

Aus dem Institut für Stammzellforschung am Helmholtz Zentrum München  
Direktor: Professor Dr. Magdalena Götz

**Temporal and cell-specific effects of the basic Helix-Loop-Helix  
Transcription factor Twist1 during breast cancer progression**

Dissertation  
zum Erwerb des Doktorgrades der Naturwissenschaften  
an der Medizinischen Fakultät der  
Ludwig-Maximilians-Universität zu München

vorgelegt von  
Johanna Maria Schmidt  
aus Gunzenhausen  
2017

Mit Genehmigung der Medizinischen Fakultät  
der Universität München

Betreuer(in): Prof. Dr. rer. nat. Magdalena Götz

Zweitgutachter(in): Prof. Dr. rer. nat. Olivier Gires

Dekan: Prof. Dr. med. dent. Reinhard Hickel

Tag der mündliche Prüfung: 24.05.2017

Dedicated to my parents.

Parts of this thesis have previously been published in Cell Reports (Schmidt et al.; 2015).

### Summary

Epithelial-Mesenchymal Transition (EMT) is a developmental process that converts epithelial cells to migratory mesenchymal cells. EMT has also been associated with metastatic dissemination of breast cancer cells and the acquisition of tumor-initiating (stem cell (sc)-like) traits (Mani et al., 2008; Scheel and Weinberg, 2012). Contradictory, metastases of breast cancers are composed of epithelial cells with strong cell-cell adhesions and numerous studies suggest tumorigenic cell populations rather to be characterized by epithelial than mesenchymal features (Celia-Terrassa et al., 2012; Korpala et al., 2011; Kowalski et al., 2003).

In my thesis I set out to reconcile these contrasting observations, by monitoring the consequences of an EMT inducing stimulus (Twist1) on mesenchymal transdifferentiation and generation of sc-like traits. Utilizing immortalized human mammary epithelial cells (HMLE) that express the EMT-transcription factor (EMT-TF) Twist1 in an inducible manner, I discovered that Twist1 converted all HMLE cells to a mesenchymal phenotype, while only a subset was additionally primed for sc-like traits. These sc-like traits exclusively emerged following Twist1-deactivation and were enriched in a small subset of cells that underwent Mesenchymal-Epithelial Transition (MET). Importantly, cells undergoing MET did not return to their original cell state as evidenced by a unique gene expression profile. Since only a subset of cells underwent MET, I hypothesized that pre-existing individual cell states determine how cells respond to transient Twist1-activation. Due to cellular heterogeneity and in order to elucidate the molecular mechanisms that pre-dispose cells for MET competence, I studied Twist1-activation in isolated HMLE single cell clones (SCCs). Studying these SCCs, I discovered that MET competence was based on partial maintenance of epithelial identity (expression of epithelial markers) during Twist1-activity. Functional studies showed that maintenance of an epithelial identity was required for proliferation in 3D environments resembling either primary tumor (collagen gels) or metastatic sites (murine lung slices), while irreversible EMT resulted in a loss of proliferative and thus a loss of colony forming ability. Finally, a cell surface proteomics screen identified 961 proteins differentially expressed on MET competent and MET incompetent cells. The identification of these proteins

generated an important fundament for future studies unraveling molecular mechanisms involved in MET competence.

In conclusion, my study suggests that irreversible mesenchymal transdifferentiation prevents, while maintenance of an epithelial cell state during Twist1-activity facilitates metastatic outgrowth. Moreover, my study emphasizes the urgent need for the development of diagnostic tools that facilitate the identification of tumor cells that have undergone MET after transient EMT-TF-activity: these tumor cells are not detectable by morphology but might have gained tumor-initiating traits that stably persist.

### **Zusammenfassung**

Der entwicklungsbiologische Prozess der Epithelial-Mesenchymalen Transition (EMT) charakterisiert die Umwandlung epithelialer Zellen in Zellen mit mesenchymalen und migratorischen Eigenschaften. Der EMT wurde zudem ein zentraler Stellenwert in der metastatischen Aussaat von Karzinomzellen sowie der Entstehung von tumorinitiierenden (Stammzell (Sz)-ähnlichen) Eigenschaften zugeschrieben (Mani et al., 2008; Scheel and Weinberg, 2012). Dem entgegengesetzt weisen die Metastasen von Mammakarzinomen zum einen einen epithelialen Phänotyp auf, zum anderen deuten zahlreiche Studien darauf hin, dass sich tumorinitiierende Karzinomzellen durch einen epithelialen und nicht durch einen mesenchymalen Phänotyp auszeichnen (Celia-Terrassa et al., 2012; Korpál et al., 2011; Kowalski et al., 2003).

Ziel dieser Arbeit war es, diese widersprüchlichen Beobachtungen aufzuklären. Hierzu wurden die Auswirkungen eines EMT induzierenden Stimulus (Twist1) auf die mesenchymale Transdifferenzierung sowie auf die Entstehung Sz-ähnlicher Eigenschaften beobachtet. Als Modellsystem dienten immortalisierte humane Brustepithelzellen (HMLE), die eine induzierbare Form des EMT-Transkriptionsfaktors (EMT-TF) Twist1 exprimierten. Hierbei entdeckte ich, dass die Aktivierung von Twist1 in allen HMLE Zellen zu einem mesenchymalen Phänotyp führte, jedoch nur in einem kleinen Bruchteil der Zellen zusätzlich Sz-ähnliche Eigenschaften initiierte. Diese Sz-ähnlichen Eigenschaften ließen sich ausschließlich nach Twist1-Deaktivierung beobachten und waren in solchen Zellen angereichert, die eine Mesenchymal-Epitheliale Transition (MET) unterlaufen hatten. Bemerkenswerterweise zeigten HMLE Zellen nach vollzogener MET ein einzigartiges Genexpressionsprofil, das darauf schließen ließ, dass diese Zellen nach MET nicht in ihren Ausgangszellstatus zurückkehrten. Basierend auf der Beobachtung, dass nur ein Bruchteil aller HMLE Zellen eine MET unterlief, stellte ich die Hypothese auf, dass ein präexistenter individueller Zellstatus die Reaktion einer Zelle auf transiente Twist1-Aktivierung bestimmt. Um die Hintergründe der MET Kompetenz von HMLE Zellen aufzuklären, die der Heterogenität dieser Zellen gerecht werden, habe ich die Folgen einer Twist1-Aktivierung in isolierten HMLE Einzel-Zell-Klonen analysiert. Dabei entdeckte ich, dass MET Kompetenz auf einer (partiellen) Aufrechterhaltung der epithelialen Identität (Expression epithelialer

Marker) während der Twist1-Aktivierung beruht. In funktionellen Studien konnte ich zeigen, dass die Aufrechterhaltung epithelialer Eigenschaften für die Proliferation in einer 3D Umgebung erforderlich ist. Im Gegensatz dazu beobachtete ich, dass eine irreversible EMT zu einem Stillstand der Proliferation sowie zum Verlust Kolonie-bildender Eigenschaften führte. Diese Beobachtungen konnten sowohl an einem Modell für Primärtumoren (Kollagengele) wie auch an einem Modell für Fernmetastasierung (Mauslungenschnitte) bestätigt werden. Im letzten Teil meiner Arbeit, konnte ich mittels Zelloberflächen-Proteomik-Analyse 961 Proteine identifizieren, die auf der Oberfläche MET kompetenter und MET inkompetenter Zellen differentiell exprimiert werden. Diese Erkenntnisse schaffen eine wichtige Grundlage für die zukünftige Aufklärung molekularer Mechanismen, die der MET Kompetenz von Mammakarzinomzellen unterliegen.

Zusammenfassend implizieren meine Studien, dass eine irreversible mesenchymale Transdifferenzierung das Auswachsen von Fernmetastasen verhindert, wohingegen die Aufrechterhaltung einer epithelialen Identität während Twist1-Aktivität, das Auswachsen von Fernmetastasen begünstigt. Meine Ergebnisse zeigen die dringende Notwendigkeit zur Entwicklung diagnostischer Hilfsmittel auf, die Tumorzellen identifizieren, welche nach transienter EMT-TF-Aktivität eine MET durchlaufen haben. Diese Tumorzellen sind anhand ihrer Morphologie nicht zu erkennen, könnten jedoch persistierende tumor-initiiierende Eigenschaften erworben haben.

## Table of contents

<b>1</b>	<b>ABBREVIATIONS .....</b>	<b>11</b>
<b>2</b>	<b>INTRODUCTION.....</b>	<b>16</b>
<b>2.1</b>	<b>Breast cancer .....</b>	<b>16</b>
<b>2.2</b>	<b>Epithelial-Mesenchymal Transition.....</b>	<b>17</b>
2.2.1	EMT and MET in development and injury.....	17
2.2.2	EMT and MET in pathological processes .....	18
2.2.3	EMT and stemness.....	19
2.2.4	Pleiotropic, interacting transcription factors orchestrate EMT .....	21
2.2.5	EMT-TFs are induced by external stimuli .....	23
2.2.6	TGF $\beta$ -signaling pathways.....	24
2.2.7	Cross-regulation between EMT-TFs.....	25
2.2.8	EMT-TFs are transiently active during cancer progression .....	26
2.2.9	EMT-TFs impart oncogenic functions independent of EMT .....	27
<b>2.3</b>	<b>Aims of the project .....</b>	<b>28</b>
<b>3</b>	<b>MATERIALS AND METHODS .....</b>	<b>30</b>
<b>3.1</b>	<b>Materials .....</b>	<b>30</b>
3.1.1	Cell lines.....	30
3.1.2	Laboratory equipment.....	30
3.1.3	Primers and Vectors.....	31
3.1.4	Instruments.....	33
3.1.5	Chemicals.....	34
3.1.6	Buffers and solutions .....	37
3.1.7	Antibodies.....	39
3.1.8	Cell culture medium.....	41
3.1.9	Software .....	41
3.1.10	Kits .....	42
<b>3.2</b>	<b>Cell Biological Methods .....</b>	<b>43</b>
3.2.1	Maintenance of cell lines .....	43
3.2.2	Isolation of Single Cell Clones (SCCs) .....	43
3.2.3	Immunofluorescence .....	43
3.2.4	Transwell Migration Assay (Boyden Chamber Assay) .....	44
3.2.5	Mammosphere Assay.....	44
3.2.6	Anoikis Assay .....	45
3.2.7	Proliferation Assay.....	46
3.2.8	Culture in 3D-floating Collagen Gels .....	46

3.2.9 Murine Lung Slice Culture .....	47
<b>3.3 Fluorescence Activated Cell Sorting (FACS) .....</b>	<b>49</b>
3.3.1 Sample preparation .....	49
3.3.2 Cell sorting .....	49
3.3.3 Cell surface marker analysis .....	50
<b>3.4 Molecular and Biochemical Biology Methods .....</b>	<b>50</b>
3.4.1 Gene Expression Analysis.....	50
3.4.2 Chromatin Immunoprecipitation (ChIP) .....	52
3.4.3 Protein Expression Analysis .....	53
<b>3.5 shRNA mediated Knockdown of ZEB1 .....</b>	<b>55</b>
3.5.1 Plasmid Preparation .....	55
3.5.2 Transfection of Virus-Producing HEK293T cells.....	56
3.5.3 Lentiviral Transduction .....	57
<b>3.6 Statistical analysis.....</b>	<b>58</b>
<b>4 RESULTS .....</b>	<b>59</b>
<b>4.1 Separation of the HMLE-Twist1-ER bulk cells into three distinct subpopulations .....</b>	<b>59</b>
<b>4.2 Twist1-activation induces Epithelial-Mesenchymal Transition (EMT) in purified epithelial, CD24<sup>pos</sup> HMLE cells .....</b>	<b>60</b>
<b>4.3 Transient Twist1-activation induces mammosphere-forming ability in CD24<sup>pos</sup> HMLE cells .....</b>	<b>63</b>
<b>4.4 The capacity of HMLE cells to undergo Mesenchymal-Epithelial-Transition (MET) following transient Twist1-activation is contained within the 24<sup>high</sup> HMLE cell population .....</b>	<b>66</b>
<b>4.5 Mammosphere-forming 24<sup>high</sup> HMLE cells display epithelial-mesenchymal plasticity .....</b>	<b>68</b>
<b>4.6 High expression of the epithelial surface marker CD24 predicts MS-formation and the ability of 24<sup>high</sup> HMLE cells to undergo MET .....</b>	<b>70</b>
<b>4.7 Twist1 induces MS-forming ability independently of EMT in 24<sup>high</sup> HMLE cells .....</b>	<b>71</b>
<b>4.8 Continuous Twist1-activity inhibits proliferation of 24<sup>high</sup> HMLE cells in a 3D environment .....</b>	<b>74</b>

<b>4.9 MS-forming 24<sup>high</sup> HMLE cells display invasive growth in 3D-collagen gels</b>	<b>77</b>
<b>4.10 24<sup>high</sup> HMLE cells display epithelial-mesenchymal plasticity in 3D collagen gels after transient Twist1-activation</b>	<b>77</b>
<b>4.11 Transient Twist1-activation permanently alters gene expression profile of HMLE cells</b>	<b>79</b>
<b>4.12 Summary of the first part</b>	<b>82</b>
<b>4.13 Single-cell cloning of 24<sup>high</sup> HMLE cells reveals resistance to Twist1-induced EMT</b>	<b>83</b>
<b>4.14 Twist1 expression levels and Twist1 TF-activity do not differ between E-SCCs and M-SCCs</b>	<b>85</b>
<b>4.15 Transcriptional programs in E-SCCs and M-SCCs are differentially activated upon TAM-treatment</b>	<b>86</b>
<b>4.16 By morphology, EMT resistant cells cannot be distinguished from EMT competent cells in co-culture</b>	<b>90</b>
<b>4.17 ZEB1-induction is required for Twist1-mediated EMT in 24<sup>high</sup> HMLE cells</b>	<b>94</b>
<b>4.18 Twist1-binding to a putative enhancer region of ZEB1 differs in M-SCCs and E-SCCs</b>	<b>96</b>
<b>4.19 E-SCCs and M-SCCs do not respond differentially to TGFβ1</b>	<b>97</b>
<b>4.20 EMT resistant and EMT competent cells show differential expression of cell surface proteins</b>	<b>99</b>
<b>4.21 Functional relevance</b>	<b>101</b>
4.21.1 Maintenance of an epithelial cell state is required for colony formation of 24 <sup>high</sup> HMLE cells in 3D collagen gels	101
4.21.2 Maintenance of an epithelial cell state is required for colony formation of 24 <sup>high</sup> HMLE cells on murine lung slices	104
<b>4.22 Summary of the second part</b>	<b>106</b>
<b>5 DISCUSSION</b>	<b>108</b>
<b>5.1 Twist1 induces mesenchymal transdifferentiation and mammosphere (MS)-formation independently of each other</b>	<b>108</b>

<b>5.2 Twist1-deactivation results in a novel, hitherto unknown permanent cell state .....</b>	<b>110</b>
<b>5.3 24<sup>high</sup> HMLE cells predisposed to undergo MET retain expression of epithelial genes during Twist1-activation.....</b>	<b>111</b>
<b>5.4 Expression of ZEB1 is directly regulated by Twist1 in 24<sup>high</sup> HMLE cells</b>	<b>112</b>
<b>5.5 Does Ovol2 represent the central brake holder of Twist1-induced EMT?</b>	<b>114</b>
<b>5.6 EMT resistance is required for proliferation at primary tumor and metastatic site.....</b>	<b>115</b>
<b>5.7 Does extracellular signaling explain differential response of E-SCCs and M-SCCs? .....</b>	<b>116</b>
<b>5.8 Closing remarks.....</b>	<b>117</b>
<b>6 REFERENCES .....</b>	<b>119</b>
<b>EIDESSTATTLICHE VERSICHERUNG.....</b>	<b>133</b>
<b>ACKNOWLEDGMENTS.....</b>	<b>134</b>

## List of tables

Table 1: qRT-PCR reaction mixture.....	51
Table 2: Cycling protocol for qRT-PCR of cDNA .....	51
Table 3: Composition of separating and stacking gel of 10% and 12.5% SDS gels.....	54
Table 4: Composition of Transfection mix.....	57

## List of figures

Figure 1: The metastatic cascade.....	19
Figure 2: Separation of the HMLE-Twist1-ER bulk cells into three distinct subpopulations. ....	60
Figure 3: Twist1-activation for 15 days induces EMT in purified epithelial, CD24 <sup>pos</sup> HMLE cells. ....	62
Figure 4: Transient Twist1-activation induces mammosphere-forming ability in CD24 <sup>pos</sup> HMLE cells. ....	65
Figure 5: The capacity of HMLE cells to undergo MET following transient Twist1-activation is contained within the 24 <sup>high</sup> HMLE cell population. ....	67
Figure 6: MS-forming 24 <sup>high</sup> HMLE cells display epithelial-mesenchymal plasticity. ....	69
Figure 7: High expression of the epithelial surface marker CD24 predicts MS-formation and the ability of 24 <sup>high</sup> HMLE cells to undergo MET. ....	71
Figure 8: Twist1 induces MS-forming ability independently of EMT in 24 <sup>high</sup> HMLE cells. ....	73
Figure 9: Continuous Twist1-activity inhibits proliferation of 24 <sup>high</sup> HMLE cells in a 3D environment. ....	76
Figure 10: MS-forming 24 <sup>high</sup> HMLE cells display invasive growth in 3D collagen gels. Immunofluorescence staining of laminin-1 (green) and DAPI (blue) of colonies formed by untreated 24 <sup>high</sup> control cells (-TAM) or MS-derived cells. Scale bar: 100 $\mu$ m. ....	77
Figure 11: 24 <sup>high</sup> HMLE cells display epithelial-mesenchymal plasticity in 3D collagen gels after transient Twist1-activation. ....	78
Figure 12: Transient Twist1-activation permanently alters gene expression profile of HMLE cells. ....	81
Figure 13: Summary of the first part. ....	82
Figure 14: Single-cell cloning of 24 <sup>high</sup> HMLE cells reveals resistance to Twist1-induced EMT. ....	84
Figure 15: Twist1 expression levels and Twist1 TF-activity do not differ between E-SCCs and M-SCCs. ....	86
Figure 16: Transcriptional programs in E-SCCs and M-SCCs are differentially activated upon TAM-treatment. ....	89

Figure 17 By morphology, EMT resistant cells cannot be distinguished from EMT competent cells in co-culture. ....91

Figure 18: EMT resistant cells reappear as epithelial islands after Twist1-deactivation. ....93

Figure 19: ZEB1-induction is required for Twist1-mediated EMT in 24<sup>high</sup> HMLE cells. ....95

Figure 20: Twist1-binding to a putative enhancer region of *ZEB1* differs in M-SCCs and E-SCCs. ....97

Figure 21: E-SCCs and M-SCCs do not respond differentially to TGFβ1. ....98

Figure 22: EMT resistant and EMT competent cells show differential expression of cell surface proteins. ....100

Figure 23: Maintenance of an epithelial cell state is required for colony formation of 24<sup>high</sup> HMLE cells in 3D collagen gels. ....103

Figure 24: Maintenance of an epithelial cell state is required for colony formation of 24<sup>high</sup> HMLE cells on murine lung slices. ....105

## 1 Abbreviations

<b>μ</b>	micro
<b>2D/3D</b>	2/3 dimensional
<b>7-AAD</b>	7-Aminoactinomycin D
<b>A</b>	ampere
<b>AML</b>	acute myeloide leucemia
<b>APC</b>	Allophycocyanin
<b>APS</b>	ammonium persulfate
<b>ATP</b>	adenosine triphosphate
<b>bFGF</b>	basic fibroblast growth factor
<b>bHLH</b>	basic helix-loop-helix
<b>BRD4</b>	bromodomain-containing protein 4
<b>BSA</b>	Bovine serum albumin
<b>CO<sub>2</sub></b>	carbon dioxide
<b>CaCl<sub>2</sub></b>	calcium chloride
<b>CD</b>	cluster of differentiation
<b>cDNA</b>	complementary DNA
<b>CFU</b>	colony forming units
<b>ChIP</b>	Chromatin Immunoprecipitation Assay
<b>CNS</b>	central nervous system
<b>CSC</b>	cancer stem cell
<b>CTBP</b>	C-terminal-binding protein
<b>CTC</b>	circulating tumor cell
<b>CTFC</b>	corrected total cell fluorescence
<b>Ctrl</b>	control
<b>d</b>	day
<b>DAPI</b>	4',6-diamidino-2-phenylindole
<b>DMEM</b>	Dulbecco's Modified Eagle Medium
<b>DMSO</b>	dimethyl sulfoxide
<b>DNA</b>	deoxyribonucleic acid
<b>Dsg3</b>	Desmoglein 3
<b>DTC</b>	disseminated tumor cell

## Abbreviations

---

<b>e.g.</b>	exempli gratia: for example
<b>E-cad</b>	E-cadherin
<b>ECL</b>	enhanced chemiluminescence
<b>ECM</b>	extracellular matrix
<b>EDTA</b>	ethylenediaminetetraacetic acid
<b>EGF</b>	epidermal growth factor
<b>EGFR</b>	epidermal growth factor receptor
<b>EGTA</b>	ethylene glycol tetraacetic acid
<b>EMT</b>	Epithelial-Mesenchymal Transition
<b>EpCAM</b>	Epithelial cell adhesion molecule
<b>ER</b>	estrogen receptor
<b>ERK</b>	extracellular signal-related kinase
<b>ESRP</b>	epithelial splicing regulatory protein
<b>FACS</b>	fluorescence-activated cell sorting
<b>FCS</b>	fetal calve serum
<b>FGF</b>	fibroblast growth factor
<b>FGFR</b>	fibroblast growth factor receptor
<b>FITC</b>	flourescein isothiocyanate
<b>FN</b>	fibronectin
<b>FOX</b>	forkhead box
<b>g</b>	gram/acceleration of gravity
<b>GFP</b>	green fluorescent protein
<b>H&amp;E</b>	Haematoxylin&Eosin
<b>H<sub>2</sub>O</b>	chemical formula for water
<b>H3K9</b>	Histone H3 Lysine 9
<b>HCl</b>	hydrogen chloride
<b>HDAC</b>	histone deacetylase
<b>HEPES</b>	4-(2-hydroxyethyl)-1-piperazineethanesulfonic acid
<b>HER2</b>	human epidermal growth factor receptor 2
<b>HGFR</b>	hepatocyt growth factor receptor
<b>HMLE</b>	Immortalized Human Mammary Epithelial Cells
<b>hTERT</b>	human telomerase reverse transcriptase
<b>Hz</b>	hertz

## Abbreviations

---

<b>i.e.</b>	id est: that is
<b>ID</b>	inhibitor of DNA binding
<b>IGFR</b>	insulin growth factor receptor
<b>IgG</b>	immunoglobulin g
<b>ITGA6</b>	Integrin, alpha 6
<b>ITGB4</b>	Integrin, beta 4
<b>JNK</b>	c-Jun N-terminal kinase
<b>K</b>	kilo
<b>kb</b>	kilobase
<b>l</b>	liter
<b>LB</b>	lysogeny broth
<b>LOXL</b>	Lysyl-oxidase like
<b>LTC</b>	lung tissue culture
<b>M</b>	molar
<b>m</b>	milli
<b>m/v</b>	mass/volume
<b>MAPK</b>	Mitogen-activated protein kinase
<b>MET</b>	Mesenchymal-Epithelial Transition
<b>MgCl<sub>2</sub></b>	magnesium chloride
<b>min</b>	minute
<b>miRNA</b>	micro RNA
<b>mRNA</b>	messenger RNA
<b>MS</b>	mammosphere
<b>n</b>	number
<b>n.d.</b>	not detectable
<b>Na<sub>3</sub>VO<sub>4</sub></b>	sodium orthovanadate
<b>NaCl</b>	sodium chloride
<b>NaOH</b>	sodium hydroxide
<b>N-cad</b>	N-cadherin
<b>neg</b>	negative
<b>NFκB</b>	nuclear factor kappa B
<b>NGS</b>	normal donor goat serum
<b>nm</b>	nanometer

## Abbreviations

---

<b>nt</b>	non-targeting
<b>ON</b>	over night
<b>Ovol</b>	Ovo-like
<b>PBS</b>	phosphate-buffered saline
<b>PC</b>	principal component
<b>Pc2</b>	polycomb 2
<b>PCA</b>	principal component analysis
<b>PCAF</b>	p300/CBP-associated factor
<b>PCR</b>	Polymerase Chain Reaction
<b>PDAC</b>	pancreatic ductal adenocarcinoma
<b>PDGFR</b>	platelet-derived growth factor receptor
<b>PDL</b>	Poly-D-Lysine
<b>PE</b>	phycoerythrin
<b>Pen/Strep</b>	Penicillin/Streptomycin
<b>PFA</b>	paraformaldehyde
<b>PI3K</b>	Phosphoinositide-3-kinase
<b>pos</b>	positive
<b>PR</b>	progesterone
<b>qRT-PCR</b>	quantitative Real-Time Polymerase Chain Reaction
<b>RB</b>	retinoblastoma protein
<b>RIPA</b>	radioimmunoprecipitation assay
<b>RLU</b>	relative light units
<b>RNA</b>	ribonucleic acid
<b>RPL32</b>	ribosomal protein L32
<b>rpm</b>	rotation per minute
<b>RT</b>	room temperature
<b>RUNX2</b>	Runt related transcription factor 2
<b>sc</b>	stem cell
<b>SCC</b>	single cell clone
<b>SD</b>	standard deviation of the mean
<b>SDS</b>	sodium dodecyl sulfate
<b>SDS-Page</b>	Sodium Dodecyl Sulfate Polyacrylamide Gel Electrophoresis
<b>sec</b>	second

## Abbreviations

---

<b>SEM</b>	standard error of the mean
<b>shRNA</b>	small hairpin RNA
<b>SIP1</b>	Smad-interacting protein 1
<b>TACSTD2</b>	Tumor-associated calcium signal transducer 2
<b>TAM</b>	4-hydroxytamoxifen
<b>TBS</b>	Tris-buffered saline
<b>TEMED</b>	tetramethylethylenediamine
<b>TF</b>	transcription factor
<b>TGFBR</b>	Transforming Growth Factor beta Receptor
<b>TGF<math>\beta</math></b>	Transforming Growth Factor beta
<b>TIC</b>	tumor-initiating cell
<b>TKR</b>	tyrosine kinase receptor
<b>TNBC</b>	triple-negative breast cancer
<b>TNS</b>	Trypsin Neutralizing Solution
<b>Trop2</b>	Trophoblast antigen 2
<b>TSS</b>	transcriptional start site
<b>U</b>	unit
<b>V</b>	volt
<b>v/v</b>	volume fraction
<b>Vim</b>	Vimentin
<b>vs</b>	versus
<b>Wnt</b>	Wingless-Type MMTV Integration Site Family Members
<b>WST-1</b>	water soluble tetrazolium 1
<b>ZEB1/2</b>	Zinc Finger E-Box Binding Homeobox 1/2
<b>ZO-1</b>	Zona occludens 1
<b><math>\beta</math>-cat</b>	$\beta$ -catenin

## **2 Introduction**

### **2.1 Breast cancer**

Breast cancer is the most frequent diagnosed cancer amongst women worldwide and one in eight women will develop breast cancer during her lifetime (RKI, 2010). One challenge in breast cancer treatment is the heterogeneity of this disease. Breast carcinomas are classified according to clinical parameters, such as tumor size or grade, and pathological markers, like the expression of estrogen receptor (ER), progesterone receptor (PR) or human epidermal growth factor receptor 2 (HER2) (Prat and Perou, 2011; Valentin et al., 2012). Tumors belonging to the class of Triple Negative Breast Cancer (TNBC) are characterized by lack of the hormone receptors ER, PR or HER2 (Podo et al., 2010). Importantly, in more than 90% of cases not the primary tumor, but distant metastases are the main cause of cancer related death (Weinberg, 2013). During the last years, mortality rates of breast cancer patients have decreased, mostly due to early diagnosis and improvement of adjuvant chemotherapy (Peto et al., 2000; Thomson et al., 2004). However, current prognostic criteria poorly predict the risk of metastasis. As a consequence, many patients are “under”- or “over-treated”. For instance, 80% of the breast cancer patients receive chemotherapy while 60% of the women may be cured by surgery or local radiotherapy alone (Weigelt et al., 2005). This clearly emphasizes the urgent need for identification of new prognostic markers that predict the risk for metastases. Moreover, identification of molecular mechanisms involved in metastatic processes might improve understanding of this disease and the development of new therapeutic strategies. Recently, the developmental process of Epithelial-Mesenchymal Transition (EMT) was found to effect early steps of the metastatic cascade such as dissemination and invasion of cancer cells (Thiery et al., 2009). Moreover, EMT was linked to the acquisition of tumor-initiating traits (stem cell (sc)-like traits), suggesting that EMT may also promote the last step of the metastatic cascade, colonization at secondary tumor sites (Mani et al., 2008). Thus, targeting EMT associated events became of central interest for the development of therapeutic strategies eradicating breast cancer.

## **2.2 Epithelial-Mesenchymal Transition**

Epithelial-Mesenchymal Transition (EMT) is the conversion from an epithelial to a mesenchymal cell state. In more detail, the process of EMT implies the switch from apico-basal polarized epithelial cells with a cobblestone-like morphology to spindle-shaped, front-to-back polarized mesenchymal cells. These morphological changes are accompanied by the dissolution of strong cell-cell adhesions, mainly by down-regulation of the adherens junction protein E-cadherin. Thereby, cells are converted from a stationary to a more motile cell state, enabling them to migrate as single cells and invade into adjacent tissue (Yang and Weinberg, 2008). Initially, the term EMT was coined by Elizabeth Hay who observed this phenomenon to be important for cell movements in chicken embryos (Hay, 1968). Since then, EMT was implicated in many more contexts: besides its importance in embryonic development, EMT was shown to be involved in wound healing and pathological processes like fibrosis and cancer progression (Chapman, 2011; Kalluri and Weinberg, 2009; Thiery et al., 2009). Importantly, EMT is not an irreversible process. The reverse process, Mesenchymal-Epithelial Transition (MET), plays a crucial role during development and pathological processes as well (Boyer and Thiery, 1993; Davies, 1996).

### **2.2.1 EMT and MET in development and injury**

During embryonic development of all metazoans, several turns of EMT and MET are required to convert the initial single layer of epithelial cells (ectoderm) to well differentiated and specialized cell types. These processes are fundamental for the formation of complex three-dimensional organs. EMT processes are well described for developmental events like mesoderm formation, neural crest development, heart valve development or secondary palate formation (Yang and Weinberg, 2008). As an example for EMT, mesoderm formation will be illustrated. The mesoderm belongs to the three germ layers and develops during gastrulation. Mesoderm formation starts at a specific region within the primitive ectoderm. During invagination, epithelial cells reorganize cell shape and redistribute their organelles. Next, cells locally break through the basement membrane and lose their strong cell-cell adhesions. Finally, cells migrate underneath the ectoderm and assemble the mesoderm (Viebahn, 1995). As

mentioned above, MET events are also crucial for successful embryogenesis. One well-studied MET process is formation of the nephron epithelium during kidney development. After outpouching of the uteric bud, nephric cells assemble around the branched tips and start to re-epithelialize by expressing laminin and components of cell-cell adhesions. Thereby, MET leads to the conversion of mesenchymal cells to differentiated, epithelial cells that finally form the kidney tubules (Davies, 1996).

Moreover, interconversions of epithelial and mesenchymal cell states occur in adult tissue as a physiological response to injury. During wound healing, keratinocytes undergo the process of EMT in response to inflammatory stimuli. Thereby, keratinocytes acquire a motile, plastic phenotype, allowing their migration to the place of injury where they finally mediate re-epithelization of the wound (Arnoux et al., 2008; Thiery et al., 2009).

### **2.2.2 EMT and MET in pathological processes**

Furthermore, EMT and MET programs are implicated in pathological processes like organ fibrosis, tumorigenesis and metastasis (Thiery et al., 2009). Interestingly, a visionary description of EMT and its implication in cancer invasion already came up 126 years ago: Ramón y Cajal discovered loss of cell adhesion and invasion to the stroma of some ductal epithelial cells in breast tumors (Ramón y Cajal, 1890). EMT and MET events during cancer progression will be described in more detail now. The majority of solid human tumors are carcinomas. For successful metastasis, initially epithelial cells of the primary tumor need to undergo a series of distinct steps including EMT and MET events. The metastatic cascade summarizes all these events (Scheel and Weinberg, 2012) (Figure1).

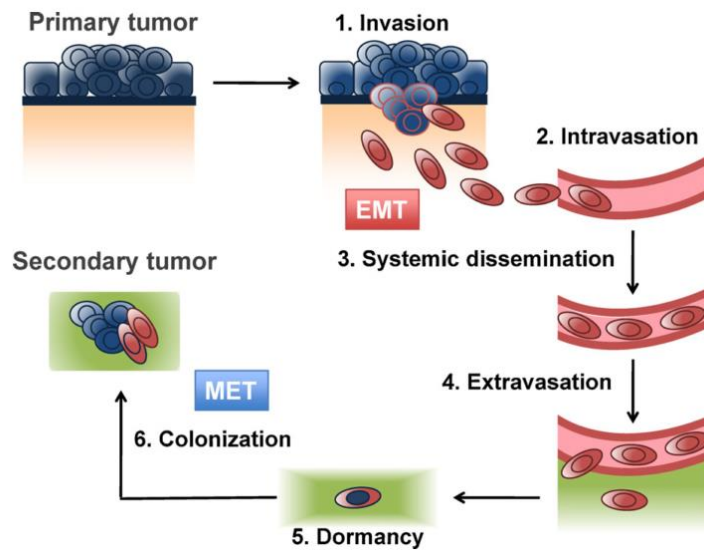


**Figure 1: The metastatic cascade**

For the early steps of the metastatic cascade (1.-4.) primary tumor cells (blue cells) undergo Epithelial-Mesenchymal Transition (red cells). After extravasation to distant tissues tumor cells remain as single cells or micro-metastases (5.). For colonization and metastatic outgrowth (6.), cells need to undergo the reverse process, Mesenchymal-Epithelial Transition (MET). (adapted from Scheel and Weinberg, 2012)

First, epithelial cells of the primary tumor undergo EMT. Thereby, they detach from neighboring cells, lose their apico-basal polarity and gain the capacity to migrate as single cells and invade surrounding tissues. After intravasation into lymph or blood vessel system, cells remain as circulating tumor cells (CTCs) and become disseminated within the body. After extravasation, tumor cells stay as non-proliferating solitary cells or micro-metastases. To complete the metastatic cascade and grow out as macro-metastases, cells finally revert back to an epithelial phenotype via MET (Celia-Terrassa et al., 2012; Kowalski et al., 2003; Ocana et al., 2012; Tsai et al., 2012).

### 2.2.3 EMT and stemness

More recently, EMT was linked to the acquisition of stem cell (sc)-like traits during breast cancer progression (Mani et al., 2008; Morel et al., 2008). The concept of stem cells was initially described for the hematopoietic system where stem cells were defined as cells with self-renewal ability that simultaneously give rise to more mature daughter cells (Reya et al., 2001). The idea of cancer stem cells (CSCs) first emerged in 1997, when Bonnet and Dick showed that a subset

of patient derived acute myeloid leukemic (AML) cells was able to re-initiate tumors after transplantation into recipient mice (Bonnet and Dick, 1997). Later, Al-Hajj and colleagues described the isolation of sc-like human breast cancer cells, characterized by the cell surface marker profile  $CD44^{high}/CD24^{neg}$ . Even after several passages,  $CD44^{high}/CD24^{neg}$  cells, in contrast to  $CD44^{pos}/CD24^{pos}$  or bulk tumor cells, gave rise to tumors, comprised of a mixture of tumorigenic  $CD44^{high}/CD24^{neg}$  and non-tumorigenic cells, in immunocompromised mice (Al-Hajj et al., 2003).

To measure self-renewal of mammary cells *in vitro*, the mammosphere assay, adapted from the neurosphere assay, is often used as a proxy-assay (Dontu et al., 2003; Reynolds and Weiss, 1992, 1996). In this assay, cells are suspended in highly viscous media and plated as single cells into culture dishes that prevent attachment of the cells to the dish surface. Under these conditions, cells that are able to proliferate at clonal density in anchorage independence grow out as mammospheres. Using this assay, Fillmore and Kupperwasser were able to enrich for tumor-initiating breast cancer cells (TICs), indicating that mammosphere (MS)-forming capacity, reflects tumor-initiating capacity *in vitro* (Fillmore and Kuperwasser, 2008). First implications linking EMT and CSCs-generation came up in 2008. Overexpression of either Twist1 or Snail1 in human immortalized breast epithelial (HMLE) cells was found to induce EMT, a  $CD44^{high}/CD24^{neg}$  surface marker profile as well as MS-forming capacity. Moreover, after transformation of these cells with the oncogene *V12H-Ras*, cells were enriched for tumor-initiation capacity in immunocompromised mice (Mani et al., 2008; Morel et al., 2008). However, at this point, it is important to mention that whereas all HMLE cells acquired a mesenchymal,  $CD44^{high}/CD24^{neg}$  phenotype during EMT, only a minority of them was able to generate MS. Furthermore, HMLE cells are heterogeneous and were shown to give rise to a small  $CD44^{high}/CD24^{neg}$ , mesenchymal subpopulation spontaneously (Chaffer et al., 2011). Therefore, it remains obscure whether transdifferentiation to a mesenchymal cell state is directly linked to the acquisition of sc-like traits. One could hypothesize that activation of the EMT program might select for pre-existing sc-like cells, but not induce the conversion of non-sc-like to sc-like cells.

#### **2.2.4 Pleiotropic, interacting transcription factors orchestrate EMT**

At the molecular level, EMT is orchestrated by a set of pleiotropic, interacting transcription factors (TFs). Together the so-called EMT-TFs coordinate repression of epithelial markers and induction of mesenchymal markers by acting as both, transcriptional repressors or activators (De Craene and Berx, 2013). There are three main EMT-TF families: 1) the Snail TF family, 2) the zinc-finger E-box-binding (ZEB) TF family and 3) the basic helix-loop-helix (bHLH) TF family. More recently, TFs of the forkhead box (FOX), GATA and SRY box (SOX) TF family were described to be involved in EMT processes during development and cancer progression (Campbell et al., 2011; Eijkelenboom and Burgering, 2013). In the following paragraphs, the three main EMT-TF families will be described in more detail.

##### **2.2.4.1 Snail transcription factors**

There are three Snail proteins in vertebrates: Snail1 (also known as Snail), Snail2 (also known as Slug) and Snail3 (also known as Smuc) (Barrallo-Gimeno and Nieto, 2005). All members of the Snail family are characterized by a common protein structure: a highly conserved carboxy-terminal region, characterized by four zinc-finger domains of the C<sub>2</sub>H<sub>2</sub>-type and a variant N-terminal domain (Knight and Shimeld; 2001). Via their zinc-fingers, Snail proteins specifically bind to E-box DNA sequences characterized by a core of six bases (5'-CATGGTG-3') (Cano et al., 2000). After binding to DNA, Snail members act as transcriptional repressors by recruiting co-repressors like the C-terminal binding protein (CTBP) or chromatin modifiers, such as histone deacetylases or demethylases (Lin et al., 2010; Tong et al., 2012). One prominent target directly repressed by Snail1 and Slug is *CDH1*, which encodes the main epithelial adherens junction protein E-cadherin (Cano et al., 2000; Hajra et al., 2002). In line with their ability to suppress components of an epithelial phenotype, Snail proteins were shown to be involved in various EMT processes during development and cancer (Barrallo-Gimeno and Nieto, 2005). During mesoderm or neural crest formation, Snail1 promotes dissociation of cell adhesion and cell migration (Nieto, 2002). Moreover, Snail1 and Slug expression are associated with metastasis and poor clinical outcome in various types of carcinomas like

breast, ovarian or colorectal cancer (Elloul et al., 2005; Moody et al., 2005; Roy et al., 2005; Shioiri et al., 2006).

### **2.2.4.2 ZEB transcription factors**

The ZEB TFs family consists of two members, ZEB1 (also known as  $\delta$ EF1) and ZEB2 (also known as SIP1) (Eger et al., 2005). Common for ZEB proteins are two zinc finger clusters, one consisting of three and one consisting of four zinc fingers. Moreover, ZEB proteins are characterized by a central homeobox-domain and additional regions, like CTBP- or SMAD-interacting sites (Peinado et al., 2007). ZEB proteins interact with DNA by simultaneous binding of both zinc finger clusters to bipartite E-boxes (Remacle et al., 1999). After binding, they recruit co-repressors (CTBP for ZEB2) or interact with transcriptional co-activators (p300/CBP-associated factor (PCAF) for ZEB1), thereby either repressing or activating gene transcription (Postigo et al., 2003). During development, ZEB1 and ZEB2 are expressed in hematopoietic, heart, skeletal and central nervous system cells (Postigo and Dean, 2000). Moreover, ZEB proteins are important regulators of cancer-related EMT. In mouse or human tumor cell lines, ZEB1 and ZEB2 were found to reduce cell-cell adhesion and promote migration as well as invasion via repression of *CDH1* (Comijn et al., 2001; Shirakihara et al., 2007).

### **2.2.4.3 (b)HLH transcription factors**

The (basic) helix-loop-helix ((b)HLH) transcription factors represent the third large family of proteins that directly or indirectly participate in the silencing of *CDH1* expression (Peinado et al., 2007). bHLH TFs belong to the huge family of HLH proteins that are subdivided into seven classes (Massari and Murre, 2000). The common protein structure is characterized by two amphipatic  $\alpha$ -helices linked via a loop. In addition, all bHLH members possess a basic domain. In regard to DNA binding, bHLH TFs act as hetero- or homodimers and recognize consensus E-box sequences (Ellenberger et al., 1994). Among all HLH proteins, the class I proteins (E12, E14), the class II proteins (Twist1 and Twist2) as well as the inhibitor of DNA binding proteins (Id1-Id4), belonging to class V, were found to be key regulators of developmental and cancer-related EMT (Xu et al., 2009). The impact of Twist1 on developmental and cancer-related EMT will be

described in more detail: Twist1 was shown to be important during development of both, invertebrates and vertebrates. Besides its function as a key factor for mesoderm specification and dorsal-ventral patterning in *Drosophila*, the absence of Twist1 was found to be lethal in mouse embryos (Chen and Behringer, 1995; Simpson, 1983). Moreover, upregulation of Twist1 expression was described for various cancer types, like breast, prostate, squamous cell and hepatocellular carcinomas (Kwok et al., 2005; Lee et al., 2006; Mironchik et al., 2005; Yuen et al., 2007). In metastatic mammary tumor cell lines, high Twist1-expression was shown to be required for successful metastatic spread to murine lungs (Yang et al., 2004).

### **2.2.5 EMT-TFs are induced by external stimuli**

EMT-TF activity and therefore the whole EMT program are regulated by external stimuli, such as growth factors or signaling molecules (Lamouille et al., 2014). Besides various tyrosine kinase receptor (TKR) pathways, like fibroblast, epidermal, platelet derived or hepatocyte growth factor receptor (FGFR, EGFR, PDGFR, HGFR) signaling, collaboration of the canonical, non-canonical Wnt- and transforming growth factor (TGF) $\beta$  -signaling pathway were shown to be sufficient to induce EMT and later maintain a mesenchymal cell state (Scheel et al., 2011; Yang and Weinberg, 2008). Moreover, the Notch signaling pathway contributes to EMT during development and tumor progression (Timmerman et al., 2004). Recently, inflammatory cytokines and hypoxia were identified to induce EMT-TF activity, as well (Lester et al., 2007; Tsai and Yang, 2013; Yang and Weinberg, 2008). Finally, EMT can be induced by mechanotransduction: matrix stiffness was found to regulate Twist1 localization and thereby Twist1-activity (Wei et al., 2015).

Interestingly, external stimuli either directly regulate EMT-TF expression or modulate EMT-TF activity on the protein level. For instance, Wnt and TGF $\beta$ -signaling are implicated in the regulation of EMT-TF expression. In murine mammary cells, Twist1 levels were found to be upregulated in response to Wnt1 (Howe et al., 2003). Moreover, Wnt signaling was found to regulate Slug expression in *Xenopus* neurel crest cells (Vallin et al., 2001). Snail expression

is modulated by TGF $\beta$ -signaling, either directly via Smad3 or indirectly via the high mobility group A2 (HMGA2) (Thuault et al., 2008; Thuault et al., 2006). At the post-transcriptional level, EMT-TF activity can be modified both, by phosphorylation or by protein-protein interactions. For instance, phosphorylation of Snail1 influences its cellular localization or degradation and thereby its function as a TF (Yang et al., 2005; Zhou et al., 2004). Besides, interaction of Snail with the lysyl-oxidase like (LOXL) proteins modulates Snail1 stability (Peinado et al., 2005). ZEB proteins are also regulated by protein-protein interactions. For example, polycomb protein Pc2 sumoylates ZEB2 thereby preventing its interaction with CTBP and thus its repressive function (Long et al., 2005). TF-activity of the bHLH family members is mainly regulated by the availability of dimerization partners and the formation of distinct homo- or heterodimers. For instance, human Twist1 exclusively binds to E-box sequences after heterodimerization with an E-protein while Twist1 homodimers lack this ability (Chang et al., 2015). Moreover, binding of Id proteins to class I or II bHLH TFs influences their function in a dominant-negative manner as Id proteins lack the DNA binding domain (Massari and Murre, 2000). In addition, bHLH TF activity is regulated by phosphorylation: Hong and colleagues revealed that mitogen-activated protein kinases (MAPK) mediated phosphorylation prevents proteasomal degradation of Twist1 (Hong et al., 2011). Besides post-transcriptional regulation of EMT-regulators by phosphorylation or protein-protein interaction, they are modulated by microRNAs (miRNAs). MiRNAs are about 22 nucleotides-long non-coding RNA molecules that negatively influence gene expression by either mRNA destabilization or translational inhibition. The miR200-family represents one prominent example. Members of this family and the EMT-TFs ZEB1 and ZEB2 were shown to repress each other in a reciprocal negative feedback loop (Bracken et al., 2008).

### **2.2.6 TGF $\beta$ -signaling pathways**

Since TGF $\beta$ -signaling will be addressed later in this thesis, it will be explained in more detail now. TGF $\beta$ -signaling is one of the best-studied pathways during developmental and cancer related EMT. Interestingly, the effects of TGF $\beta$ -signaling are cell context dependent and change during cancer progression.

While TGF $\beta$ -signaling induces cell cycle arrest and cell death in normal and premalignant tumor cells, it can favor malignant progression by EMT promotion as well: malignant tumor cells show resistance to TGF $\beta$ -induced cell death and utilize TGF $\beta$ -signaling to gain the capacity to invade, systemically disseminate and extravasate at distant sites (Massague, 2008). Interestingly, this so-called TGF $\beta$ -switch was found to be conveyed by forced expression of the EMT-TF Snail1 (Franco et al., 2010). At the molecular level, TGF $\beta$ -signaling is subdivided in the canonical (Smad-dependent) and the non-canonical (Smad-independent) pathway. During canonical signaling, direct binding of TGF $\beta$  ligands to TGF- $\beta$  receptor type II (TGFBR2), a transmembrane serine/threonine protein kinase receptor, induces dimerization with the serine/threonine kinase TGF- $\beta$  receptor type I (TGFBR1). Thereby, TGFBR1 becomes trans-phosphorylated and activated. Subsequently, Smad2/3 are recruited and phosphorylated, allowing the interaction with Smad4. Upon generation of the heterotrimeric Smad2/3/4 complex, this complex translocates into the nucleus and regulates gene expression. Independently of the Smad proteins, TGF $\beta$ -signaling activates mitogen-activated protein (MAP) kinase family members- like the extracellular signal-related kinase 1/2 (ERK1/2), the c-Jun N-terminal kinase (JNK) or p38 MAPK. Moreover, non-canonical TGF $\beta$ -signaling regulates focal adhesion signaling, phosphoinositide-3-kinase (PI3K) signaling and the activation of Rho-family GTPases (Parvani et al., 2011).

### **2.2.7 Cross-regulation between EMT-TFs**

Besides external stimuli, EMT-TFs regulate each other's transcription themselves. For instance, cross-regulation of EMT-TFs reinforces transcriptional repression of E-cadherin: while Snail1, Slug and ZEB-TFs directly bind to the E-cadherin promotor, Twist1 indirectly represses E-cadherin transcription by induction of other EMT-TFs expression (Casas et al., 2011; Dave et al., 2011; Peinado et al., 2007). Specifically, Twist1 was described to bind to an E-box sequence within the Slug promotor, thereby inducing its transcription. In contrast, knockdown of Slug completely prevented suppression of E-cadherin by Twist1 (Casas et al., 2011). In *Drosophila* Twist1 was found to directly induce Snail1 and thereby promote EMT processes during mesoderm formation (Leptin, 1991).

Moreover, Snail1 and Twist1 functionally cooperate during EMT: Snail1 as well as Twist1 directly regulate expression of ZEB1 during TGF $\beta$ -induced EMT in mouse breast epithelial NMuMG cells (Dave et al., 2011). Up-regulation of ZEB1 by Snail1 was discovered in other mammalian epithelial cell lines as well and Snail1 was found to be required for expression of the ZEB1 homolog (Zfh1) in *Drosophila* (Guaita et al., 2002; Lai et al., 1991). Interestingly, EMT-TFs were also discovered to negatively regulate each other. Recently, a temporal and spatial cooperation between Snail1 and Twist1 in breast cancer metastasis was described: during early steps of transient TGF $\beta$ -induced EMT, Snail1 was found to bind within the promotor of Twist1 thereby directly repressing its transcription (Tran et al., 2011).

### **2.2.8 EMT-TFs are transiently active during cancer progression**

EMT-TFs are important key regulators during cancer progression as they repress cell-cell adhesion genes and induce a migratory, mesenchymal phenotype (Peinado et al., 2007). In addition, as discussed above EMT-TF activity was linked to the acquisition of sc-like traits (Mani et al., 2008). Contradictory, metastases of invasive breast cancers are composed of epithelial cells with strong cell-cell adhesion (Kowalski et al., 2003). These observations suggest that EMT-TFs may be merely transiently active during cancer progression. Moreover, they indicate that a mesenchymal cell state and sc-like traits are not necessarily linked to each other. One example supporting this hypothesis was described during the progression of squamous cell carcinoma in mice: in the primary tumor, Twist1-activity induced cell invasion by EMT-induction and promotion of invadopodia-mediated extracellular matrix (ECM) degradation. However, at the metastatic site, Twist1-deactivation was crucial for outgrowth of metastases (Tsai et al., 2012). In addition, transient Snail-activation was described to be crucial during cancer progression: Tran and colleagues found that continuous Snail1 overexpression increased the amount of disseminated tumor cells (DTC), but not the number of lung metastases. In contrast, transient Snail1 expression increased both, DTCs and lung metastases (Tran et al., 2014). Moreover, the recently discovered EMT inducer homeobox factor Prrx1 promotes mesenchymal transdifferentiation and invasion while its loss is absolutely required for cancer

cell outgrowth at metastatic sites (Ocana et al., 2012). Extending these observations, I discovered that transient but not continuous Twist1-activation induces mammosphere-forming capacity in HMLE cells (Schmidt et al., 2015).

### **2.2.9 EMT-TFs impart oncogenic functions independent of EMT**

The fact that EMT-TF expression is already detectable in non-invasive neoplastic lesions of human tumor samples, suggests that these factors might have oncogenic functions in primary tumors besides initiation of mesenchymal transdifferentiation and invasion (Ansieau et al., 2013; Geradts et al., 2011). Indeed, EMT-TFs have been found to convey survival advantages for tumor cells under oncogenic stress signals (Puisieux et al., 2014). For instance, Twist1 was shown to prevent apoptosis and allow escape from cell cycle control by suppression of p53- and retinoblastoma protein (RB)-pathways, respectively (Ansieau et al., 2008; Maestro et al., 1999; Valsesia-Wittmann et al., 2004). In addition, ZEB1 was described to be involved in overcoming cell cycle arrest by repression of the cyclin-dependent kinase inhibitors p15<sup>NK4B</sup> and p16<sup>NK4A</sup> (Ohashi et al., 2010). Finally, members of the Snail TF family were implicated in p53 downregulation and inhibition of its transcriptional activity as well (Lee et al., 2009; Wu et al., 2005).

### 2.3 Aims of the project

The developmental process EMT has been associated with the acquisition of aggressive traits by breast cancer cells, including the ability to complete various steps of the metastatic cascade and tumor-initiating traits (stem cell (sc)-like traits (Thiery et al., 2009; Mani et al., 2008; Morel et al., 2008). Recent studies suggesting a link between EMT and the acquisition of sc-like traits (measured as mammosphere (MS)-forming ability) were carried out using bulk populations of immortalized human mammary epithelial cells (HMLE) (Elenbaas et al., 2001; Mani et al., 2008). Importantly, HMLE bulk cells are heterogeneous and contain pre-existing subpopulations that are phenotypically and functionally distinct: besides epithelial cells, HMLE bulk cells contain a small mesenchymal subpopulation enriched for MS-forming ability (Mani et al., 2008; Scheel et al., 2011). Furthermore, HMLE cells were shown to give rise to this small CD44<sup>high</sup>/CD24<sup>neg</sup>, mesenchymal subpopulation spontaneously (Chaffer et al., 2011). Thus, one cannot distinguish whether EMT generates mesenchymal, MS-forming cells *de novo* or whether the EMT process selects and expands pre-existing mesenchymal, MS-forming cells.

To elucidate this issue, the initial aim of my project was to study the following questions: Does EMT select for pre-existing MS-forming cells or are there actually cells residing within the HMLE bulk population that obtain this trait during EMT? What are the characteristics of these “specific” cells (if they exist)?

To address these questions, the dynamics and functional consequences of the EMT-TF Twist1 were assessed using the HMLE-Twist1-ER cell line (Casas et al., 2011). To exclude the possibility of selection and figure out which particular cells might acquire MS-forming capacity during EMT, HMLE cells were separated into subpopulations based on the cell surface markers CD44 and CD24. Subsequently, the pre-existing mesenchymal CD44<sup>high</sup>/CD24<sup>neg</sup> fraction was excluded and Twist1 was activated in two pure epithelial subpopulations (CD24<sup>high</sup> and CD24<sup>low</sup>). Thereby, I discovered that Twist1 induced both, mesenchymal transdifferentiation (EMT) and MS-forming ability of CD24<sup>pos</sup> HMLE cells. However, these traits were induced sequentially and independently of each other, suggesting that acquisition of a mesenchymal phenotype and MS-forming ability are not linked to each other. Moreover, MS-forming cells were enriched in a small subset of CD24<sup>high</sup> cells that underwent MET after Twist1-

deactivation. These data were published in Cell Reports in January 2015 (Schmidt et al., 2015). Based on the observations from the first part of my thesis, I developed the hypothesis that a pre-existing cell state predisposed cells to undergo MET. In the second part of my thesis I set out to investigate the molecular mechanisms that predispose cells to undergo MET. Given that single cells within the FACS purified CD24<sup>high</sup> subpopulation responded differently (some underwent MET while most remained in a mesenchymal phenotype) to transient Twist1-activation, single cell clones (SCCs) were isolated from the CD24<sup>high</sup> subpopulation and studied during Twist1-activation. Thereby, I discovered both, EMT competent (M-SCCs) and EMT resistant (E-SCCs) cell clones. Moreover, none of the EMT competent cells underwent MET after subsequent Twist1-activation. These observations were contradictory to the results from the CD24<sup>high</sup> bulk population. Therefore, I set out to elucidate why EMT resistance was not detected in the bulk population, while some cells appeared to revert back to an epithelial cell state via MET following Twist1-deactivation. Moreover, I investigated what predisposes cells to resist Twist1-induced EMT and which functional consequences might result from EMT resistance.

### 3 Materials and Methods

#### 3.1 Materials

##### 3.1.1 Cell lines

Cell line	Origin/Citation
HEK293T	Human embryonic kidney cells that express SV40 large-T antigen. (DuBridg e et al. 1987)
HMLE	Immortalized Human Mammary Epithelial Cells; Cells that were transformed by infection with retroviruses containing the SV40 large T early region and hTERT gene, but which are not tumorigenic and are ER-negative. (Elenbaas et al. 2001; Ince et al. 2007)
HMLE-Twist1-ER	HMLE-derived cell line; HMLE cells that were transduced with pWZL-mTwist1-ER plasmid followed by selection with 5 ng/ml blasticidin; HMLE-Twist1-ER cells express an inducible Twist1 protein upon treatment with 4-hydroxytamoxifen. (Casas et al., 2011)

##### 3.1.2 Laboratory equipment

Equipment	Manufacturer
10 cm cell culture dishes	Becton-Dickinson, Heidelberg
6-, 24-, 96-well plates	Becton-Dickinson, Heidelberg
Cell culture inserts with 8 $\mu$ m pores	Becton-Dickinson, Heidelberg
Cell scraper	VWR, Radnor (USA)
Cell strainer 40 $\mu$ m nylon	Becton-Dickinson, Heidelberg
Conicals Falcon	Corning, Midland (USA)
Cover glass, 13 mm, round	VWR, Radnor (USA)
Cryotubes	Thermo Scientific, Waltham (USA)
F96 MicroWell white polystyrene plate	Thermo Scientific, Waltham (USA)
FACS tube 5 ml with strainer cap 35 $\mu$ m	Becton-Dickinson, Heidelberg
GeneChip® Human Gene 2.0 ST Array	Affymetrix, Santa Clara (USA)
KOVA Glasstic SLIDE 10 with GRIDS	VWR, Radnor (USA)

Equipment	Manufacturer
Micro cover glasses, 22 mm x 40 mm	VWR, Radnor (USA)
Microscope slides, cut edges, matt strip	Thermo Scientific, Waltham (USA)
Optical 384-well reaction plate	Life Technologies, Darmstadt
Pipette tips filtered and unfiltered	Starlab, Hamburg
PVDF Blotting Membrane	GE Healthcare, Farifield (USA)
PVDF filter pore size 0.45 µM	Millipore, Darmstadt
QIAshredder	Qiagen; Hilden
Reaction Tubes	Eppendorf, Hamburg
Rotilabo® - Blotting papers, thick 1.5 mm, 580x600 mm	Carl Roth, Karlsruhe
Scalpels	VWR, Radnor (USA)
Stripettes	Greier Bio-One, Kremsmünster (Österreich)
Superfrost ultra plus microscope slides	Thermo Scientific, Waltham (USA)
Ultra-low attachment 96-well plates	Sigma, St. Louis (USA)

### 3.1.3 Primers and Vectors

#### 3.1.3.1 Primers used for RT-PCR

Gene	Forward (5')	Reverse (3')
E-cadherin	TGCCCAGAAAATGAAAAAG G	GTGTATGTGGCAATGCGTT C
Fibronectin	CAGTGGGAGACCTCGAGA AG	TCCCTCGGAACATCAGAAA C
FOXC2	GCCTAAGGACCTGGTGAA GC	TTGACGAAGCACTCGTTGA G
mTwist1	GTCCGCAGTCTTACGAGG AG	TGGAGGACCTGGTAGAGG AA
N-cadherin	ACAGTGGCCACCTACAAA GG	CCGAGATGGGGTTGATAAT G
Ovol2	ACAGGCATTCGTCCCTACA AA	CGCTGCTTATAGGCATACT GC

Gene	Forward (5')	Reverse (3')
RPL32	CAGGGTTCGTAGAAGATTC AAGG	CTTGGAGGAAACATTGTGA GCGATC
Slug	GGGGAGAAGCCTTTTTCTT G	TCCTCATGTTTGTGCAGGA G
Wnt5a	ATGGCTGGAAGTGCAATG TCT	ATACCTAGCGACCACCAAG AA
ZEB1	GCACAAGAAGAGCCACAA GTAG	GCAAGACAAGTTCAAGGGT TC

### 3.1.3.2 Primers used for ChIP analysis

Gene	Forward (5')	Reverse (3')
ZEB1_-ve site	TTCCATATTGAGCTGTTGC CG	AAAGCGAACAGCTCTTTCC GA
ZEB1_+ve site	GCAGAGGCCATCATTCCA CAA	TTGCAAAATCTGGCAAACA CTATCA

### 3.1.3.3 Vectors

Name	Gene/Insert	Source/Citation
pCMV-dR8.2 dvpr	none (2nd generation lentiviral packaging plasmid)	Laboratory of Robert Weinberg
pCMV-VSV-G	none (Envelope protein for producing lentiviral particles)	Laboratory of Robert Weinberg
pGIPZ non targeting shRNAs	non targeting shRNA: #RHS4346	Thermo Scientific, Waltham (USA)

Name	Gene/Insert	Source/Citation
pGIPZ ZEB1 targeting shRNAs	shRNA constructs: V3LHS_356186 (sh1) V3LHS_356187 (sh2)	Dharmacon, Lafayette (USA)
pRRL-cPPT-CMV-GFP-W	GFP	Laboratory of Timm Schröder
pRRL-cPPT-CMV-mCherry-W	mCherry	Laboratory of Timm Schröder

### 3.1.4 Instruments

Instrument	Manufacturer
Axioplan 2 Imaging Microscope	Carl Zeiss, Jena
ChemiDoc™ MP System	Bio-Rad, Hercules (USA)
FACSAria IIIu	Becton-Dickinson, Heidelberg
FV1000 inverted confocal laser scanning microscope	Olympus, Shinjuku (Japan)
Heracell 240i CO2 incubator	Thermo Scientific, Waltham (USA)
Heraeus Megafuge 40R Centrifuge	Thermo Scientific, Waltham (USA)
Hyrax V55 Vibratome	Carl Zeiss, Jena
iMark™ Microplate Absorbance Reader	Bio-Rad, Hercules (USA)
Leica CM3050 S Research Cryostat	Leica, Wetzlar
Leica DM IL LED	Leica, Wetzlar
Leica RM2125 RTS microtome	Leica, Wetzlar
LTQ-Orbitrap XL	Thermo Scientific, Waltham (USA)
Luminometer Centro XS <sup>3</sup> LB 960	Berthold Technologies, Bad Wildbad
Mastercycler nexus gradient	Eppendorf, Hamburg
Mini-PROTEAN® Tetra Cell Systems	Bio-Rad, Hercules (USA)
NanoDrop® ND 1000 Spectrophotometer	Thermo Scientific, Waltham (USA)
QuantStudio 12K Flex qPCR System	Life Technologies, Darmstadt
Sonopuls HD 2070 Sonicator	Bandelin, Hagen

Instrument	Manufacturer
SteREO Lumar.V12	Carl Zeiss, Jena
Thermomixer comfort 1.5 ml	Eppendorf, Hamburg
Ultimate 3000 nano HPLC system	Thermo Scientific, Waltham (USA)
Wet/Tank Blotting System	Bio-Rad, Bio-Rad, Hercules (USA)

### 3.1.5 Chemicals

Chemicals	Manufacturer
(Z)-4-Hydroxytamoxifen	Sigma, St. Louis (USA)
1,7-Dichloro-octamethyltetrasiloxane	Santa Cruz, Santa Cruz (USA)
16% formaldehyde solution	Sigma, St. Louis (USA)
4',6-diamidino-2-phenylindole (DAPI)	Sigma, St. Louis (USA)
7-Aminoactinomycin D (7-AAD)	Becton-Dickinson, Heidelberg
Agarose, low gelling temperature	Sigma, St. Louis (USA)
Aluminum potassium sulfate	Sigma, St. Louis (USA)
Aminoxy-Biotin	Biotium, Hayward (USA)
Ammonium Persulfate (APS)	Thermo Scientific, Waltham (USA)
Amphotericin	Sigma, St. Louis (USA)
Ampicillin	Sigma, St. Louis (USA)
Anilin	Sigma, St. Louis (USA)
AQUA-POLY MOUNT	Polysciences, Warrington (USA)
B27 (50x)	Life Technologies, Darmstadt
Basic FGF, human recombinant	Millipore, Darmstadt
Blasticidine S hydrochloride	Sigma, St. Louis (USA)
Bovine Serum Albumin (BSA)	Sigma, St. Louis (USA)
Carmine	Sigma, St. Louis (USA)
CellTiter-Glo®	Promega, Madison (USA)
Collagen type I rat tail	Corning, Midland (USA)
Collagenase type I	Sigma, St. Louis (USA)
cOmplete™ protease inhibitor cocktail	Roche, Basel (Schweiz)
Dimethyl sulfoxide (DMSO)	Sigma, St. Louis (USA)
DMEM	Life Technologies, Darmstadt

Chemicals	Manufacturer
DMEM/F12	Life Technologies, Darmstadt
DMEM/Ham's F12	Life Technologies, Darmstadt
DNase/Rnase free water	Life Technologies, Darmstadt
EGF, human recombinant	Millipore, Darmstadt
Ethanol	VWR, Radnor (USA)
Ethylene glycol tetraacetic acid (EGTA)	Sigma, St. Louis (USA)
Ethylenediaminetetraacetic acid (EDTA)	Sigma, St. Louis (USA)
Fetal calf serum (FCS)	Pan Biotech, Aidenbach
Formaldehyde 37%	Sigma, St. Louis (USA)
Glycine	Carl Roth, Karlsruhe
H&E	Carl Roth, Karlsruhe
Heparin sodium salt from porcine intestinal mucosa	Sigma, St. Louis (USA)
HEPES	Applichem, Darmstadt
Hydrochloric acid solution	Applichem, Darmstadt
Hydrocortisone	Sigma, St. Louis (USA)
Insulin from bovine pancreas	Sigma, St. Louis (USA)
LB Agar Miller	Sigma, St. Louis (USA)
LB-Medium (Lennox)	Carl Roth, Karlsruhe
Mammary epithelial growth medium	PromoCell, Heidelberg
Methanol, ROTIPURAN	Carl Roth, Karlsruhe
Methylcellulose Stock Solution	R&D Systems, Wiesbaden
Sodium Chloride	Carl Roth, Karlsruhe
Non-fat dried milk powder	Carl Roth, Karlsruhe
Normal Donor Donkey Serum	Genetex, Irvine (USA)
Normal Donor Goat Serum	Biozol, Eching
NP-40	Thermo Scientific, Waltham (USA)
PageRuler Prestained Protein Ladder	Thermo Scientific, Waltham (USA)
PBS, pH 7.4	Life Technologies, Darmstadt
Penicillin	Sigma, St. Louis (USA)
Penicillin/streptomycin	Invitrogen, Karlsruhe

Chemicals	Manufacturer
Phosphatase Inhibitor Cocktail 2	Sigma, St. Louis (USA)
Phosphatase Inhibitor Cocktail 3	Sigma, St. Louis (USA)
PNGase F	NEB, Massachusetts (USA)
Poly-D-Lysine	Sigma, St. Louis (USA)
Power SYBR green PCR Master Mix	Life Technologies, Darmstadt
Protamine Sulfate	Sigma, St. Louis (USA)
Recombinant TGFβ1	R&D Systems, Wiesbaden
RNase-Free H2O	Life Technologies, Darmstadt
Rotiphorese® Gel 30 (37.5:1)	Carl Roth, Karlsruhe
SDS, ultrapure	Carl Roth, Karlsruhe
Sodium deoxycholate	Merck, Darmstadt
Sodium metaperiodate	Merck, Darmstadt
Sodium orthovanadate	Sigma, St. Louis (USA)
Sodium pyrophosphate	Santa Cruz, Santa Cruz (USA)
Streptavidin beads	IBA, Edina (USA)
Streptomycin	Sigma, St. Louis (USA)
Tetramethylethylenediamine (TEMED)	Carl Roth, Karlsruhe
Tissue-TEK® O.C.T. Compound	VWR, Radnor (USA)
Tris Hydrochloride	Carl Roth, Karlsruhe
TritonX-100	Sigma, St. Louis (USA)
Trizma® base	Sigma, St. Louis (USA)
Trypsin Neutralizing Solution (TNS)	PromoCell, Heidelberg
Trypsin-EDTA 0.05% (1x)	Invitrogen, Karlsruhe
Trypsin-EDTA 0.25% (1x)	Invitrogen, Karlsruhe
Tween®20	Sigma, St. Louis (USA)
WST-1	Roche, Basel (Schweiz)
XL10-Gold Ultracompetent Cells	Agilent Technologies, Santa Clara (USA)
X-treme GENE HP DNA Transfection Reagent	Roche, Basel (Schweiz)
β-glycerophosphate	Santa Cruz, Santa Cruz (USA)

Chemicals	Manufacturer
$\beta$ -Mercaptoethanol	Sigma, St. Louis (USA)

### 3.1.6 Buffers and solutions

Buffer	Ingredients
4% PBS-buffered formaldehyde	4% (v/v) Paraformaldehyde in 1x PBS
APS	10% (m/v) APS
Biotinylation buffer	1 mM NaIO <sub>4</sub> 500 $\mu$ M Aminoxy-Biotin 10 mM Aniline in 1xPBS
Blocking Solution for Immunoblotting	5% (m/v) non-fat dried milk powder or 5% (m/v) Bovine Serum Albumin in 1x TBS/T
Carmine staining solution	1 g Carmine 2.5 g aluminum potassium sulfate in 500 ml MilliQ water
Collagenase I solution	300 U/ml Collagenase type I in 1xPBS
FACS Buffer	0.1% (v/v) BSA in 1x PBS
Laemmli Running Buffer 1x	192 mM Glycine 3.5 mM SDS ultrapure 25 mM Trizma® base
Lysis buffer (Proteomics)	1% (v/v) NP40 10 mM NaCl 10 mM Tris/HCl pH 7.6 add freshly before use 1x cOmplete™ protease inhibitor cocktail
Neutralizing Solution	10% (v/v) 1 M HEPES in 2x PBS adjust to pH 7.3 with NaOH (1 M)
PBS/CaCl <sub>2</sub> /MgCl <sub>2</sub> Buffer	1 mM CaCl <sub>2</sub> 500 $\mu$ M MgCl <sub>2</sub> in 1xPBS adjust to pH 6.7 with HCl (1 M)

Buffer	Ingredients
PBS-buffered blocking solution for Immunofluorescence	10% (v/v) Normal Goat Serum or 10% (v/v) Normal Donkey Serum in 0.1% (v/v) BSA in 1x PBS
Permeabilization Buffer for Immunofluorescence	0.2 % (v/v) TritonX-100 in 1x PBS
Protamine Sulfate Solution	980 $\mu$ M Protamine Sulfate
RIPA Buffer	20 mM Tris/HCl (pH 7.5) 150 mM NaCl 1 mM Na <sub>2</sub> EDTA 1 mM EGTA 1% (v/v) NP40 1% (v/v) Sodium Deoxycholate 2.5 mM Sodium Pyrophosphate 1 mM Beta-glycerophosphate add freshly before use 10% (v/v) Phosphatase Inhibitor Cocktail 2 and 3, and 1 mM Sodium Orthovanadate Solution
SDS loading Buffer 5x	30% (v/v) Glycerol 10% (v/v) 2-Mercaptoethanol 35 mM SDS 250 mM Tris/HCl (pH 6.8) pinch of Bromphenol Blue
Sodium Orthovanadate Solution	1 M Na <sub>3</sub> VO <sub>4</sub>
Stripping Buffer	200 mM Glycine 35 mM SDS 1% (v/v) Tween® 20 adjust to pH 2.2-2.6 with HCL (1 M)
TBS 10x	1.5 M Sodium chloride 0.1 M Trizma® base adjust to pH 7.2-7.4 with HCl (1 M)

Buffer	Ingredients
TBS/T	10x TBS supplemented with 0.1% (v/v) Tween® 20
Transfer Buffer	192 mM Glycine 20% (v/v) Methanol 26 mM Trizma® base
Tris/HCl	1 M Trizma® base adjust to pH 6.8 or 8.8 with HCl (1 M)

### 3.1.7 Antibodies

#### 3.1.7.1 Immunofluorescence Antibodies

##### 3.1.7.1.1 Primary Antibodies

Antibody	Manufacturer	Species	Dilution
E-cadherin [EP700Y]	Biozol, Eching	rabbit	1:250
E-cadherin-Alexa 488 [24E10]	New England Biolabs, Ipswich (USA)	rabbit	1:50
Laminin [L9393]	Sigma, St. Louis (USA)	rabbit	1:100
Phalloidin-Atto 647N	Sigma, St. Louis (USA)	-	1:250
Twist1 [Twist2C1a]	Santa Cruz, Santa Cruz (USA)	mouse	1:500
Vimentin [D21H3] XP	Biozol, Eching	rabbit	1:100
Vimentin [V9]	Abnova, Heidelberg	mouse	1:100
Z0-1-Alexa 594 [1A12]	Invitrogen, Carlsbad (USA)	mouse	1:100
ZEB1 [H-102]	Santa Cruz, Santa Cruz (USA)	rabbit	1:250

##### 3.1.7.1.2 Secondary Antibodies

Antibody	Manufacturer	Species	Dilution
Alexa Flour 488 donkey-anti-mouse IgG (H+L)	Life Technologies, Darmstadt	donkey	1:250
Alexa Flour 488 goat-anti-rabbit IgG (H+L)	Life Technologies, Darmstadt	goat	1:250

Antibody	Manufacturer	Species	Dilution
Alexa Flour 594 donkey-anti-rabbit IgG (H+L)	Life Technologies, Darmstadt	donkey	1:250
Alexa Flour 594 goat-anti-mouse IgG (H+L)	Life Technologies, Darmstadt	goat	1:250

### 3.1.7.2 FACS Antibodies

Antibody	Manufacturer	Species	Dilution
APC Mouse Anti-Human CD44 [G44-26]	Becton-Dickinson, Heidelberg	mouse	1:25
FITC Mouse Anti-Human CD24 [ML5]	Becton-Dickinson, Heidelberg	mouse	1:12.5
FITC Mouse Anti-Human CD326, EpCAM [VU-1D9]	Biozol, Eching	mouse	1:20
FITC Mouse Anti-Human Trop2/TACSTD2 [01]	Sino Biological Inc., North Wales (UK)	mouse	1:20

### 3.1.7.3 ChIP Antibodies

Antibody	Manufacturer	Species
ER $\alpha$ [HC-20, sc-543]	Santa Cruz, Santa Cruz (USA)	rabbit
IgG [ab37415]	Abcam, Cambridge (USA)	rabbit

### 3.1.7.4 Western Blot Antibodies

#### 3.1.7.4.1 Primary Antibodies

Antibody	Manufacturer	Species	Dilution
Phospho-Smad2 (Ser465/467)/Smad3 (Ser423/425) [D27F4]	Cell signaling, Danvers (USA)	rabbit	1:1000
Smad 2/3 [D7G7] XP	Cell signaling, Danvers (USA)	rabbit	1:1000

Antibody	Manufacturer	Species	Dilution
Twist1 [Twist2C1a]	Santa Cruz, Santa Cruz (USA)	mouse	1:200
ZEB1 [H-102]	Santa Cruz, Santa Cruz (USA)	rabbit	1:200
$\beta$ -Actin [AC-15]	Sigma, St. Louis (USA)	mouse	1:6000

### 3.1.7.4.2 Secondary Antibodies

Antibody	Manufacturer	Species	Dilution
Anti-mouse IgG (H+L) peroxidase conjugated	Jackson ImmunoResearch	goat	1:12.500
Anti-rabbit IgG (H+L) peroxidase conjugated	Jackson ImmunoResearch	goat	1:12.500

### 3.1.8 Cell culture medium

Medium	Ingredients
Freezing medium	PC Medium, 20% FCS, 10% DMSO
PC medium	Mammary epithelial growth medium, 0.004 ml/ml bovine pituitary extract, 10 ng/ml EGF, 5 $\mu$ g/ml hydrocortisone and 1% (v/v) Penicillin/Streptomycin (10.000 U/ml; 10 $\mu$ g/ml)
Mammosphere medium (MS medium)	DMEM/F-12, 5 ng/ml EGF, 20 ng/ml bFGF, 0.5 $\mu$ g/ml hydrocortisone, 10 $\mu$ g/ml insulin, 4 $\mu$ g/ml heparin, 1x B27, 0.3% methylcellulose
sterile cultivation medium for mouse lung slices	DMEM/Ham's F12; penicillin (100 U/ml), streptomycin (100 $\mu$ g/ml), amphotericin B (2.5 $\mu$ g/ml)

### 3.1.9 Software

Software	Manufacturer/Source
CARMAweb	Medical University Innsbruck (Austria)
FlowJo V10	FlowJo, LLC, Ashland (USA)

Software	Manufacturer/Source
FV10-ASW	Olympus, Shinjuku (Japan)
Genomatix Pathway System (GePS)	Genomatix, München
Image Lab™	Bio-Rad, Hercules (USA)
Photoshop CS5	Adobe, San Jose´ (USA)
Progenesis QI Software	Nonlinear Dynamics, Newcastle (UK)
QuantStudio 12K Flex	Life Technologies, Darmstadt
statistical programming environment R	R Development Core Team
MikroWin, Version 4.41	Mikrotek Laborsysteme GmbH, Overath
ImageJ 1.48	NIH
FACS Diva 6.0	Becton-Dickinson, Heidelberg
Flowing Software 2.5	Cell Imaging Core, Turku Centre for Biotechnology, Finland
Axiovision Rel 4.7	Carl Zeiss, Jena

### 3.1.10 Kits

Kit	Manufacturer
Amersham™ ECL Advance Western Blotting Detection Kit	GE Healthcare, Fairfield (USA)
Biorad DC Protein Assay Kit	Bio-Rad, Hercules (USA)
EasyScript Plus	Applied Biological Materials, Richmond (Canada)
Hemacolor Rapid staining Set	Merck, Darmstadt
miRNeasy Mini Kit	Qiagen, Hilden
Ovation Pico WTA System V2	NuGEN, San Carlos (USA)
Plasmid Midi Kit	Qiagen, Hilden
RNase-Free DNase Set	Qiagen, Hilden

Kit	Manufacturer
RNasy Mini Kit	Qiagen, Hilden

## 3.2 Cell Biological Methods

### 3.2.1 Maintenance of cell lines

Cell lines were cultured in 6-well plates or 10 cm cell culture dishes at 37°C and 5% CO<sub>2</sub> in a Heracell 240i CO<sub>2</sub> incubator. HMLE-Twist1-ER cells were propagated in PC medium supplemented with blasticidin at a final concentration of 10 µg/ml. HEK 293T cells were propagated in DMEM supplemented with 10% FCS and 1% Penicillin/Streptomycin. Cells were passaged every 2-3 days using 0.15% Trypsin-EDTA. For HMLE-Twist1-ER cells Trypsin reaction was stopped with TNS in a 3:1 ratio, for HEK 293T cells Trypsin reaction was stopped with medium containing FCS in a 10:1 ration. For the induction of the transcription factor Twist1 in HMLE-Twist1-ER cells, cells were treated with 4-hydroxytamoxifen (TAM) at a final concentration of 20 nM for the indicated number of days.

### 3.2.2 Isolation of Single Cell Clones (SCCs)

To study effects of Twist1 at the single cell level, HMLE-Twist1-ER CD24<sup>high</sup> cells were diluted to a cell number of 3 cells per 1 ml PC medium supplemented with blasticidin at a final concentration of 10 µg/ml. Cell suspension was plated into 96-well plate (100 µl/well = 0.3 cells/well). Each well was checked by eye for single cells. Only wells including one single cell were further passaged and cells were expanded to a minimum of 1x10<sup>6</sup> cells. Isolation of the SCCs was done in collaboration with Dr. Benjamin Hirschi.

### 3.2.3 Immunofluorescence

Immunofluorescence is a method to detect localization and relative abundance of proteins of interest using specific antibodies.

Cells were grown on poly-D-lysine-coated cover glasses for a minimum of 24 hours. Medium was removed, cells were washed once with PBS and either fixed with 4% PBS-buffered formaldehyde at RT for 12 min or ice-cold methanol at RT for 5 min. Then, cells were washed 3 times with PBS, permeabilized with

0.2% PBS buffered Triton-X-100 at RT for 2 min, again washed 3 times with PBS and blocked with PBS-buffered blocking solution at RT for 1 hour. Afterwards, cells were washed 3 times with PBS and stained with primary antibodies (see 3.1.7.1.1) diluted in PBS-buffered blocking solution at 4°C in a moisturized chamber protected from light overnight. The following day, cells were washed with PBS and stained with secondary antibodies (see 3.1.7.1.2) diluted in PBS-buffered blocking solution at RT in a moisturized chamber protected from light for 1-3 hours. Then, cells were washed 3-5 times with PBS, cell nuclei were stained with PBS-buffered DAPI solution (167 ng/ml) for 1 min. Afterwards cells were washed once with PBS and once with MilliQ water. Finally, cover glasses were mounted with AQUA-POLY/MOUNT mounting medium on microscope slides. Microscope slides were air-dried and either directly imaged using an Axioplan 2 imaging light/fluorescence microscope (20-fold magnification) or stored at -20°C. Images were processed with Axiovision Rel 4.7 and Adobe Photoshop CS5 software. In this study, each immunofluorescence staining was repeated independently at least three times.

### **3.2.4 Transwell Migration Assay (Boyden Chamber Assay)**

To measure single cell migration  $2.5 \times 10^4$  cells were plated into 24-well culture inserts with 8  $\mu\text{m}$  pores. After 24 hours non-migrated cells were removed from the upper side of the insert using a cotton swab. Migrated cells that had squeezed through the pores and were subsequently located on the lower side of the insert were fixed and stained with the Hemacolor Rapid staining Set, which is based on the principle of Pappenheim staining, according to manufacturer's instruction. The stained cells were counted on a Leica DM IL LED light microscope using a 10-fold magnification. For each condition triplicates were plated and each transwell migration assay was repeated independently at least three times in this study.

### **3.2.5 Mammosphere Assay**

To determine anchorage-independent growth at clonal density, mammosphere assays were performed as previously described by Dontu et al. with modifications (Dontu et al., 2003). Cells were trypsinized, filtered through a 40  $\mu\text{m}$  cell strainer and counted in triplicates. 100 or less cells per well were

plated in an ultra-low attachment 96-well plate with MS medium. MS medium was either supplemented or not supplemented with TAM (final concentration of 20 nM). Mammospheres were counted 7-10 days after initial plating. For each cell line 10-20 replicates were plated per condition and each mammosphere assays was repeated independently at least three times in this study.

### **3.2.5.1 Serial Passaging**

For serial passaging mammospheres were collected, spun down at 1500 rpm for 5 min, dissociated into single cells by trypsinization, filtered through a 40 µm cell strainer and re-plated as described in 3.2.5.

### **3.2.5.2 Immunofluorescence of Mammosphere Sections**

For immunofluorescence of mammosphere sections, mammospheres were collected, spun down at 1500 rpm for 5 min, fixed with 4% PBS-buffered formaldehyde at RT for 15 min, embedded in TissueTek® O.C.T Compound and frozen to  $-80^{\circ}\text{C}$ . 10 µm sections were prepared using the Leica CM3050 S Research Cryostat and placed on Superfrost ultra plus microscope slides. The sections were air-dried and either stored at  $-80^{\circ}\text{C}$  or directly used for immunofluorescence staining according to standard protocol as described in 3.2.3.

### **3.2.6 Anoikis Assay**

To determine survival in anchorage-independence, anoikis assays were performed as previously described by Onder et al. with modifications (Onder et al., 2008). In contrast to the mammosphere assay, cells were kept as single cells by permanent rotation of the cell suspension instead of using viscous methylcellulose. In addition, cells were not supplied with nutrients during this assay.

Cells were trypsinized and filtered through a 40 µm cell strainer.  $5 \times 10^4$  cells were suspended in 50 ml DMEM/F12 in a 50 ml conical tube and rotated at  $37^{\circ}\text{C}$  for 24 hours. For each condition triplicates were performed. Surviving cells were spun down at 1500 rpm for 5 min and plated in 6-well plates with PC medium. After 4-6 days cells were fixed and stained with Hemacolor Rapid staining Set, which is based on the principle of Pappenheim staining, according to

manufacturer's instruction. Colonies were counted on a Leica DM IL LED light microscope using a 10-fold magnification. Each anoikis assay was repeated independently at least three times in this study.

### **3.2.7 Proliferation Assay**

To measure cell proliferation  $2 \times 10^3$ - $2.5 \times 10^3$  cells were plated in white polystyrene 96-well plates in PC medium supplemented with blasticidin at a final concentration of 10  $\mu\text{g/ml}$ . For each condition 5-10 replicates were plated. Cell proliferation was monitored for a period of 72 hours, adding fresh medium every 24 hours. The viability of the cells was measured every day using the WST-1 reagent: 10  $\mu\text{l}$  WST-1 was added per well and cells were incubated at 37°C for 1 hour. Afterwards, absorbance at 450 nm was measured on an iMark Microplate Absorbance Reader. Wavelength 595 nm was used as reference. Data were normalized to respective control at day 0. Each proliferation assay was repeated independently at least three times in this study.

### **3.2.8 Culture in 3D-floating Collagen Gels**

3D-floating collagen gels were prepared as previously described by Linnemann et al. with modifications (Linnemann et al., 2015). Cells were trypsinized, filtered through a 40  $\mu\text{m}$  cell strainer and counted in triplicates. Desired cell number was suspended in corresponding media and mixed with neutralizing solution and collagen I at a final collagen-concentration of 1.3 mg/ml. The mixture was plated into siloxane-coated 24- (400  $\mu\text{l/well}$ ) or 6- (2 ml/well) wells. Gels were allowed to polymerize at 37°C for 1 hour. Afterwards, gels were detached from the well and corresponding medium was added. Medium was changed every 2-3 days. Measurements of proliferation or colonization as well as immunofluorescence staining of 3D collagen cultures were performed 7-10 days after initial plating. For each condition, cultivation of HMLE cells in 3D-floating collagen gels and subsequent analyses were repeated independently at least three times in this study.

#### **3.2.8.1 Proliferation measurement**

To measure cell proliferation of cells grown in 3D-floating collagen gels, gels were digested with Collagenase I (300 U/ml) at 37°C for 1 hour. Then, cells were

spun down at 300 g for 5 min, trypsinized and counted. The cell number was normalized to initial plating density. The number of doublings (n) was calculated using following formula:  $2^n = (\text{number of cells at endpoint} / \text{number of initially plated cells})$ .

### **3.2.8.2 Colony formation**

To measure colony formation of cells grown in 3D-floating collagen gels, gels were washed with PBS for 10 min, fixed with 4% PBS-buffered formaldehyde for 15 min and washed again with PBS for 10 min. To quench the formaldehyde gels were incubated in 0.15 M Glycine for 10 min followed by a final washing step with PBS for 10 min. Gels were stained with carmine staining solution at RT overnight. All washing, fixation, quenching and staining steps were performed using an orbital shaker. Colonies were imaged using a Zeiss SteREO Lumar.V12 microscope with a NeoLumar S 0.8x objective (10- to 20-fold magnification) and counted with the ImageJ 1.48 software.

### **3.2.8.3 Immunofluorescence staining**

For immunofluorescence staining of cells grown in 3D-floating collagen gels, gels were fixed as described in 3.2.8.2. Immunofluorescence staining was performed as described in 3.2.3 with modifications: the cells were permeabilized for 10 min, incubated in blocking solution at 4°C overnight and stained with primary antibodies at 4°C overnight. All washing steps were performed on an orbital shaker for 10 min. After immunofluorescence staining and mounting, slides were air-dried overnight, sealed and either directly imaged using an FV1000 inverted confocal laser scanning microscope or stored at -20°C. Images were processed with FV-10-ASW 1.7 Viewer and Adobe Photoshop CS5 software.

### **3.2.9 Murine Lung Slice Culture**

To mimic colonization and proliferation at distant metastases HMLE cells were grown on murine lung slices. Murine lung slice culture and each subsequent analysis were repeated independently three times in this study.

#### **3.2.9.1 Preparation of murine lung slices**

All steps were performed by the laboratory of Dr. Dr. Melanie Königshoff from the Comprehensive Pneumology Center at the Helmholtz Center Munich. 3D-lung

tissue cultures (3D-LTCs) were generated as previously described (Uhl et al., 2015). Briefly, C57BL6/N mice of 8-12 weeks were intubated and after the dissection of the diaphragm, lungs were flushed through the heart with sterile sodium chloride solution. Using a syringe pump, lungs were filled with low gelling temperature agarose (2% by weight, kept at 40°C) in sterile cultivation medium. Separated lobes were cut with a Hyrax V55 vibratome to a thickness of 300 µm using a speed of 10–12 µm/sec, a frequency of 80 Hz and an amplitude of 1 mm. The 3D-LTCs were cultivated in sterile cultivation medium containing 0.1% FCS.

### **3.2.9.2 Co-culture of murine lung slices and HMLE cells**

For culture on murine lung slices HMLE cells were lentiviral transduced with pRRL-cPPT-CMV-GFP-W (EMT resistant Clone #3) or pRRL-cPPT-CMV-mCherry-W (EMT competent Clone #3) as described in 3.5.3. Cells were trypsinized, filtered through a 40 µm cell strainer and counted in triplicates. Subsequent, cells were suspended in PC medium to a final concentration of  $2 \times 10^4$  cells per ml. Medium was removed from the murine lung slices and 1 ml cell-suspension was added on top of the slices. The following day murine lung slices with cells on top were transferred to a fresh 24-well and 1 ml fresh PC-medium was added. Murine lung slices and cells were cultured for 5 days, changing the medium every day. Afterwards murine lung slices and cells were fixed with 4% PBS-buffered formaldehyde as described for 3D-floating collagen gels in 3.2.8.2 and afterwards either stored at 4°C or directly used for immunofluorescence staining.

### **3.2.9.3 Immunofluorescence staining**

Immunofluorescence staining of murine lung slice cultures was performed as described for 3D-floating collagen gels in 3.2.8.3. To quantify the proliferation of the HMLE cells, the DAPI fluorescence was assessed using the ImageJ 1.48 software. Afterwards corrected total cell fluorescence (CTCF) of DAPI was calculated using following formula:  $CTCF = \text{integrated density} - (\text{area of selected cells} \times \text{mean fluorescence of background readings})$ .

### **3.2.9.4 Paraffin sections and H&E staining**

Murine Lung slices were fixed with 4% PBS-buffered formaldehyde as described for 3D-floating collagen gels in 3.2.8.2. All subsequent steps were performed by

the laboratory of Prof. Dr. Thomas Kirchner from the Institute of Pathology at the Ludwig Maximilian University Munich. Paraffin sections (3  $\mu\text{m}$ ) were prepared according to standard protocols using a Leica RM2125 RTS microtome. Sections were stained H&E (Haematoxylin&Eosin) according to standard protocols.

### **3.3 Fluorescence Activated Cell Sorting (FACS)**

Fluorescence Activated Cell Sorting (FACS) is a technique that allows detection and sorting of pre-labelled cells.

#### **3.3.1 Sample preparation**

Cells were trypsinized, counted and suspended in FACS buffer to a final concentration of  $1 \times 10^6$  cells per ml. For cell surface marker analyses  $1 \times 10^5$  cells were suspended in 100  $\mu\text{l}$  FACS buffer. Cells were stained with FACS antibodies (see 3.1.7.2) on ice protected from light for 45 min. Cells that were sorted for GFP or mCherry were not stained with any antibody. Afterwards cells were washed with PBS, suspended in FACS buffer to a maximum concentration of  $1 \times 10^7$  cells per ml and filtered through a 35  $\mu\text{m}$  cell strainer into a 5 ml round-bottom FACS tube. Prior to sorting or analyses, 7AAD was added to distinguish dead and live cells. For controls, cells were either single stained for corresponding antibody, 7AAD or processed without any staining. Cells that were not transduced with GFP or mCherry vector served as a control for sorting of GFP<sup>pos</sup> or mCherry<sup>pos</sup> cells.

#### **3.3.2 Cell sorting**

Cells were sorted on a BD FACSAriaIIIu using the 70  $\mu\text{m}$  nozzle. FITC fluorescence of CD24, CD326, Trop2 or GFP were analyzed with the 488 nm laser and detected by the 530/30 nm filter. APC fluorescence of CD44 was analyzed with the 633 nm laser and detected by the 660/20 nm filter. mCherry fluorescence was analyzed with the 561 nm laser and detected by the 610/20 nm filter. 7AAD was analyzed with the 488 nm laser and detected by the 695/40 nm filter. Forward and side scatter were used to gate for single cells. In addition, live cells were discriminated by absence of 7AAD fluorescence. Positive and negative gates were set using unstained and single stained controls as references. Using the "4-way purity" sort mode, cells were sorted into highly

purified populations. Sorted populations were first collected in tubes containing PC medium and then plated into 6-well plates for further expansion.

### **3.3.3 Cell surface marker analysis**

Cells were analyzed on a BD FACSAriaIIIu using the same settings as described in 3.3.2. For each sample  $1 \times 10^4$  to  $1 \times 10^5$  events were recorded and further analyzed with FlowJoV10 or Flowing Software 2.5. Each cell surface marker analyses were repeated independently at least three times in this study.

## **3.4 Molecular and Biochemical Biology Methods**

### **3.4.1 Gene Expression Analysis**

#### **3.4.1.1 RNA Isolation and Reverse Transcription**

For RNA isolation, cells were grown in 6-well plates or 10 cm cell culture dishes to a maximum of 80% confluency. Cells were washed once with PBS and lysed either with RLT/ $\beta$ MerCaptoethanol (for mRNA only) or QIAzol Lysis reagent (for total RNA). Then, RNA was isolated using either RNeasy Mini Kit (for mRNA only) or miRNeasy Mini Kit (for total RNA) according to manufacturer's instructions. In both cases, RNA was isolated via a silica-membrane-based purification. In addition, a DNA digestion step was included using the RNase-Free DNase Set according to manufacturer's instructions. Concentration of isolated RNA was determined using the NanoDrop® ND 1000 Spectrophotometer at 260 nm and RNA was stored at  $-80^\circ\text{C}$ .

Reverse transcription of 1  $\mu\text{g}$  RNA was performed using the EasyScriptPlus cDNA Synthesis Kit according to manufacturer's instructions. cDNA was stored at  $-20^\circ\text{C}$ .

#### **3.4.1.2 Quantitative Real Time-Polymerase Chain Reaction (qRT-PCR)**

To measure relative expression levels of the genes of interest, qRT-PCR was performed. This method links the amplification of double-stranded nucleic acid molecules to the generation of a fluorescence signal which is monitored during each PCR cycle.

For cDNA amplification 100 ng cDNA was mixed with corresponding forward and reverse primer as well as Power SYBR Green PCR Master Mix (for details see Table 1). The housekeeping gene RPL32 was used as a loading control and

each primer was run in a water control. Primer sequences used for the experiments are listed in 3.1.3.1.

**Table 1:** qRT-PCR reaction mixture

Components	
Forward Primer (20 $\mu$ M)	0.25 $\mu$ l
Reverse Primer (20 $\mu$ M)	0.25 $\mu$ l
Power SBYR Green PCR Master Mix	5 $\mu$ l
RNase/DNase free water	2.5 $\mu$ l
cDNA	100 ng
<b>Total reaction volume</b>	<b>10 <math>\mu</math>l</b>

Samples were run in triplicates on a QuantStudio 12K Flex qPCR System using the cycling protocol shown in Table 2. Afterwards, a melting curve was performed to check for primer-dimer artifacts and to ensure reaction specificity.

**Table 2:** Cycling protocol for qRT-PCR of cDNA

Step	Duration of cycles	Temperature	Number of cycles
Initial Activation	10 min	95°C	1x
Denaturation	15 sec	95°C	} 40x
Annealing	30 sec	60°C	
Extension	16 sec	72°C	

To compare expression levels of different genes of interest relative to an internal control (RPL32) data were processed using the  $\Delta$ Ct method as described previously (Yang et al., 2004). In detail, first the threshold cycle Ct for each gene was defined as that PCR cycle at which the fluorescence signal (SYBR Green) crosses an arbitrarily set threshold that is slightly above the background. Next, the  $\Delta$ Ct value was defined. Meaning, gene expression of the gene of interest was normalized to gene expression of the internal control gene by subtracting its Ct value from the Ct value of the internal control gene ( $\Delta$ Ct=Ct(internal control)–Ct(gene of interest)). Finally, fold expression of gene of interest compared to control gene expression was calculated by the formula  $2^{\Delta$ Ct}. Each qRT-PCR analysis was repeated independently at least three times in this study.

### **3.4.1.3 Expression profiling and statistical transcriptome analysis**

Total RNA of three independent biological replicates for each condition was isolated as described in 3.4.1.1. All subsequent steps were performed in collaboration with Prof. Dr. Johannes Beckers and Dr. Martin Irmeler from the Institute of Experimental Genetics at the Helmholtz Center Munich. In detail, total RNA (about 30 ng) was amplified using the Ovation Pico WTA System V2 in combination with the Encore Biotin Module (Nugen). Amplified cDNA was hybridized on an Affymetrix Human Gene 2.0 ST arrays. Staining and scanning was done according to the Affymetrix expression protocol including minor modifications as suggested in the Encore Biotin protocol. Expression console (v.1.3.0.187, Affymetrix) was used for quality control and to obtain annotated normalized RMA gene-level data (standard settings including median polish and sketch-quantile normalization). Statistical analyses were performed by utilizing the statistical programming environment R (R Development Core Team (2008)) implemented in CARMAweb (Rainer et al. (2006)). Genewise testing for differential expression was done employing the (limma) t-test and Benjamini-Hochberg multiple testing correction (FDR <10%). Heatmaps were generated with CARMAweb and cluster dendrograms with R scripts (hclust, agnes, diana). Sets of regulated genes were defined based on limma t-test p-value<0.05, fold change>1.3x and average expression in at least one group>10 arbitrary units. To define the 189 gene set a filter for higher expression (FC>1.3x) in the three groups (Snail ms, Twist ms, +/-Twist) versus +Twist was applied. GO term and pathway enrichment analyses (p<0.01) were done with GePS (Genomatix, Germany). Array data has been submitted to GEO (GSE61206).

### **3.4.1.4 Principal Component Analysis (PCA)**

Principal Component Analysis was performed by Prof. Dr. Fabian Theis and Dr. Steffen Sass from the Institute for Computational Biology (ICB) at the Helmholtz Center Munich. PCA was performed using the prcomp function within the R environment for statistical computing (R Development Core Team; 2008).

### **3.4.2 Chromatin Immunoprecipitation (ChIP)**

ChIP is a technique that allows detection of protein-DNA interactions. In brief, proteins are crosslinked to DNA. After fragmentation of the chromatin, including

protein-DNA complexes, protein of interest is purified via an antibody-based retrieval. Finally, DNA sequences bound by the protein of interest can be amplified by PCR.

Cells were grown on 10 cm cell culture dishes to a confluency of 90%. Cells were washed with PBS and proteins were crosslinked by incubating cells with 1% PBS-buffered formaldehyde for 20 min at RT. Formaldehyde was quenched with 125 mM Glycine for 5 min on a slowly rotating shaker. Cells were washed twice with ice-cold PBS, then scraped from the culture dish and collected in 1 ml ice-cold PBS. All subsequent steps were performed in collaboration with Prof. Dr. Steven A. Johnson, Dr. Vivek K. Mishra and Vijayalakshmi Kari from the Department of General, Visceral and Pediatric Surgery at the University Medical Center Göttingen according to a previously published protocol (Nagarajan et al., 2014). Antibodies used for these experiments are listed in 3.1.7.3. Primer sequences used for these experiments are listed in 3.1.3.2.

### **3.4.3 Protein Expression Analysis**

#### **3.4.3.1 Whole Cell Lysate Preparation**

For protein isolation cells were grown on 6-well plates to a confluence of 100%. Cells were washed with PBS and lysed with RIPA buffer (150  $\mu$ l per 6-well) on ice for 5 min. Cells were scraped from the culture dish, collected and incubated on ice for 5-10 min. Cell lysates were centrifuged at 14.000 g and 4°C for 10 min. Supernatant containing protein fraction was stored at -80°C.

#### **3.4.3.2 Protein Concentration Measurement**

Protein concentration was measured using the Biorad DC Protein Assay Kit according to manufacturer's instructions. This assay is a colorimetric protein assay based on the Lowry method.

For each sample 5  $\mu$ l isolated protein solution was used for the assay and absorbance was measured in duplicates at 750 nm using an iMark™ Microplate Absorbance Reader. Protein standards of 50  $\mu$ g, 25  $\mu$ g, 10  $\mu$ g, 7.5  $\mu$ g, 5  $\mu$ g, 2.5  $\mu$ g, 1.25  $\mu$ g and 0.625  $\mu$ g BSA in RIPA buffer were used as reference and RIPA buffer only was used as blank.

### 3.4.3.3 Sodium Dodecyl Sulfate Polyacrylamide Gel Electrophoresis

Sodium Dodecyl Sulfate Polyacrylamide Gel Electrophoresis or short SDS-Page is a technique to separate proteins according to their size. By binding to the proteins SDS denatures their primary structure and confers a negative charge on them. Thus protein-SDS complexes migrate to the positive electrode during gel electrophoresis and proteins become separated.

To separate proteins according to their size 10-40  $\mu\text{g}$  of each protein lysate was mixed with 5x SDS loading buffer, incubated at 95°C for 5 min and loaded on a SDS gel. The percentage of the separating gel was chosen depending on the size of the protein of interest. SDS gels were prepared according to Table 3.

**Table 3:** Composition of separating and stacking gel of 10% and 12.5% SDS gels

Reagent	Separating Gel		Stacking Gel
	10% (30-200 kDa)	12.5% (10-120 kDa)	
Rotiphorese® Gel 30 (37.5:1)	3.3 ml	3.9 ml	833 $\mu\text{l}$
MilliQ water	6.1 ml	5.5 ml	3.46 ml
1 M Tris pH 6.8	---	---	625 $\mu\text{l}$
1 M Tris pH 8.8	2.5 ml	2.5 ml	---
SDS (10%)	100 $\mu\text{l}$	100 $\mu\text{l}$	50 $\mu\text{l}$
Temed	7.5 $\mu\text{l}$	7.5 $\mu\text{l}$	5 $\mu\text{l}$
APS (10%)	75 $\mu\text{l}$	75 $\mu\text{l}$	25 $\mu\text{l}$

In addition to the samples, 8  $\mu\text{l}$  of PageRuler Prestained Protein Ladder was loaded on the SDS gel. Electrophoresis was performed at 120 V for 1 hour.

### 3.4.3.4 Immunoblotting

After separating proteins by SDS gel electrophoresis, proteins were transferred to a PVDF blotting membrane using Wet/Tank Blotting procedure. Proteins were transferred to a PVDF membrane at 2 mA per  $\text{cm}^2$  of membrane for 1.5 hours. After transferring proteins to a PVDF membrane, membrane was washed with TBS/T for 2 min and incubated in blocking solution at RT for 1 hour. Then, the membrane was incubated with primary antibody (see 3.1.7.4.1) diluted in blocking solution at 4°C overnight. The following day, membrane was washed

3 times with TBS/T for 10 min each. Then, the membrane was incubated with secondary antibody (see 3.1.7.4.2) diluted in blocking solution at RT for 1 hour. Afterwards, the membrane was washed 3 times with TBS/T for 10 min each and once with TBS for 5 min. The membrane was developed using ECL Western Blotting Detection Kit according to manufacturer's instructions. Finally, chemiluminescence was detected using the ChemiDoc System from Bio-Rad. Protein expression levels were quantified using the ImageJ 1.48 software. Each immunoblotting was repeated independently at least three times in this study.

### **3.4.3.5 Proteomics analysis of cell surface proteins**

Glycosyl residues on intact cells were labelled with aminosy-biotin under mild oxidative conditions as described before (Graessel et al. 2015; Grosche et al. 2015). All subsequent steps were performed in collaboration with the laboratory of Dr. Stefanie Hauck from the Research Unit Protein Science at the Helmholtz Center Munich. In detail, after cell lysis, glycosylated cell surface proteins were enriched with streptavidin beads. After stringent washing steps, proteins were on-bead proteolysed with trypsin, followed by deglycosylation with PNGase F. Eluted peptides were combined, acidified and directly used for analysis on a LTQ-OrbitrapXL connected with an Ultimate 3000 nano HPLC system as described (Hauck et al., 2010). The full-scan MS spectra were acquired in the Orbitrap with a resolution of 60,000 and up to 10 most abundant peptide ions were selected for fragmentation in the linear ion trap. Peptides were identified and quantified using the Progenesis QI software and the Mascot search algorithm with the Ensembl Human public database as described (Graessel et al. 2015; Hauck et al. 2010; Grosche et al. 2015). Identified peptides were filtered for following criteria: peptide count  $\geq 5$ , confidence score  $> 100$ , E/M ration (-TAM)  $> 1$  and additionally E/M ration (+TAM)  $> 1$ . Finally, peptides were sorted by size of E/M ration (+TAM).

## **3.5 shRNA mediated Knockdown of ZEB1**

### **3.5.1 Plasmid Preparation**

#### **3.5.1.1 Transformation of XL10-Gold Ultracompetent Cells**

pGIPZ vectors encoding for shRNAs targeting ZEB1 or a non-targeting control (nt), each additionally encoding for GFP, were purchased as glycerol stocks from

Dharmacon or Thermo Scientific. Plasmid-DNA was cloned by transformation into XL10-Gold Ultracompetent Cells from Agilent Technologies according to manufacturer's instructions. In brief, XL10-Gold Ultracompetent Cells were gently mixed with 0.5 -1 µg plasmid-DNA, incubated on ice for 30 min and then heat-shocked for 45 sec at 42°C. Afterwards, the suspension was incubated on ice for 2 min and then mixed with LB medium. Subsequently, the suspension was plated on a selective plate containing antibiotics (100 µg/ml ampicillin) and incubated at 37°C overnight.

### **3.5.1.2 Isolation of pGIPZ plasmid DNA**

3 ml LB medium containing antibiotics (100 µg/ml ampicillin) were inoculated with single bacterial colony picked from selective plate (see 3.5.1.1) and incubated at 37°C and 300 rpm for 6-8 hours. Afterwards, inoculated LB medium was transferred to a chicane flask containing additional 100 ml of LB medium with antibiotics (100 µg/ml ampicillin) and incubated at 37°C and 250 rpm for 16 hours. Bacterial cells were harvested by centrifugation at 6000 g and 4°C for 15 min. Plasmid isolation from bacterial cells was done using the Plasmid Midi Kit from QIAGEN® according to manufacturer's instructions. This Kit combines alkaline lysis procedure, followed by binding of plasmid DNA to a resin column under low-salt and pH conditions. After washing steps under medium-salt conditions plasmid DNA is eluted under high-salt concentration and finally precipitated by isopropanol.

Afterwards, DNA concentration was determined with NanoDrop® ND 1000 Spectrophotometer at 260 nm and DNA was stored at -20°C.

### **3.5.2 Transfection of Virus-Producing HEK293T cells**

Transfection is the process by which naked nucleic acids (DNA or RNA) are introduced into eukaryotic cells.

For the production of lentivirus the human embryonic kidney cell line HEK293T (DuBridge et al., 1987) was simultaneously transfected with isolated plasmid DNA (see 3.5.1.2), envelope protein encoding plasmid pCMV-VSV-G and packaging plasmid pCMV-dR8.2 dvpr using x-treme GENE reagent.

Transfection mix was prepared according to Table 4 and incubated at RT for 15 min.

**Table 4:** Composition of Transfection mix

<b>Components (for one 10 cm culture dish)</b>	
plasmid-DNA	2.5 µg
pCMV-dR8.2 dvpr	2.25 µg
pCMV-VSV-G	0.25 µg
x-treme GENE	15 µl
DMEM w/o supplements	X µl
<b>Total reaction volume</b>	<b>500 µl</b>

Transfection mix was added dropwise to medium of HEK293T cells growing in cell culture dish and cells were incubated at 37°C for 16 hours. Afterwards, medium was removed and replaced by PC medium. 24 hours after medium change, PC medium (= virus supernatant containing lentiviral particles) was collected, filtered through a PVDF filter (pore size of 0.45 µm) and either directly used for lentiviral transduction or frozen at -80°C. These steps were repeated after additional 24 hours.

### 3.5.3 Lentiviral Transduction

Lentiviral transduction is the infection of eukaryotic cells by replication-deficient lentivirus containing DNA sequence of interest. During transduction, replicates of the sequence of interest become more or less randomly integrated into genome of target cells. The number of integrations is dependent on the virus titer.

Target cells were incubated with virus supernatant (see 3.5.2) at 37°C for 6-8 hours. Afterwards medium containing viral particles was replaced by fresh PC medium and cells were incubated at 37°C overnight. The following day medium was replaced by virus supernatant (see 3.5.2), cells were incubated for 6-8 hours until medium was replaced by fresh PC medium again.

Puromycin selection of successfully transduced HMLE-Twist1-ER cells was not possible since these cells were already puromycin resistant. Therefore successfully transduced cells were purified using FACS (see 3.3). HMLE-Twist1-ER cells successfully transduced with shRNAs targeting ZEB1, non-targeting control or CMV-GFP, respectively, were GFP<sup>pos</sup>. HMLE-Twist1-ER cells successfully transduced with CMV-Cherry were Cherry<sup>pos</sup>.

### **3.6 Statistical analysis**

Data are presented as mean  $\pm$  standard error (SEM) or mean  $\pm$  standard deviation (SD). The student's t test (two-tailed) was used to compare two groups. A p-value  $p < 0.05$  was considered significant.

## 4 Results

### 4.1 Separation of the HMLE-Twist1-ER bulk cells into three distinct subpopulations

The initial aim of my project was to determine whether the process of Epithelial-Mesenchymal-Transition (EMT) and the acquisition of stem cell (sc)-like traits, such as mammosphere (MS) formation, are directly linked to each other. Therefore, functional consequences of the EMT-transcription factor (TF) Twist1 were studied using the HMLE-Twist1-ER cell line. These are immortalized human mammary epithelial cells (HMLE) transduced with a retroviral construct containing Twist1 cDNA fused to a mutated estrogen receptor (ER) ligand binding domain (Casas et al., 2011; Elenbaas et al., 2001). Upon 4-hydroxytamoxifen (TAM) treatment, the Twist1-ER fusion protein undergoes a conformational change that allows binding to DNA and hence, TF-activity. Importantly, HMLE-Twist1-ER bulk cells are heterogeneous and contain pre-existing subpopulations that are phenotypically and functionally distinct.

Besides CD44<sup>pos</sup> cells expressing a variable range of the epithelial surface marker CD24, HMLE-Twist1-ER cells were found to contain a small CD44<sup>high</sup>/CD24<sup>neg</sup>, mesenchymal subpopulation enriched for sc-like traits (Mani et al., 2008).

To prevent selection for this pre-existing mesenchymal CD44<sup>high</sup>/CD24<sup>neg</sup> population and address the impact of the epithelial surface marker CD24 on mesenchymal transdifferentiation and acquisition of MS-forming ability, the heterogeneity of the HMLE-Twist1-ER cells was unraveled. For this purpose, cells were sorted by Fluorescence Activated Cell Sorting (FACS) into the following three subpopulations based on the expression of the surface markers CD44 and CD24: i) CD44<sup>high</sup>/CD24<sup>neg</sup>, ii) CD44<sup>pos</sup>/CD24<sup>low</sup> and iii) CD44<sup>pos</sup>/CD24<sup>high</sup> (Figure 2A). In 2D culture following cell sorting, the CD44<sup>high</sup>/CD24<sup>neg</sup> cells presented as single, scattered, spindle-shaped cells with a front-to-back polarized morphology, indicating a mesenchymal phenotype. In contrast, CD44<sup>pos</sup> cells additionally expressing high or low levels of the surface marker CD24 (24<sup>high</sup> and 24<sup>low</sup>) grew in closely adhering islands and showed a cobblestone-like morphology, indicating an epithelial phenotype (Figure 2B).

Importantly, post-sort analysis confirmed successful separation of the CD44<sup>pos</sup> cells into subpopulations with different CD24 expression levels (Figure 2C).

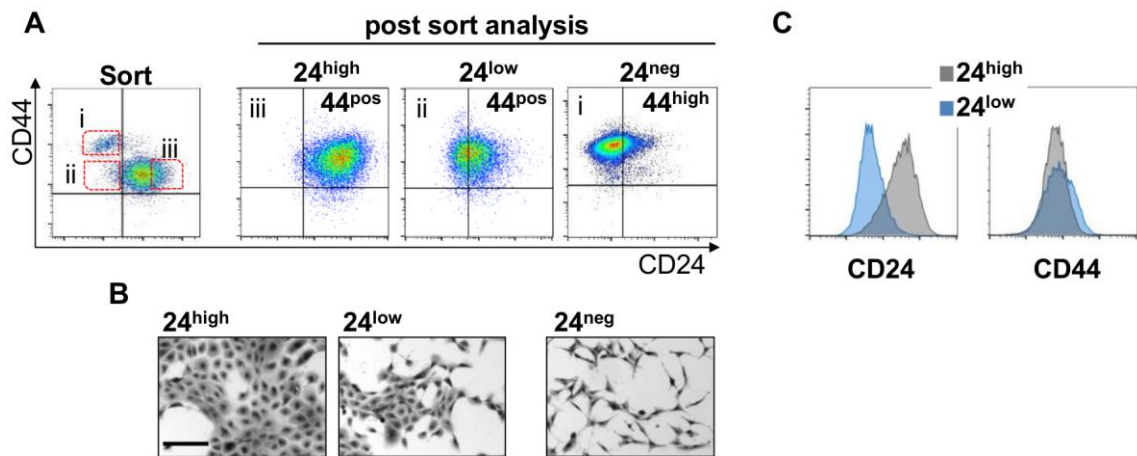


**Figure 2: Separation of the HMLE-Twist1-ER bulk cells into three distinct subpopulations.** (A) FACS sorting strategy of HMLE-Twist1-ER cells based on the CD44 and CD24 surface marker (left panel) and post-sort analysis of the sorted subpopulations after 3 days in culture (right panel). (B) Representative bright-field microscopic pictures of FACS-purified HMLE-Twist1-ER subpopulations after 3 days in culture. Scale bar: 100  $\mu$ m. (C) Overlaid histograms of the CD24 or CD44 marker of FACS-purified 24<sup>high</sup> (grey) and 24<sup>low</sup> (blue) cells after 3 days in culture.

Taken together, based on expression of the surface markers CD44 and CD24 HMLE-Twist1-ER bulk cells were separated into a pure mesenchymal CD44<sup>high</sup>/CD24<sup>neg</sup> and two distinct epithelial subpopulations (CD44<sup>pos</sup>/CD24<sup>low</sup> and CD44<sup>pos</sup>/CD24<sup>high</sup>). All further experiments described below were performed using the purified epithelial subpopulations, referred to as 24<sup>high</sup> and 24<sup>low</sup>.

#### 4.2 Twist1-activation induces Epithelial-Mesenchymal Transition (EMT) in purified epithelial, CD24<sup>pos</sup> HMLE cells

To determine whether Twist1 induces mesenchymal transdifferentiation in purified epithelial subpopulations, 24<sup>high</sup> and 24<sup>low</sup> cells were treated with TAM for a period of 15 days, adding TAM to the cells every 48 hours. During this period, expression of epithelial and mesenchymal markers was monitored at protein and transcriptional level by immunofluorescence and qRT-PCR analysis. At the protein level both, 24<sup>high</sup> and 24<sup>low</sup> cells showed progressive loss of E-cadherin (epithelial marker) expression as well as upregulation and re-organization of vimentin (mesenchymal marker), starting at day 6 after Twist1-activation (Figure 3A). Consistently, E-cadherin expression was downregulated at the

transcriptional level (Figure 3B). By contrast, transcript levels of the mesenchymal markers N-cadherin, ZEB1, FOXC2 and Wnt5a were upregulated. Consequently, both 24<sup>high</sup> and 24<sup>low</sup> cells completely transdifferentiated from their initially epithelial to a mesenchymal phenotype. Since single-cell migration is a functional hallmark of mesenchymal cells, cells were assessed for their motility before and after Twist1-activation using the transwell migration assay (Boyden chamber assay). Twist1-activation for 15 days significantly increased the number of migrating cells, further confirming the acquisition of a mesenchymal phenotype (Figures 3C and 3D). Previously, it was described for the bulk HMLE-Twist1-ER cells that all of these cells acquired a CD44<sup>high</sup>/CD24<sup>neg</sup> surface marker profile upon TAM-treatment (Mani et al., 2008). To determine the dynamics of the CD44 and CD24 marker expression in purified 24<sup>high</sup> and 24<sup>low</sup> cells upon TAM-treatment, cells were treated with TAM for 15 days and analyzed by FACS. During TAM-treatment, the number of CD44<sup>high</sup> cells increased compared to untreated control cells in both 24<sup>high</sup> and 24<sup>low</sup> cells (Figures 3E and 2A). However, dynamics of CD24 marker expression differed between the two subpopulations: whereas 94% of the 24<sup>low</sup> cells acquired a CD24<sup>neg</sup> profile during EMT, 78% of the CD24<sup>high</sup> cells still expressed the epithelial marker CD24 after 15 days of TAM-treatment.

Together, these data revealed that long-term (15 days) Twist1-activation induced EMT in purified epithelial, CD24<sup>pos</sup> HMLE cells. However, whereas the majority of the 24<sup>low</sup> cells lost CD24 expression during Twist1-induced EMT, 24<sup>high</sup> cells retained expression of this epithelial marker.

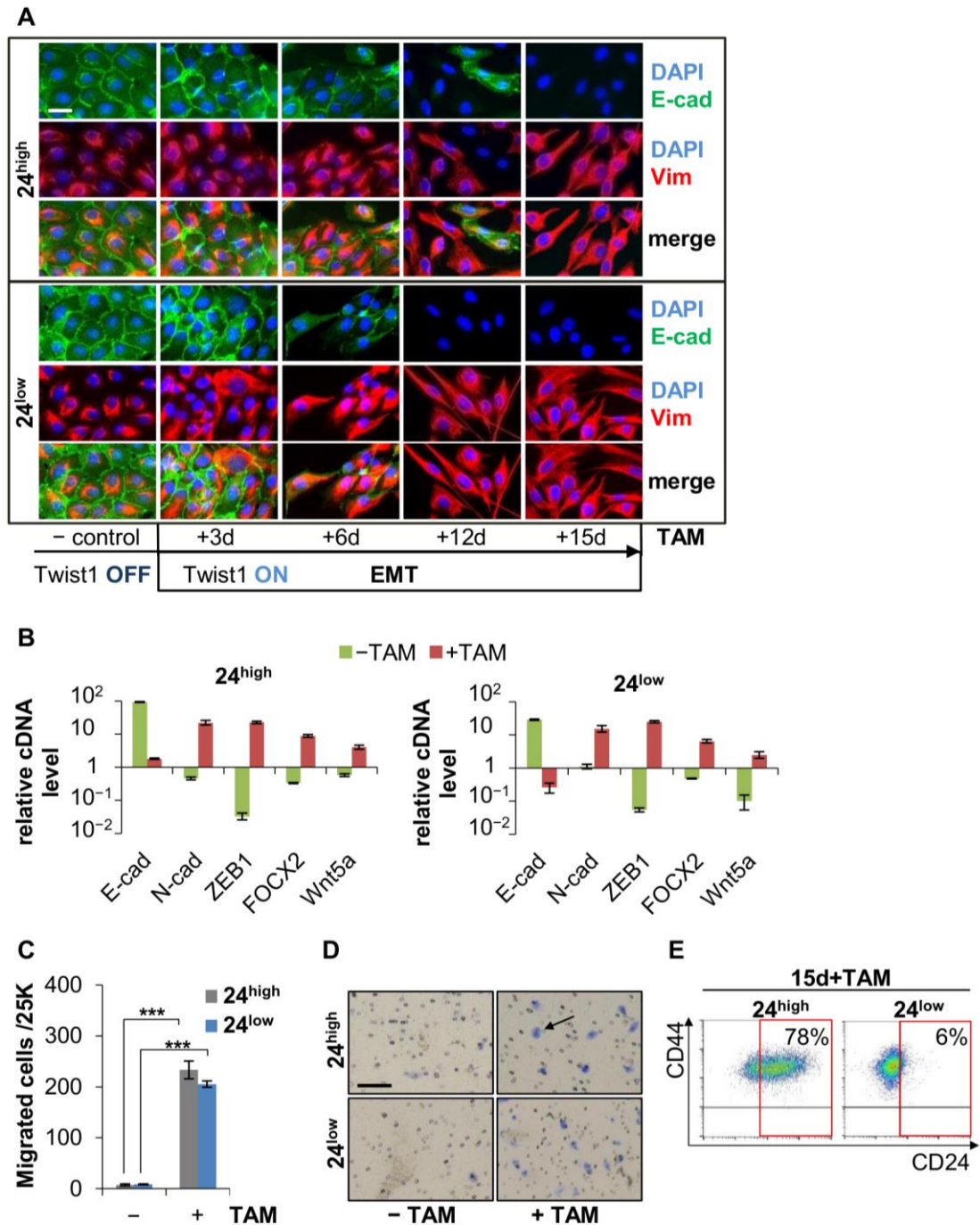


**Figure 3: Twist1-activation for 15 days induces EMT in purified epithelial, CD24<sup>pos</sup> HMLE cells.**

(A) Immunofluorescence staining of E-cadherin (green), vimentin (red) and DAPI (blue) of FACS-purified 24<sup>high</sup> and 24<sup>low</sup> control cells (-) or cells treated with 4-hydroxytamoxifen (TAM) for indicated number of days. Scale bar: 20  $\mu$ m. (B) Relative mRNA expression of E-cadherin, N-cadherin, ZEB1, FOXC2, Wnt5a of 24<sup>high</sup> and 24<sup>low</sup> control cells (green) and cells treated with TAM for 15 days (red). n=3. (C) Quantification of migration ability of 24<sup>high</sup> (grey) and 24<sup>low</sup> (blue) control cells (-) and cells treated with TAM for 15 days (+). n=3. \*p<0.05, \*\*p<0.005, \*\*\*p<0.0005. (D) Representative bright-field microscopic pictures of stained, migrated 24<sup>high</sup> and 24<sup>low</sup> cells. Arrow indicates one representative, migrated cell. Scale bar: 100  $\mu$ m. (E) FACS analysis based on the CD44 and CD24 surface marker of 24<sup>high</sup> and 24<sup>low</sup> cells treated with TAM for 15 days.

Data are presented as mean  $\pm$  SEM.

### 4.3 Transient Twist1-activation induces mammosphere-forming ability in CD24<sup>pos</sup> HMLE cells

To determine whether Twist1 induces sc-like traits in addition to EMT, 24<sup>high</sup> and 24<sup>low</sup> cells were plated into the mammosphere (MS)-assay. This assay was initially adapted from the neurosphere assay and is often used as a proxy-assay to measure self-renewal in mammary epithelial cells as well as tumorigenicity in breast cancer cells (Dontu et al., 2003; Reynolds and Weiss, 1992, 1996). Functionally, the MS-assay tests the ability of cells to proliferate in anchorage independence (suspension culture) at clonal density. MS forming ability was determined for 24<sup>high</sup> and 24<sup>low</sup> cells cultured as depicted in Figure 4A. Specifically, in condition 1) cells were not treated with TAM (-), in condition 2) cells were pre-treated with TAM for 15 days followed by either continued treatment (+) or in condition 3) with no further treatment with TAM upon plating into the MS-assay (+/-). Untreated control cells (-) within both populations did not give rise to MS. In addition, cells continuously treated with TAM during the MS-assay (+) did not generate any MS either. By contrast, cells pre-treated in 2D and not further treated during the MS-assay (+/-) generated MS. Under this condition, MS forming ability of 24<sup>high</sup> cells was 6-fold higher than that of 24<sup>low</sup> cells (Figure 4B). Of note, two types of multicellular clusters were observed in the MS-assay, tight, round spheres and loose, planar sheets of cells (Figure 4C).

Since emergence of MS-formation was only observed after transient Twist1-activation (i.e. following Twist1-deactivation), I hypothesized that a prolonged period of TAM-withdrawal might further increase the frequency of MS-forming cells. To test this hypothesis, 24<sup>high</sup> and 24<sup>low</sup> cells were cultured as depicted in Figure 4D. Specifically, in condition 1) cells were not treated with TAM (-) and in condition 2) cells were pre-treated with TAM for 15 days and not further treated with TAM upon plating into the MS-assay (+/-). Finally, in condition 3) cells were pre-treated with TAM for 15 days, then TAM was withdrawn and cells were further cultured for additional 9 days in 2D prior to plating into the MS-assay (+/- 9d). Whereas prolonged TAM-withdrawal in 2D did not influence MS-forming ability of 24<sup>low</sup> cells, the frequency of MS-forming cells was 20-fold increased for 24<sup>high</sup> cells. Of note, the number of both compact and loose MS increased to a similar extent (Figure 4E). To quantify the MS-forming efficiency more precisely,

serial passaging in limiting dilution was performed using 24<sup>high</sup> cells (Rota et al., 2012). After four passages, the number of MS-forming cells was increased from 1 out of 15 cells to 1 out of 3 cells, indicating acquisition of long-term repopulating ability (Figure 4F).

In summary, these data indicated that transient, but not continuous Twist1-activation induced stable MS-forming ability of CD24<sup>pos</sup> HMLE cells. Furthermore, these data revealed that the frequency of MS-forming cells generated by transient Twist1-activation was enriched in the 24<sup>high</sup> subpopulation of HMLE cells.

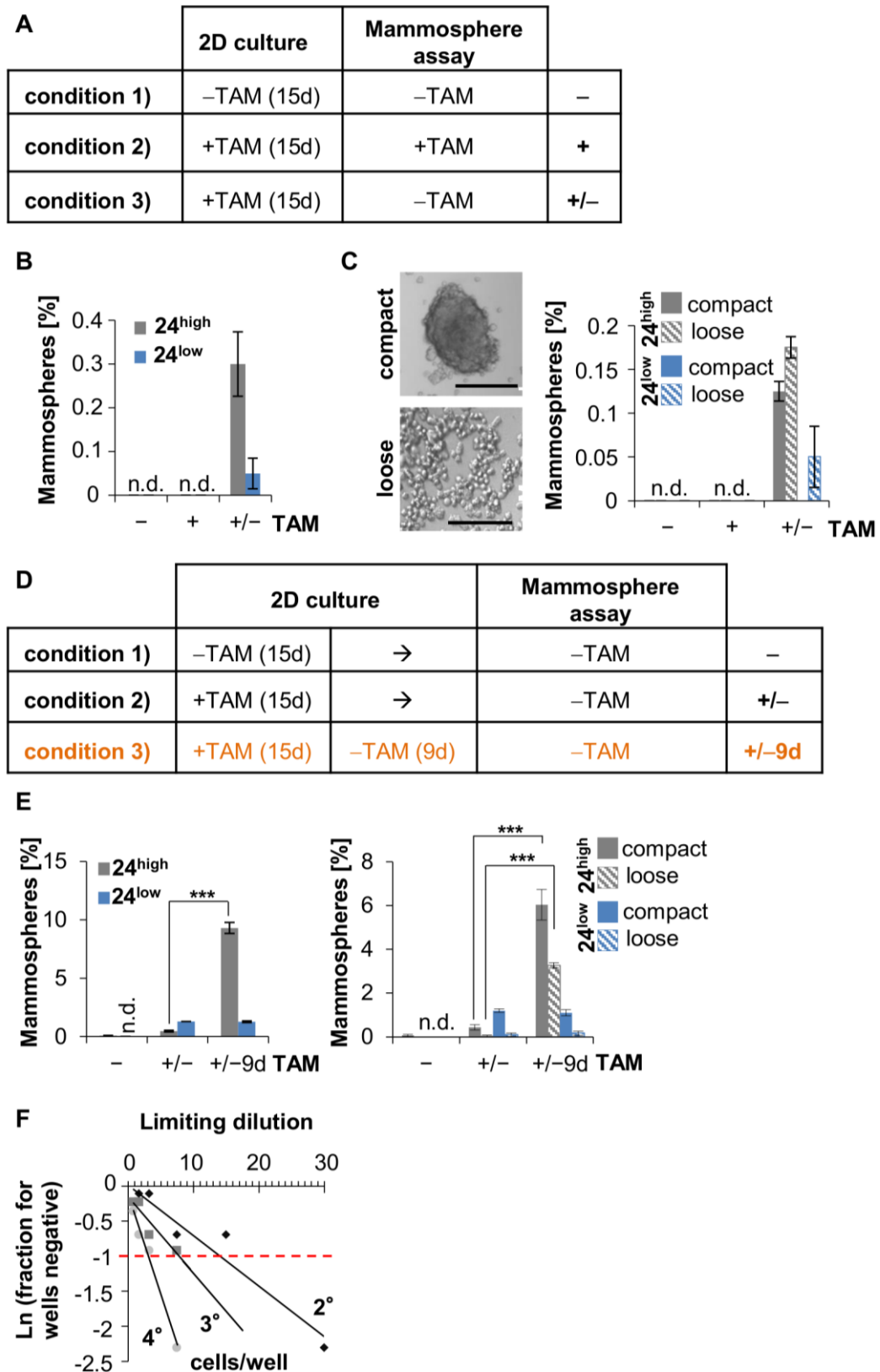


**Figure 4: Transient Twist1-activation induces mammosphere-forming ability in CD24<sup>pos</sup> HMLE cells.**

(A) Experimental setup for MS-assay: 24<sup>high</sup> or 24<sup>low</sup> cells were either not treated with TAM (-) or pre-treated with TAM for 15 days prior to plating. Upon plating TAM-treatment was either continued (+) or discontinued (+/-). (B) Quantification of MS formed by 24<sup>high</sup> (grey) or 24<sup>low</sup>

(blue) cells treated as described in (A). n.d.= not detectable. n=20. **(C)** Representative bright-field microscopic pictures and quantification of compact (filled bars) and loose (striped bars) MS formed by 24<sup>high</sup> (grey) or 24<sup>low</sup> (blue) cells. Cells were treated as described in (A). n.d.= not detectable. n=20. Scale bar: 100  $\mu$ m. **(D)** Modified experimental setup for MS-assay: 24<sup>high</sup> or 24<sup>low</sup> cells were treated as described in (A) or cells were cultured without TAM for 9 days prior plating (+/-9d).  $\rightarrow$ : cells were directly transferred to mammosphere assay after 2D culture for 15 days. **(E)** Quantification of total number of MS and quantification of compact (filled bars) and loose (striped bars) MS formed by 24<sup>high</sup> (grey) or 24<sup>low</sup> (blue) cells treated as described in (D). n.d.= not detectable. n=20. \*p<0.05, \*\*p<0.005, \*\*\*p<0.0005. **(F)** Limiting dilution analysis of 24<sup>high</sup> cells serially passaged for 4 generations. Cells were treated for 15 days with TAM followed by 9 days of TAM-withdrawal prior to plating into MS-assay. n=10/generation.

Data are presented as mean  $\pm$  SEM.

#### **4.4 The capacity of HMLE cells to undergo Mesenchymal-Epithelial-Transition (MET) following transient Twist1-activation is contained within the 24<sup>high</sup> HMLE cell population**

Following TAM-withdrawal, a small subset of 24<sup>high</sup> cells, but not 24<sup>low</sup> cells was observed to revert back to an epithelial phenotype in 2D culture. To confirm that 24<sup>high</sup> cells underwent MET, immunofluorescence and qRT-PCR analysis were performed. As determined by immunofluorescence, 20% of the 24<sup>high</sup> cells re-expressed E-cadherin and downregulated vimentin protein expression. By contrast, 100% of the 24<sup>low</sup> population maintained high vimentin protein expression and total loss of E-cadherin (Figure 5A). Consistently, at the transcriptional level, 24<sup>high</sup> cells showed E-cadherin up-regulation to levels comparable to untreated control cells, while transcript levels of the mesenchymal markers N-cadherin, ZEB1, FOXC2 decreased after TAM-withdrawal. Importantly, downregulation of the direct Twist1 target gene *Wnt5a* to transcriptional levels comparable to untreated control confirmed Twist1-deactivation (Shi et al., 2014) (Figure 5B). To investigate, whether differences between 24<sup>high</sup> and 24<sup>low</sup> cells upon TAM-withdrawal were due to different Twist1 protein levels, localization or activity, cells were analyzed by immunofluorescence. However, before, during and after TAM-treatment Twist1 protein expression was similarly heterogeneous at the single-cell level in both 24<sup>high</sup> and 24<sup>low</sup> cells (Figure 5C).

In summary, these data indicated that a proportion of HMLE cells residing within the 24<sup>high</sup> subpopulation were able to undergo MET after Twist1-deactivation. In

contrast, all HMLE cells residing within the  $24^{\text{neg}}$  subpopulation retained a mesenchymal phenotype.

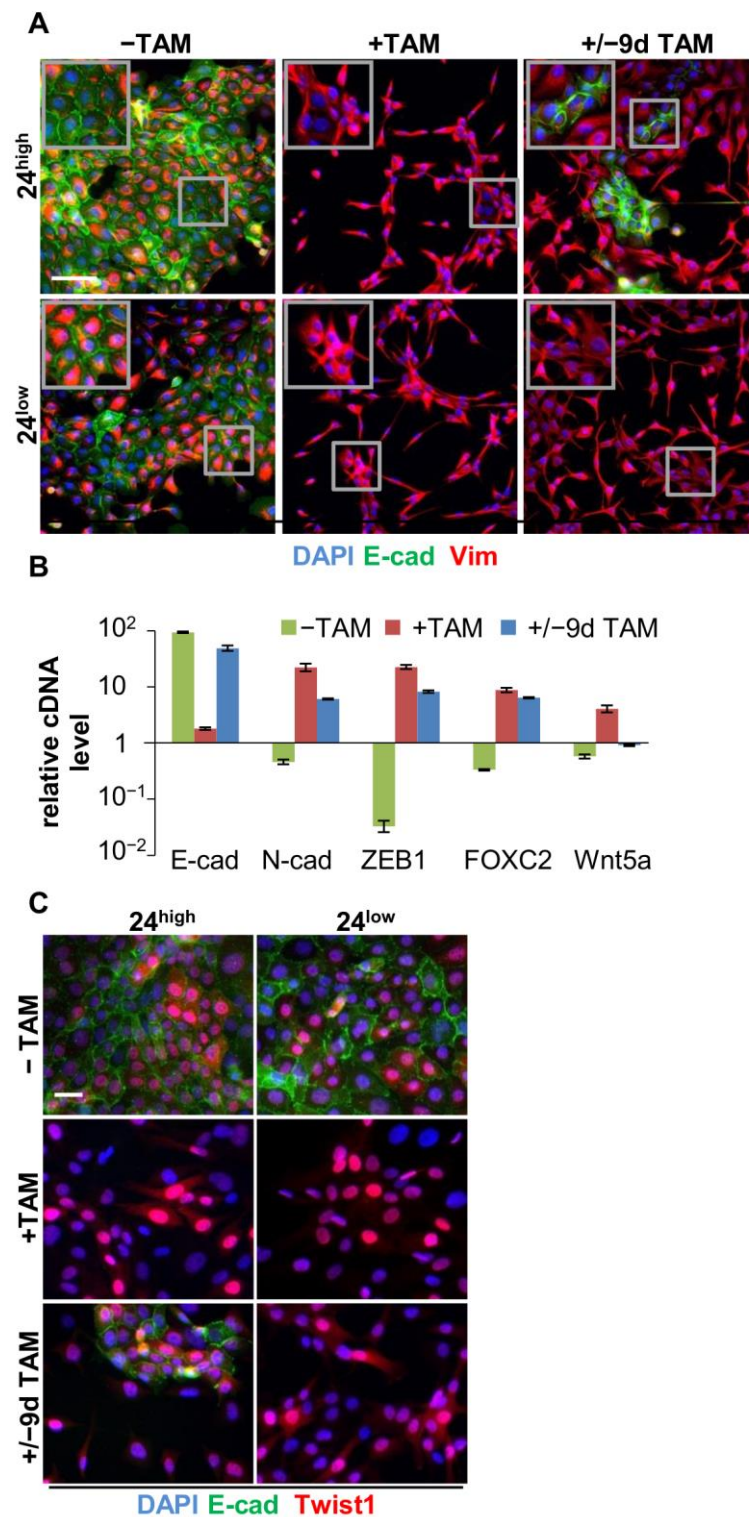


**Figure 5: The capacity of HMLE cells to undergo MET following transient Twist1-activation is contained within the  $24^{\text{high}}$  HMLE cell population.**

(A) Immunofluorescence staining of E-cadherin (green), vimentin (red) and DAPI (blue) of  $24^{\text{high}}$  and  $24^{\text{low}}$  control cells (-TAM) or cells treated with TAM for 15 days (+TAM) or cells treated for 15 days followed by 9 days of TAM-withdrawal (+/-9d TAM). Scale bar: 100  $\mu\text{m}$ . (B) Relative mRNA expression of E-cadherin, N-cadherin, ZEB1, FOXC2, Wnt5a in  $24^{\text{high}}$  control cells (green), cells

treated with TAM for 15 days (red) and cells treated for 15 days followed by 9 days of TAM-withdrawal (blue). n=3. **(C)** Immunofluorescence staining of E-cadherin (green), Twist1 (red) and DAPI (blue) of 24<sup>high</sup> and 24<sup>low</sup> treated as described in (A). Scale bar: 50  $\mu$ m.

Data are presented as mean  $\pm$  SEM.

### **4.5 Mammosphere-forming 24<sup>high</sup> HMLE cells display epithelial-mesenchymal plasticity**

As described before, a subset of 24<sup>high</sup> cells underwent MET after Twist1-deactivation, whereas the majority of cells retained a mesenchymal phenotype (Figure 5A). Moreover, only 1 out of 15 cells generated MS after transient Twist1-activation as determined by limiting dilution (Figure 4F). Therefore, it was unclear which cells exactly acquired MS-forming ability during transient Twist1-activation: MS-forming cells could be contained within those cells that were able to revert back to an epithelial phenotype or those that had transdifferentiated to a stable mesenchymal phenotype. To determine which cells within the 24<sup>high</sup> cell population gave rise to MS, Twist1 was transiently activated in 24<sup>high</sup> cells. Specifically, 24<sup>high</sup> cells were pre-treated with TAM for 15 days, afterwards TAM was withdrawn and cells were cultured for additional 9 days in 2D culture (+/-9d). Subsequently, differential trypsinization was performed as illustrated in Figure 6A. Thereby, three different fractions of cells were obtained: one fraction of mesenchymal cells (M), one fraction mainly consisting of epithelial cells with 5-10% mesenchymal cells (E) and one strongly trypsin-resistant pure epithelial fraction (E+). Mesenchymal or epithelial phenotype was confirmed at protein and transcriptional level using immunofluorescence and qRT-PCR analysis (Figures 6A and 6B). When plated into the MS-assay, cells of the E fraction were detected to be highly enriched for MS-forming cells. Specifically, 9% of the cells residing within the E fraction formed MS, whereas only 1% of the E+ and 0.1% of the M fraction cells were able to do so (Figure 6C). To further characterize which cell state enabled MS-forming ability, MS (originated from 24<sup>high</sup> cells) were analyzed for expression of epithelial and mesenchymal markers at the protein and transcriptional level. Immunofluorescence revealed E-cadherin- and vimentin-positive cells in both, loose and compact MS (Figure 6D). At the transcriptional level, MS-derived cells expressed E-cadherin, but also the mesenchymal markers ZEB1 and FOXC2. Moreover, transcript levels of these markers were

## Results

between epithelial control cells (-TAM) and mesenchymal cells (+TAM). Importantly, Wnt5a transcript levels were comparable to epithelial control cells, indicating that Twist1 was not active in MS-derived cells (Figure 6E).

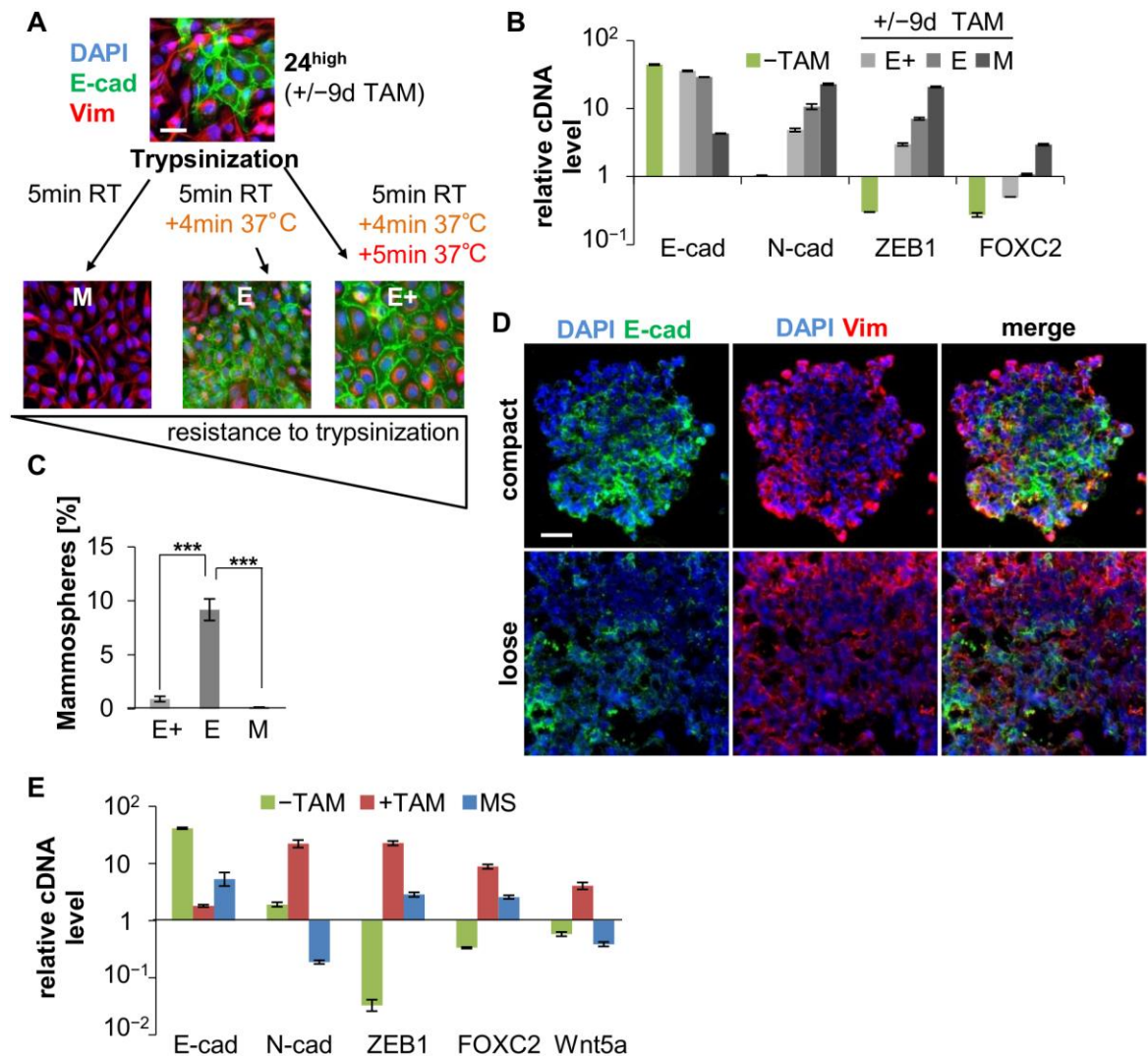


**Figure 6: MS-forming 24<sup>high</sup> HMLE cells display epithelial-mesenchymal plasticity.**

**(A)** Experimental setup of differential trypsinization: 24<sup>high</sup> cells were treated for 15 days with TAM, followed by 9 days of TAM-withdrawal (+/-9d TAM). 24<sup>high</sup> (+/-9d TAM) cells were trypsinized for 5 min at RT, detached cells were collected and re-seeded in 2D culture (M), remaining cells were trypsinized for additional 4 min at 37°C and detached cells were collected and re-seeded in 2D culture (E). Still remaining cells were trypsinized for additional 5 min at 37°C, collected and re-seeded in 2D culture (E+). Also shown, immunofluorescence staining of E-cadherin (green), vimentin (red) and DAPI (blue) of cells before differential trypsinization and of cells of the M, E and E+ fraction. Scale bar: 20 µm. **(B)** Relative mRNA expression of E-cadherin, N-cadherin, ZEB1 and FOXC2 of 24<sup>high</sup> untreated control cells (green) and cells of M (dark grey), E (middle grey) and E+ (light grey) fraction. n=3. **(C)** Quantification of MS formed by cells of M, E and E+ fraction. n=20. \*p<0.05, \*\*p<0.005, \*\*\*p<0.0005. **(D)** Immunofluorescence staining of E-cadherin (green), vimentin (red) and DAPI (blue) of compact and loose MS. Scale bar: 100 µm.

**(E)** Relative mRNA expression of E-cadherin, N-cadherin, ZEB1, FOXC2 and Wnt5a of 24<sup>high</sup> control cells (green), cells treated with TAM for 15 days (red) and MS-derived cells (blue). n=3.

Data are presented as mean  $\pm$  SEM.

Together, these observations indicated that neither cells with a fixed epithelial (enriched in the E+ fraction) nor a fixed mesenchymal cell phenotype (enriched in M fraction) were enriched for MS-forming ability. Otherwise, the majority of MS-forming cells would have been expected to be found within the E+ or M, but not in the E fraction. Moreover, these data revealed MS-forming cells to simultaneously express epithelial and mesenchymal markers and thus suggested MS-forming cells to be characterized by epithelial-mesenchymal plasticity.

#### **4.6 High expression of the epithelial surface marker CD24 predicts MS-formation and the ability of 24<sup>high</sup> HMLE cells to undergo MET**

As shown in Figure 4, MS-forming cells were found to be enriched in the 24<sup>high</sup> subpopulation of HMLE cells. Furthermore, FACS analysis showed that the majority of 24<sup>high</sup> cells retained expression of the epithelial cell surface marker CD24 during Twist1-induced EMT (Figure 3E).

Therefore, I set out to investigate whether expression of CD24 predicts MS-forming ability. For this purpose, 24<sup>high</sup> cells, treated with TAM for 15 days, were separated by FACS into CD24<sup>neg</sup> and CD24<sup>high</sup> cells (Figure 7A). Subsequently, cells were plated into the MS-assay and in 2D culture. The MS-assay revealed MS-forming cells to be 8-fold enriched in CD24<sup>high</sup> cells compared to CD24<sup>neg</sup> cells (Figure 7B). Of note, FACS analysis of MS-derived cells (originating from 24<sup>high</sup> cells) showed that CD24 expression was retained after plating into the MS-assay (Figure 7C). Interestingly, in 2D culture, CD24<sup>neg</sup> cells retained a mesenchymal phenotype while CD24<sup>high</sup> cells underwent MET (Figure 7D).

Together, these data revealed MS-forming cells to be characterized by expression of the epithelial surface marker CD24. Moreover, these observations demonstrated MS-forming cells to be contained in HMLE cells that retain expression of CD24 during EMT and undergo MET after Twist1-deactivation.

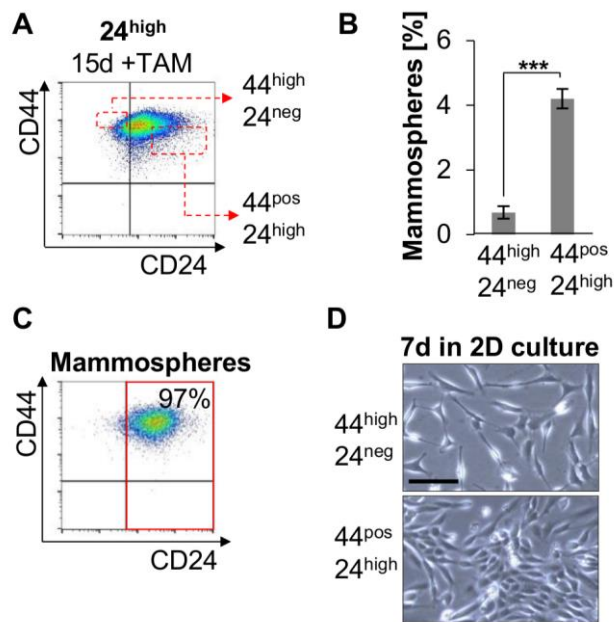


**Figure 7: High expression of the epithelial surface marker CD24 predicts MS-formation and the ability of 24<sup>high</sup> HMLE cells to undergo MET.**

(A) FACS sorting strategy based on the CD44 and CD24 surface marker of 24<sup>high</sup> cells treated with TAM for 15 days. (B) Quantification of MS formed by CD44<sup>high</sup>/CD24<sup>neg</sup> and CD44<sup>pos</sup>/CD24<sup>high</sup> cells, purified by FACS sorting according to (A). n=20. \*p<0.05, \*\*p<0.005, \*\*\*p<0.0005. (C) FACS analysis based on the CD44 and CD24 surface marker of MS. (D) Representative bright-field microscopic pictures of FACS-sorted CD44<sup>high</sup>/CD24<sup>neg</sup> and CD44<sup>pos</sup>/CD24<sup>high</sup> cells after 7 days in 2D culture. Scale bar: 50 μm.

Data are presented as mean ± SEM.

#### 4.7 Twist1 induces MS-forming ability independently of EMT in 24<sup>high</sup> HMLE cells

Based on the results shown in Figure 6 and 7, I hypothesized that maintenance of epithelial marker expression (e.g. CD24) during Twist1-induced EMT enables 24<sup>high</sup> HMLE cells to undergo MET once Twist1 is deactivated. Additionally, I hypothesized that reversion to an epithelial phenotype favors MS-forming ability. Consequently, this raised the question whether generation of MS-forming cells necessitated passage through a complete EMT at all.

Since the progressive loss of E-cadherin and the upregulation of vimentin protein expression were not observed until day 6 after Twist1-activation, I set out to investigate MS-forming ability early after Twist1-activation. For this purpose, 24<sup>high</sup> HMLE cells were treated for 24, 48 or 72 hours with TAM and then plated directly into the MS-assay (referred to as direct). As a second approach cells were treated for 24, 48 or 72 hours with TAM. Afterwards TAM was withdrawn

and cells were further cultured for 9 days in 2D prior to plating into the MS-assay (referred to as delay) (Figure 8A).

Functionally, no MS-formation was detected in 24<sup>high</sup> cells directly plated into the MS-assay. However, 48 hours of TAM-treatment followed by 9 days of TAM-withdrawal elicited MS-forming capacity: 20% of the wells contained at least one MS. Moreover, the number of MS doubled when cells were treated for 72 hours prior to TAM-withdrawal (Figure 8B). Finally, to determine whether short-term Twist1-activation induced MS-forming capacity as a stable trait as long-term Twist1-activation did, MS were serially passaged. Indeed, MS-formation was stable over several passages and the percentage of wells containing at least one MS increased from passage 1° to 3°, from 20% to 100% (Figure 8C).

To verify that cells had not undergone EMT prior to plating into the MS-assay, immunofluorescence and qRT-PCR analysis were performed. Following Twist1-activation and subsequent deactivation, all cells retained high levels of membranous E-cadherin and low vimentin protein expression, indicating an epithelial phenotype (Figure 8D). Consistently, E-cadherin and N-cadherin transcript levels were comparable to untreated control cells. Transcript levels of the EMT-TF ZEB1 were upregulated by transient Twist1-activation: cells treated with TAM for 72 hours (directly or delayed plated into the MS-assay) expressed 10-fold higher levels compared to control cells. Since directly plated cells did not form MS, these data suggested that ZEB1 did not contribute to MS-formation. Of note, expression level of the direct Twist1 target gene *Wnt5a* confirmed successful Twist1-activation and deactivation (Figure 8E).

Taken together, these data indicated that short-term Twist1-activation was sufficient to induce stable MS-forming ability in a subset of 24<sup>high</sup> HMLE cells. However, as observed for long-term Twist1-activation, MS-forming ability exclusively arose after TAM-withdrawal. Importantly, passage through an EMT did not appear to be required for Twist1 to induce MS-forming ability in 24<sup>high</sup> HMLE cells, suggesting that Twist1 induced this trait independently of EMT.

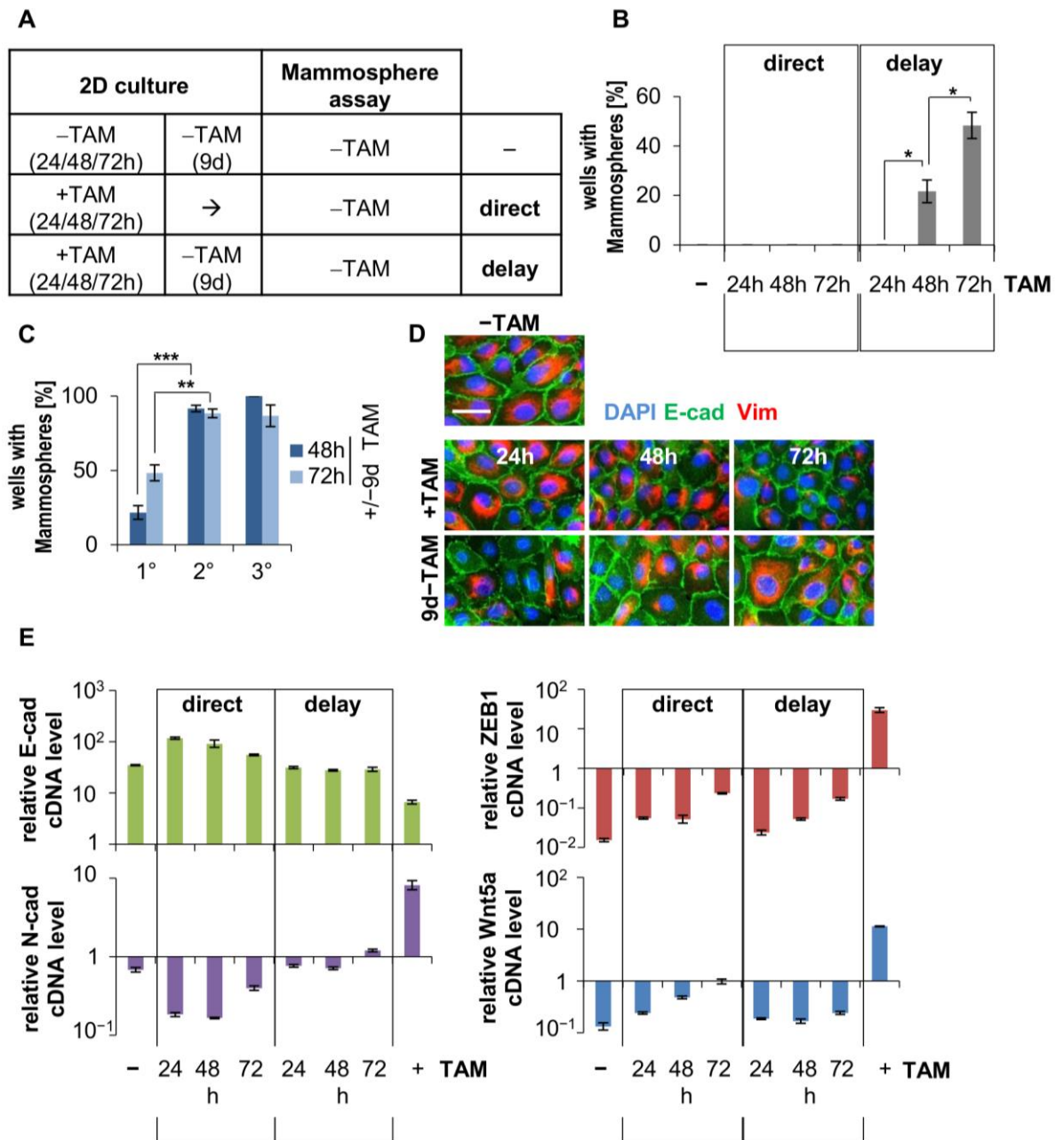


**Figure 8: Twist1 induces MS-forming ability independently of EMT in  $24^{\text{high}}$  HMLE cells.** (A) Experimental setup for MS-assay:  $24^{\text{high}}$  cells were not treated with TAM (-), pre-treated with TAM for 24, 48 or 72 hours in 2D and either directly plated into the MS-assay without further TAM-treatment (direct) or TAM was withdrawn for 9 days in 2D culture prior to plating (delay). →: cells were directly transferred to mammosphere assay after 2D culture for 15 days. (B) Quantification of MS formed by  $24^{\text{high}}$  cells treated as described in (A).  $n=20$ . \* $p<0.05$ , \*\* $p<0.005$ , \*\*\* $p<0.0005$ . (C) Quantification of 1<sup>st</sup>, 2<sup>nd</sup> and 3<sup>rd</sup> generation of MS formed by  $24^{\text{high}}$  cells treated with TAM for 48 or 72 hours followed by 9 days of TAM-withdrawal prior to plating into MS-assay.  $n=30$ /generation. \* $p<0.05$ , \*\* $p<0.005$ , \*\*\* $p<0.0005$ . (D) Immunofluorescence staining of E-cadherin (green), vimentin (red) and DAPI (blue) of  $24^{\text{high}}$  cells treated as described in (A). Scale bar: 20  $\mu\text{m}$ . (E) Relative mRNA expression of E-cadherin, N-cadherin, ZEB1 and Wnt5a of  $24^{\text{high}}$  cells treated as described in (A) and cells treated with TAM for 15 days (+).  $n=3$ .

Data are presented as mean  $\pm$  SEM.

#### **4.8 Continuous Twist1-activity inhibits proliferation of 24<sup>high</sup> HMLE cells in a 3D environment**

Figure 4B and 8B showed that transient TAM-treatment was required to induce MS-forming ability in HMLE cells. Moreover, no MS-formation was observed in HMLE cells during continuous TAM-treatment upon plating into the MS-assay. Therefore, I hypothesized that Twist1-activation was required to prime HMLE cells for MS-forming ability. However, this trait subsequently emerged only following Twist1-deactivation.

Since the MS-assay functionally tests two parameters: 1) survival in anchorage-independence and 2) proliferation at clonal density, I set out to separate these functional aspects and determine which one depends specifically on transient Twist1-activation. First, survival in anchorage-independence was assessed using a modified anoikis assay as previously described (Onder et al., 2008; Figure 9A). Anoikis as a form of programmed cell death was shown to be initiated upon disruption of epithelial cell-matrix interactions, while EMT was implicated conferring anoikis resistance (Frisch and Francis, 1994; Onder et al., 2008). To induce anchorage-independence, single-cell suspensions were rotated in Falcon tubes overnight. The following day, surviving cells were collected by centrifugation and plated in 2D culture without continuing TAM-treatment. Subsequently, colonies generated by anoikis-surviving cells were counted. Whereas untreated control cells did not form any colonies, 1.2% of cells with active Twist1 and 0.4% of cells assessed after transient Twist1-activation showed colony forming ability after the anoikis assay (Figure 9B). Consequently, Twist1-activity induced survival in anchorage independence, and this trait was partially maintained once Twist1 was deactivated.

Next, I determined whether lack of MS-formation in the presence of active Twist1 was due to a lack of proliferation. Since 24<sup>high</sup> HMLE cells with active Twist1 robustly proliferated in 2D culture, I hypothesized that proliferation was specifically inhibited by active Twist1 in a 3D environment (Figure 9C). To test this hypothesis, cells were plated in floating collagen gels (Linnemann et al., 2015). Since collagen is an abundant component of the extracellular matrix in breast stroma, collagen gels provided a physiologically relevant 3D environment (Lo et al., 2012). The following cells were assessed for their colony formation at

different plating densities: 1) untreated 24<sup>high</sup> control cells, 2) 24<sup>high</sup> cells treated for 15 days with TAM in 2D, followed by TAM-treatment during 3D culture (i.e. cells with active Twist1), and 3) MS-derived cells (i.e. cells after transient Twist1-activation). To visualize colonies and quantify colony formation, carmine staining was performed. Untreated control 24<sup>high</sup> cells and MS-derived cells formed similar numbers of colonies while colony formation was strongly suppressed in cells with active Twist1. Of note, at low plating densities no colonies were generated by cells with active Twist1 at all (Figures 9D and 9E). Thus, differences in colony formation demonstrated a lack of proliferation in 3D. To quantify proliferation more precisely, cells were isolated from the gels and the total cell number was counted. As depicted in Figure 9F, both control and MS-derived cells had undergone 12-fold more cell doublings during 3D culture than cells with active Twist1.

In summary, these data indicated that Twist1 induced survival under anchorage-independence in 24<sup>high</sup> HMLE cells and this trait was maintained after Twist1-deactivation. Moreover, active Twist1 was shown to inhibit proliferation under 3D conditions. Consequently, the lack of MS-formation in the presence of active Twist1 was due to a lack of proliferation upon plating into the MS-assay.

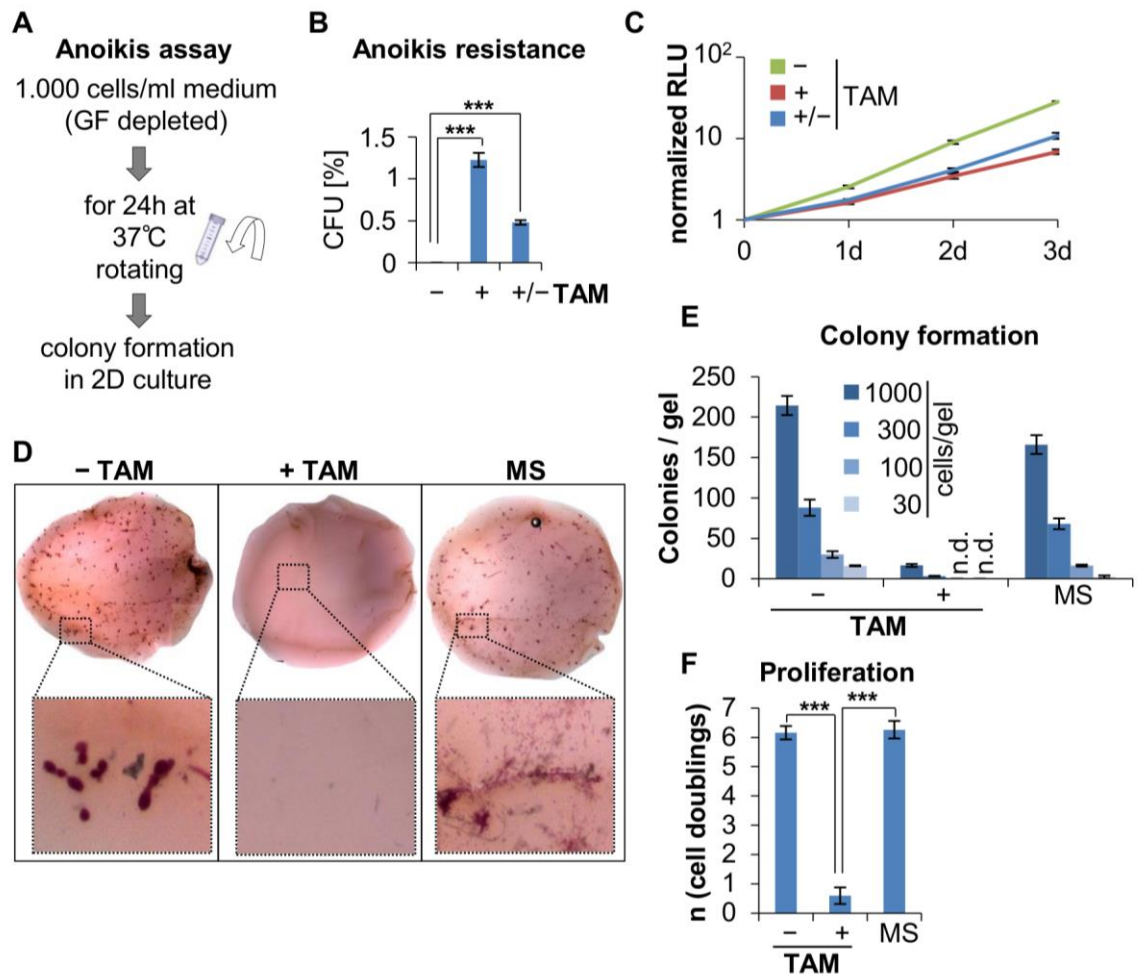


**Figure 9: Continuous Twist1-activity inhibits proliferation of 24<sup>high</sup> HMLE cells in a 3D environment.**

**(A)** Experimental setup for the Anoikis assay. GF=growth factor. **(B)** Quantification of Anoikis assay: colony forming units (CFU) of 24<sup>high</sup> cells either not treated with TAM (-) or pre-treated with TAM for 15 days (+) or pre-treated for 15 days followed by 3 days of TAM withdrawal (+/-) prior to Anoikis assay. n=3. \*p<0.05, \*\*p<0.005, \*\*\*p<0.0005. **(C)** Quantification of proliferation over a period of 3 days in 2D culture. 24<sup>high</sup> cells were either not treated with TAM (-), pre-treated for 15 days and further treated (+) or pre-treated for 15 days and not further treated (+/-) during this period. n=10. **(D)** Representative bright-field microscopic pictures of carmine stained colonies formed by 24<sup>high</sup> cells either not treated with TAM (-TAM) or pre-treated for 15 days and further treated during 3D culture (+TAM) or by MS-derived cells not treated with TAM during 3D culture. Plating density: 1000 cells per gel. n=3. **(E)** Quantification of carmine stained colonies formed by 24<sup>high</sup> cells treated as described in (D). n.d.=not detectable. n=3. **(F)** Quantification of the number of cell doublings in 3D culture. 24<sup>high</sup> cells were treated as described in (D). Plating density: 1000 cells per gel. n=3. \*p<0.05, \*\*p<0.005, \*\*\*p<0.0005.

Data are presented as mean ± SEM.

#### 4.9 MS-forming 24<sup>high</sup> HMLE cells display invasive growth in 3D-collagen gels

During quantification of the colony formation in 3D collagen gels, I discovered that colonies formed by untreated 24<sup>high</sup> control cells and MS-derived cells markedly differed in their morphology: untreated control cells formed colonies with clearly defined edges while MS-derived cells generated colonies characterized by diffuse margins. To investigate the morphologies of colonies formed by untreated 24<sup>high</sup> control and MS-derived cells more precisely, immunofluorescence staining for the basement membrane-component laminin-1 and subsequent confocal microscopy was performed. Colonies generated by untreated 24<sup>high</sup> control cells displayed smooth margins with continuous laminin-1 expression, indicating non-invasive 3D-growth. In contrast, colonies formed by MS-derived cells showed patchy laminin-1 expression and cell-clumps as well as single cells detaching from the margins, indicating invasive 3D-growth (Figure 10).

In summary, these data revealed that transient Twist1-activation induced invasive traits of 24<sup>high</sup> HMLE cells in 3D culture. Moreover, these results, together with the observations from the MS-assay, demonstrated that transient Twist1 permanently altered functional traits of 24<sup>high</sup> HMLE cells.

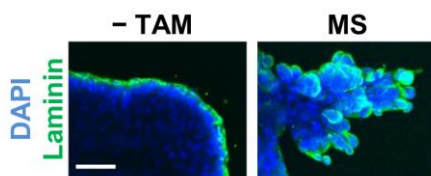


**Figure 10: MS-forming 24<sup>high</sup> HMLE cells display invasive growth in 3D collagen gels.** Immunofluorescence staining of laminin-1 (green) and DAPI (blue) of colonies formed by untreated 24<sup>high</sup> control cells (-TAM) or MS-derived cells. Scale bar: 100  $\mu$ m.

#### 4.10 24<sup>high</sup> HMLE cells display epithelial-mesenchymal plasticity in 3D collagen gels after transient Twist1-activation

Since invasive traits are often linked to a mesenchymal cell state and non-invasive traits are often linked to an epithelial cell state, 24<sup>high</sup> HMLE cells growing in 3D collagen gels were characterized for expression of epithelial and mesenchymal markers by immunofluorescence and subsequent confocal

microscopy. In detail, 1) untreated  $24^{\text{high}}$  control cells, 2)  $24^{\text{high}}$  cells with active Twist1 and 3)  $24^{\text{high}}$  cells transiently treated with TAM (15 days treated with TAM in 2D followed by TAM-withdrawal upon plating into 3D collagen gels) were analyzed for the expression of following markers: A) E-cadherin, B) vimentin, C) the tight-junction component ZO-1 (epithelial marker) and D) F-actin. Of note, cortical organization of actin filaments is characteristic for epithelial cells while mesenchymal cells display actin stress fibers. (Confocal microscopy for E-cadherin and vimentin were performed in collaboration with Diana Dragoi, PhD student in the Scheel group).

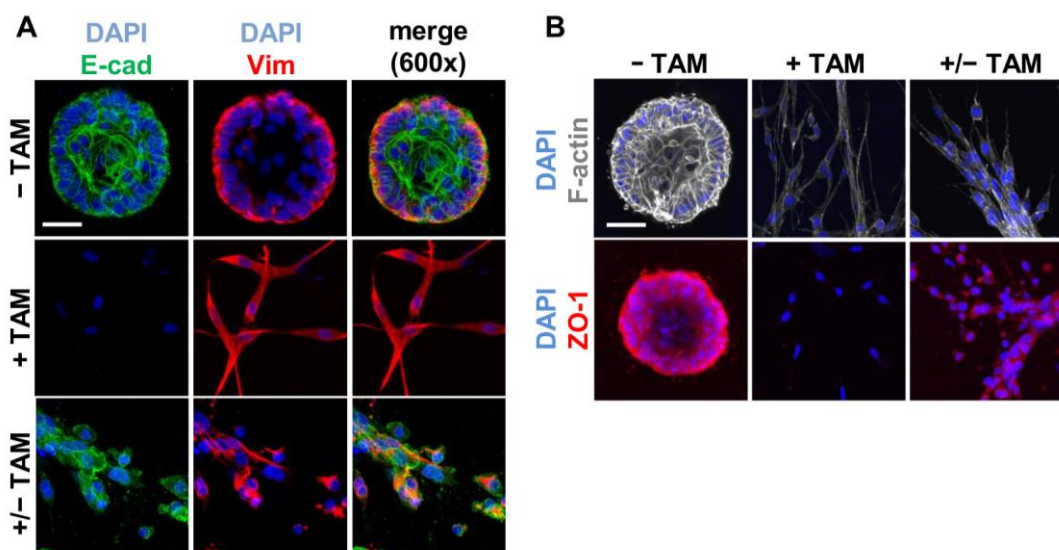


**Figure 11:  $24^{\text{high}}$  HMLE cells display epithelial-mesenchymal plasticity in 3D collagen gels after transient Twist1-activation.**

(A) Immunofluorescence staining of E-cadherin (green), vimentin (red) and DAPI (blue) of colonies formed by untreated  $24^{\text{high}}$  control cells (-TAM) or  $24^{\text{high}}$  cells treated with TAM for 15 days and further treated in 3D culture (+TAM) or  $24^{\text{high}}$  cells treated with TAM for 15 days and not further treated with TAM in 3D culture (+/-TAM). Scale bar: 50  $\mu\text{m}$ . (B) Immunofluorescence staining of F-actin (white), ZO-1 (red) and DAPI (blue) of colonies formed by cells treated as described in (A). Scale bar: 50  $\mu\text{m}$ .

Untreated  $24^{\text{high}}$  control cells generated colonies characterized by a basal layer of E-cadherin- and vimentin-positive cells. In addition, untreated  $24^{\text{high}}$  control cells showed expression of the tight-junction component ZO-1 and cortical F-actin.  $24^{\text{high}}$  HMLE cells with active Twist1 were characterized by high vimentin protein expression as well as actin stress fibers and a lack of E-cadherin and ZO-1 expression. In contrast,  $24^{\text{high}}$  HMLE cells transiently treated with TAM displayed E-cadherin, high vimentin as well as ZO-1 expression. Moreover,

colonies generated by these cells contained both, cortical F-actin localization and actin stress fibers (Figures 11A and 11B).

Taken together, colonies formed by untreated control 24<sup>high</sup> HMLE cells harbored cells characterized by an epithelial cell state. 24<sup>high</sup> HMLE cells with active Twist1 were characterized by a mesenchymal cell state. In contrast, colonies generated by transiently treated 24<sup>high</sup> HMLE cells were composed of cells simultaneously expressing epithelial and mesenchymal markers. Consequently, these observations confirmed the findings from the MS-assay (Figures 6D and 6E), suggesting that transient Twist1-activation induces epithelial-mesenchymal plasticity in 24<sup>high</sup> HMLE cells.

#### **4.11 Transient Twist1-activation permanently alters gene expression profile of HMLE cells**

As described in Figure 9, 10 and 11, 24<sup>high</sup> HMLE cells growing in a 3D environment showed different traits depending on Twist1-activity: 1) before Twist1-activation cells displayed a proliferative, non-invasive, epithelial phenotype, 2) during Twist1-activation cells showed a non-proliferative, invasive, mesenchymal phenotype and 3) after transient Twist1-activation cells were characterized by a proliferative, invasive phenotype with epithelial-mesenchymal plasticity, a hitherto unknown cell state.

For further characterization of this novel cell state, gene expression profiling was performed in collaboration with Dr. Martin Irmeler from the Institute of Experimental Genetics at the Helmholtz Center Munich for. The gene expression profiles of 1) 24<sup>low</sup> and 24<sup>high</sup> cells before Twist1-activation (–TAM), 2) 24<sup>low</sup> and 24<sup>high</sup> cells during Twist1-activation (15 days +TAM), 3) 24<sup>high</sup> cells after transient Twist1-activation (+/–TAM) and MS-derived cells were assessed. Our group recently showed that not only Twist1 but also the EMT-TF Snail1 primed 24<sup>high</sup> HMLE cells for stable MS-forming capacity and epithelial-mesenchymal plasticity (Master Thesis Elena Panzilius, 2013; Schmidt et al., 2015). Intending to derive a common plasticity gene signature, the gene expression profiles of HMLE-Snail1-ER 24<sup>high</sup> cells before Snail1-activation (–TAM) and of MS-derived cells of MS formed by HMLE-Snail1-ER 24<sup>high</sup> cells were included in the analysis (Figure

12A). Following unsupervised clustering, principle component analysis (PCA) was performed in collaboration with Dr. Steffen Sass from the Institute for Computational Biology (ICB) at the Helmholtz Center Munich (Figure 12B). With respect to principal component (PC) 2, all analyzed cell populations fell into three different clusters characteristic for: 1) an epithelial cell state (untreated 24<sup>low</sup> and 24<sup>high</sup> HMLE-Twist1-ER cells and untreated 24<sup>high</sup> HMLE-Snail1-ER cells), 2) a mesenchymal cell state (24<sup>low</sup> and 24<sup>high</sup> HMLE-Twist1-ER treated with TAM) and 3) a cell state in-between (cells after transient Twist1-activation and MS-derived cells). Thus, in accordance with my functional findings, 24<sup>high</sup> HMLE cells were found to differ in their gene expression profile depending on EMT-TF-activity. With respect to PC1, the gene expression profile of MS-derived cells was different from those of all other cell populations. Thus, 3D culture conditions influenced the gene expression profile of HMLE cells. To identify genes within a specific plasticity gene signature, genes were filtered for those genes expressed in 2D and 3D independent of cell culture conditions and specifically expressed in HMLE cells after transient EMT-TF-activation, but not in a fixed epithelial or mesenchymal cell state. Indeed a subset of 189 genes representing a unique plasticity gene signature was identified consisting of genes associated with intracellular protein kinase signaling (Figures 12C, 12D and 12E).

Together, these data suggested that transient Twist1- or Snail1-activation permanently altered the cell state of 24<sup>high</sup> HMLE cells. The acquired cell state was characterized by a unique gene expression profile represented by a 189-genes signature.

## Results

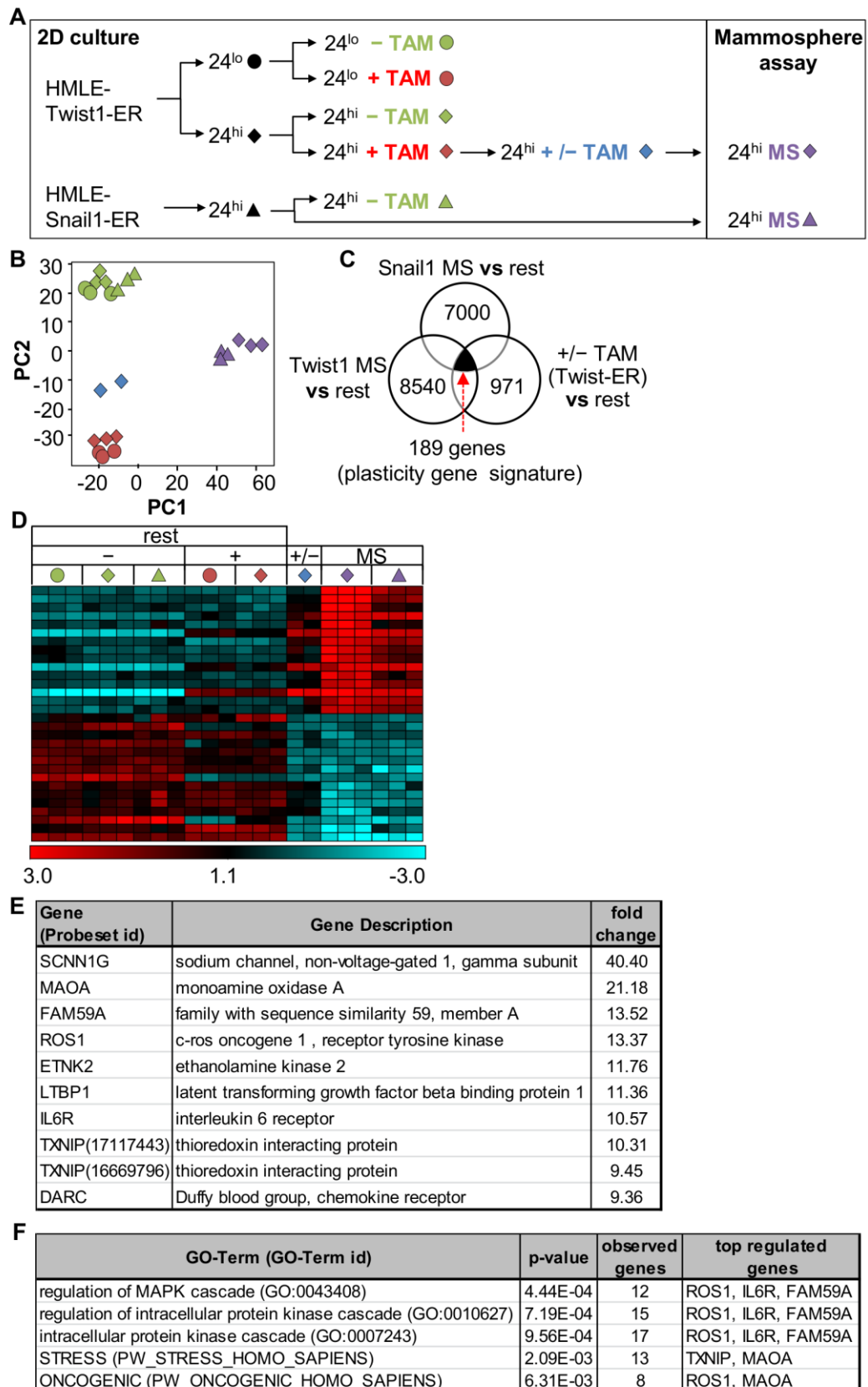


**Figure 12: Transient Twist1-activation permanently alters gene expression profile of HMLE cells.**

(A) Schematic overview of cells (for each n=3) included in the gene expression profiling: 24<sup>high</sup> (24<sup>hi</sup>; rhomb) or 24<sup>low</sup> (24<sup>lo</sup>; circle) HMLE-Twist1-ER or 24<sup>high</sup> HMLE-Snail1-ER cells (triangle) either not treated with TAM (green) or treated with TAM for 15 days (red) or treated with TAM for

15 days followed by 9 days of TAM-withdrawal (blue) or MS-derived cells (purple). **(B)** Principal Component Analysis (PCA) after unsupervised clustering of the gene expression profiles of the cells described in (A). **(C)** Venn diagram of differentially expressed genes in MS-derived cells from MS formed by HMLE-Snail1-ER or HMLE-Twist1-ER cells and in HMLE-Twist1-ER cells after transient Twist1-activation. The 189-gene signature represents the overlap of differentially regulated genes shared by these three groups. rest = HMLE-Twist1-ER or HMLE-Snail1-ER cells not treated with TAM and HMLE-Twist1-ER cells treated with TAM for 15 days. **(D)** Heatmap showing the top 15 up- and downregulated expression values of the 189-gene signature described in (C). Samples are labeled as described in (A). Red (high) and blue (low) indicates log2 expression values. Scale bar in log2. **(E)** Top 10 upregulated genes of the 189-gene signature generated as described in (C). The corresponding fold-changes are shown for MS-derived cells from MS formed by HMLE-Twist1-ER cells. **(F)** Significantly enriched GO-terms containing the top 10-upregulated genes of the 189-gene signature generated as described in (C).

#### 4.12 Summary of the first part

In the first part of my thesis, I showed that Twist1-activation induced mesenchymal transdifferentiation and MS-forming ability in purified epithelial cells ( $24^{neg}$  and  $24^{high}$ ). Importantly, these traits were induced independently of each other and MS-formation only emerged after subsequent Twist1-deactivation. In addition, I discovered that whereas most of the  $24^{high}$  HMLE cells retained a mesenchymal phenotype, a small subset of the cells underwent MET and acquired a hitherto unknown cell state: this cell state neither resembled those of epithelial cells before Twist1-activation nor those of mesenchymal cells with active Twist1 (Figure 13). Specifically, this subset of  $24^{high}$  HMLE cells was characterized by epithelial-mesenchymal plasticity, invasive traits in 3D collagen gels as well as a unique gene expression profile consisting of 189 genes. Since only a subset of  $24^{high}$  HMLE cells underwent MET and acquired the described “novel” cell state, I concluded that there exists cellular heterogeneity even within the FACS purified  $24^{high}$  HMLE subpopulation. Moreover, I hypothesized that a pre-existing cell state might determine how a cell responds to transient Twist1-activation.

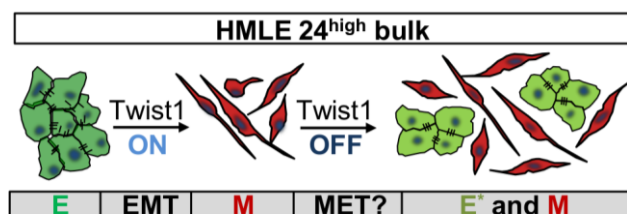


**Figure 13: Summary of the first part.**

Schematic representation: Before Twist1-activation HMLE  $24^{high}$  cells show an epithelial phenotype (E). During Twist1-activation for 15 days all  $24^{high}$  cells undergo EMT and acquire a mesenchymal phenotype (M). After subsequent Twist1-deactivation for 9 days a subset of  $24^{high}$  cells undergoes MET and acquires a unique cell state (E\*).

### **4.13 Single-cell cloning of 24<sup>high</sup> HMLE cells reveals resistance to Twist1-induced EMT**

As common metastatic models suggest that MET is required for outgrowth of cancer cells at metastatic sites (colonization), I sought to study the molecular process predisposing a cell to undergo MET. For this purpose, I set out to identify those 24<sup>high</sup> HMLE cells that were able to undergo MET after Twist1-deactivation. Since, I discovered in the first part of my thesis that even the FACS purified 24<sup>high</sup> subpopulation was heterogeneous with respect to Twist1-responsiveness, I wished to further unravel cellular heterogeneity and study the effects of Twist1 at the single cell level.

For this purpose, single-cell clones (SCCs) were isolated from the purified 24<sup>high</sup> subpopulation. Next, Twist1 was activated for 15 days in 32 isolated SCCs. During this period, 23 SCCs started to scatter and acquire a spindle-shaped, front-to-back polarized morphology, indicating transdifferentiation to a mesenchymal cell state (M-SCCs). In contrast, five SCCs retained an epithelial, cobblestone-like morphology (E-SCCs) and four SCCs (D-SCCs) died upon Twist1-activation. During subsequent Twist1-deactivation for 9 days, the E-SCCs maintained an epithelial morphology. Remarkably, all M-SCCs retained a mesenchymal morphology after TAM-withdrawal, indicating that, in contrast to bulk 24<sup>high</sup> HMLE cells, none of these SCCs underwent MET (Figure 14A).

In addition, ten representative SCCs (five E-SCCs and five M-SCCs) were analyzed by immunofluorescence 1) before Twist1-activation (–TAM), 2) after Twist1-activation (15d+TAM) and 3) after transient Twist1-activation (+/–9d TAM). Before Twist1-activation, SCCs showed high levels of membranous E-cadherin and low vimentin protein expression. Thus, all SCCs displayed an epithelial phenotype before TAM-treatment. After Twist1-activation for a period of 15 days, M-SCCs had lost membranous E-cadherin and gained high vimentin protein expression, confirming transdifferentiation to a mesenchymal phenotype. In contrast, E-SCCs retained membranous E-cadherin and low vimentin protein expression, confirming maintenance of an epithelial phenotype. After subsequent Twist1-deactivation for 9 days, none of the M-SCCs showed re-expression and membranous localization of E-cadherin or

downregulation of vimentin protein expression, indicating a stable mesenchymal transdifferentiation. E-cadherin and vimentin protein levels of the E-SCCs were not influenced by TAM-withdrawal (Figure 14B).

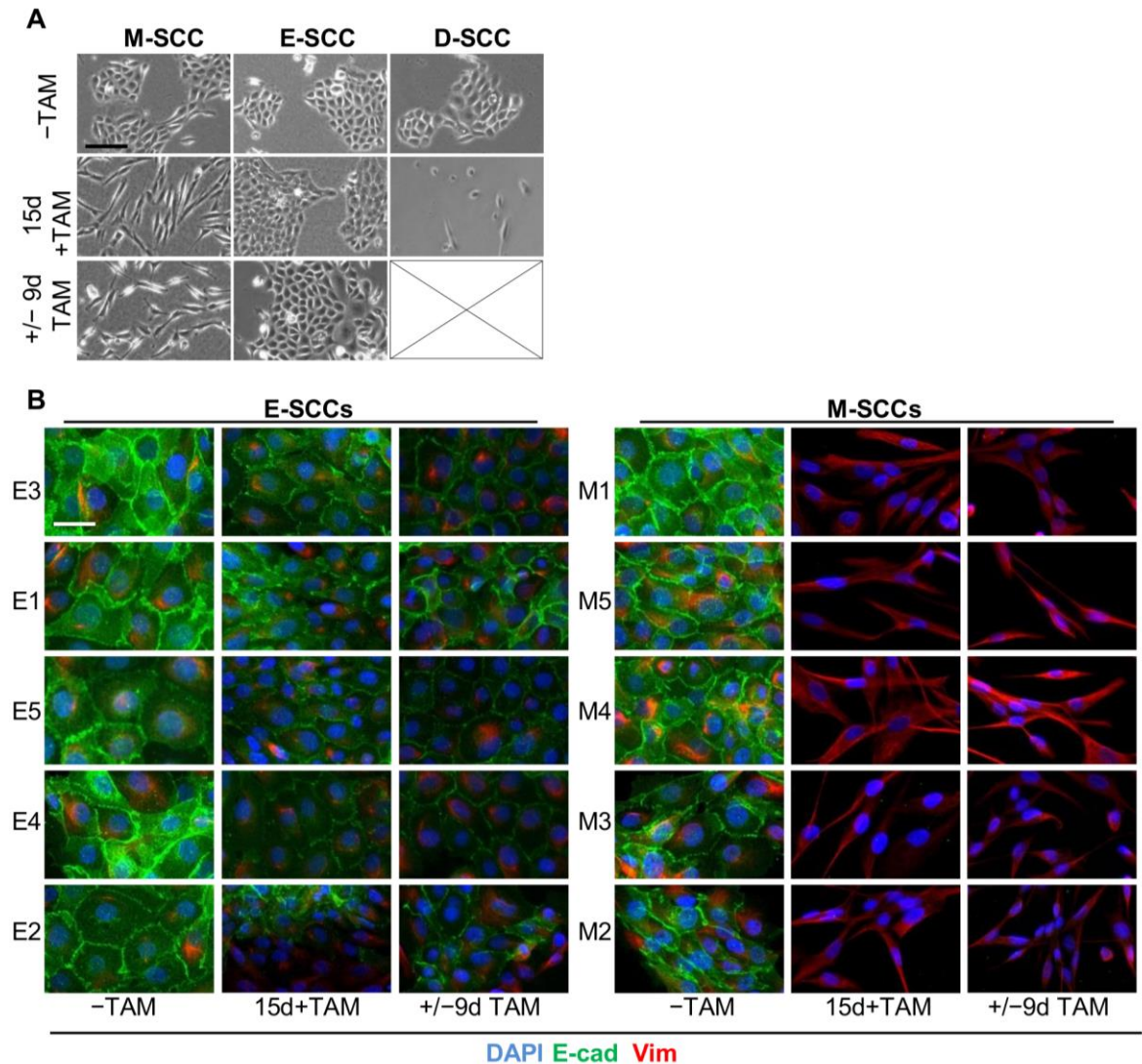


**Figure 14: Single-cell cloning of 24<sup>high</sup> HMLE cells reveals resistance to Twist1-induced EMT.**

**(A)** Representative bright-field microscopic pictures of single cell clones (SCCs) isolated from purified 24<sup>high</sup> HMLE-Twist1-ER cells. Cells were not treated with TAM (-), treated with TAM for 15 days (+TAM) or treated with TAM for 15 days followed by 9 days of TAM-withdrawal. Scale bar: 100  $\mu$ m. **(B)** Immunofluorescence staining of E-cadherin (green), vimentin (red) and DAPI (blue) of five isolated EMT resistant (E-SCC) and five isolated EMT competent (M-SCC) SCCs. Cells were treated as described in (A). Scale bar: 20  $\mu$ m.

Taken together, these data showed that Twist1 elicited different effects in SCCs isolated from 24<sup>high</sup> HMLE cells compared to 24<sup>high</sup> HMLE bulk cells. Whereas M-SCCs underwent Twist1-induced EMT and acquired a stable mesenchymal cell state (referred to as “EMT competence”), E-SCCs resisted Twist1-induced EMT

and retained an epithelial cell state (referred to as “EMT resistance”). Consequently, these data raised three main questions: 1) why did the isolated SCCs respond differentially to TAM-treatment, 2) why was EMT resistance not observed in the bulk 24<sup>high</sup> HMLE cells and 3) why was MET not detected in the isolated M-SCCs?

#### **4.14 Twist1 expression levels and Twist1 TF-activity do not differ between E-SCCs and M-SCCs**

First, I focused on the question why isolated SCCs responded differentially to TAM-treatment. The HMLE-Twist1-ER cell line was originally generated by retroviral transduction of HMLE cells with the pWZL-mTwist1-ER plasmid (Casas et al., 2011). During retroviral transductions, the copy-number and the integration sites of the plasmid DNA into the target genome are random. Based on that, I hypothesized that the isolated 24<sup>high</sup> HMLE SCCs might respond differentially to TAM-treatment due to different Twist1 expression levels. Additionally, I hypothesized that M-SCCs might express higher Twist1 levels compared to E-SCCs. To test these hypotheses, I analyzed Twist1 expression in ten representative SCCs (five E-SCCs and five M-SCCs) at transcriptional and protein level by qRT-PCR and Western-blot analysis. At the transcriptional level, Twist1 levels varied in-between the ten SCCs. However, Twist1 transcript levels were not consistently lower in E-SCCs and higher in M-SCCs. For instance, E-SCC 3, 4 and M-SCC 4 showed comparable Twist1 transcript levels (Figure 15A). Similarly, Twist1 protein levels varied in-between the ten SCCs, but were not generally higher in the EMT competent M-SCCs (Figure 15B). Thus, Twist1 expression levels did not correlate with different abilities of E-SCCs and M-SCCs to undergo EMT in response to TAM-treatment.

Upon TAM-treatment, the Twist1-ER fusion protein undergoes a conformational change that allows DNA binding and thereby TF-activity. Therefore, I set out to investigate whether Twist1 target gene expression might differ in E-SCCs and M-SCCs upon TAM-treatment. For this purpose, expression levels of the direct Twist1 target gene *Wnt5a* were assessed by qRT-PCR analysis before and after TAM-treatment (Shi et al., 2014). To quantify *Wnt5a* up-regulation, the fold changes of *Wnt5a* transcript levels were calculated. Upon TAM-treatment, all

SCCs showed upregulation of the direct Twist1 target gene *Wnt5a*. However, fold-changes in *Wnt5a* expression did not correlate with EMT resistance (E-SCCs) or EMT competence (M-SCCs) (Figure 15C).

Together, these data suggested that differences between E-SCCs and M-SCCs upon TAM-treatment did neither result from different Twist1 transcript or protein levels nor from general disparities in Twist1 TF-activity.

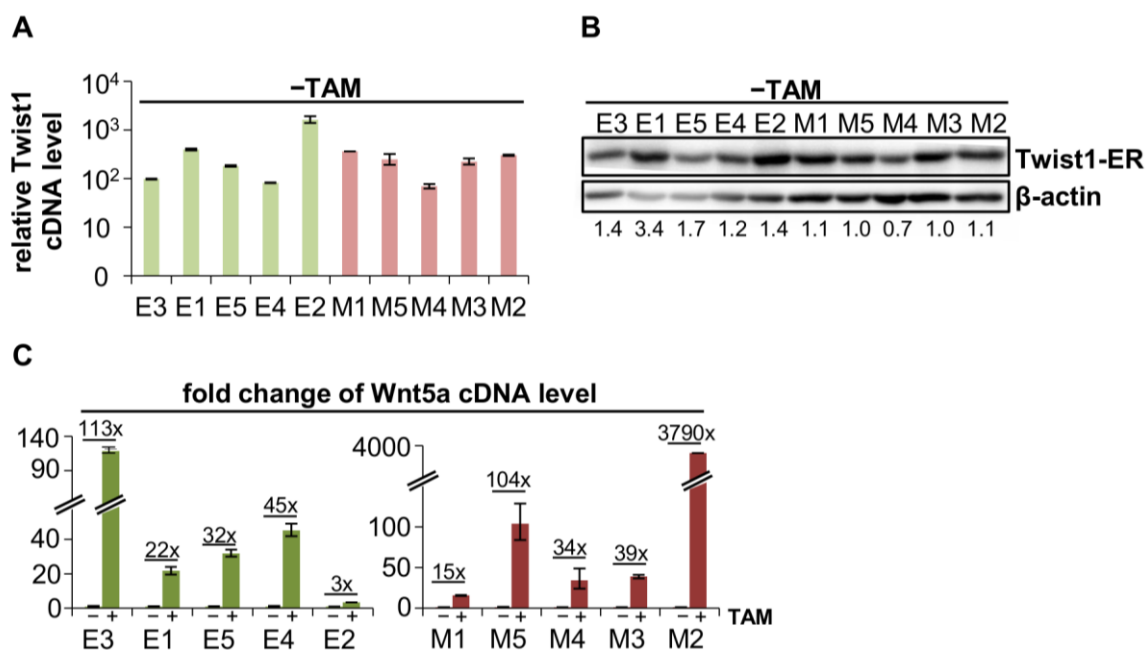


**Figure 15: Twist1 expression levels and Twist1 TF-activity do not differ between E-SCCs and M-SCCs.**

(A) Relative mRNA expression of Twist1 of E-SCCs and M-SCCs. Cells were not treated with TAM. n=3. (B) Western-blot analysis of Twist1-ER and  $\beta$ -actin in E-SCCs and M-SCCs. Cells were not treated with TAM. Twist1-ER protein levels were quantified relatively to  $\beta$ -actin. (C) Fold change of the cDNA level of *Wnt5a* of E-SCCs and M-SCCs not treated (-) versus treated with TAM for 7 days (+). n=3.

Data are presented as mean  $\pm$  SEM.

#### 4.15 Transcriptional programs in E-SCCs and M-SCCs are differentially activated upon TAM-treatment

Not only Twist1, but a set of additional EMT-TFs are involved in the regulation of the EMT-program and coordinate repression of epithelial markers (e.g. E-cadherin) as well as induction of mesenchymal markers. Since Twist1 TF-activity was equally induced in both, E-SCCs and M-SCCs, I set out to investigate

whether components of the EMT-transcriptional program might not be initiated in E-SCCs in contrast to M-SCCs.

For this purpose, the transcriptional programs of E-SCCs and M-SCCs were analyzed by qRT-PCR. Consequently, ten representative SCCs (five E-SCCs and five M-SCCs) were examined 1) before (–TAM), 2) during (7d+TAM) and 3) after long-term Twist1-activation (14d+TAM). Specifically, transcript levels of the adherens junction proteins E-cadherin and N-cadherin, the EMT-TFs ZEB1 and Slug as well as the Ovo-like zinc finger 2 TF (Ovol2) were assessed (Figure 16A). ZEB1 and Slug are direct repressors of E-cadherin, while Ovol2 represents a transcriptional repressor of the EMT-TF ZEB1 and was found to induce MET in human cancer (Roca et al., 2013; Watanabe et al., 2014). Before Twist1-activation, all SCCs expressed high levels of E-cadherin, Slug and Ovol2. ZEB1 transcript levels were nearly undetectable for all SCCs and N-cadherin transcript levels varied in-between the SCCs but did not correlate with E-SCC- or M-SCC-cell-state. Thus, with respect to these markers E-SCCs and M-SCCs did not differ from each other before Twist1-activation. During TAM-treatment, transcript levels of N-cadherin (except E-SCC 3) and Slug were consistently up-regulated in both E-SCCs and M-SCCs: after Twist1-activation for 14 days, N-cadherin transcript levels were increased by 5- to 10-fold and Slug transcript levels by 10-fold compared to untreated control cells. In contrast, E-cadherin, Ovol2 and ZEB1 transcript levels changed differentially in E-SCCs and M-SCCs upon TAM-treatment. After Twist1-activation for 14 days, E-SCCs still expressed high levels of the epithelial makers E-cadherin and Ovol2 while M-SCCs showed a 10- to 1000-fold downregulation of these markers compared to untreated control cells. Although all SCCs displayed up-regulation of ZEB1 transcript levels (100- to 1000-fold) during Twist1-activation for 14 days, ZEB1 transcript levels strongly varied between E-SCCs and M-SCCs at day 7 after Twist1-activation (Figure 16A). To quantify ZEB1 up-regulation at day 7 more precisely, fold-changes of ZEB1 transcript levels were calculated. Whereas ZEB1 transcript levels increased 3- to 6-fold in E-SCCs, a 30- to 70-fold increase of ZEB1 levels was revealed in M-SCCs upon TAM-treatment (Figure 16B). Next, I investigated whether differences in ZEB1 up-regulation between E-SCCs and M-SCCs were detectable at the protein level as well. For this purpose, Western-blot analysis

was performed for ten SCCs after TAM-treatment for 7 days. None of the E-SCCs showed ZEB1 protein expression. In contrast, M-SCCs (except M-SCC 1) showed robust ZEB1 expression at the protein level (Figure 16C). Of note, ZEB1 protein levels correlated with ZEB1 transcript levels (Figure 16A).

In summary, qRT-PCR analysis indicated that the transcriptional programs of EMT resistant (E-SCCs) and EMT competent (M-SCCs) SCCs are activated differentially upon Twist1-activation. Loss of E-cadherin and Ovol2 expression as well as strong ZEB1 up-regulation (at day 7) correlated with mesenchymal transdifferentiation, while maintenance of high E-cadherin and Ovol2 transcript levels as well as delayed ZEB1 up-regulation correlated with EMT resistance.

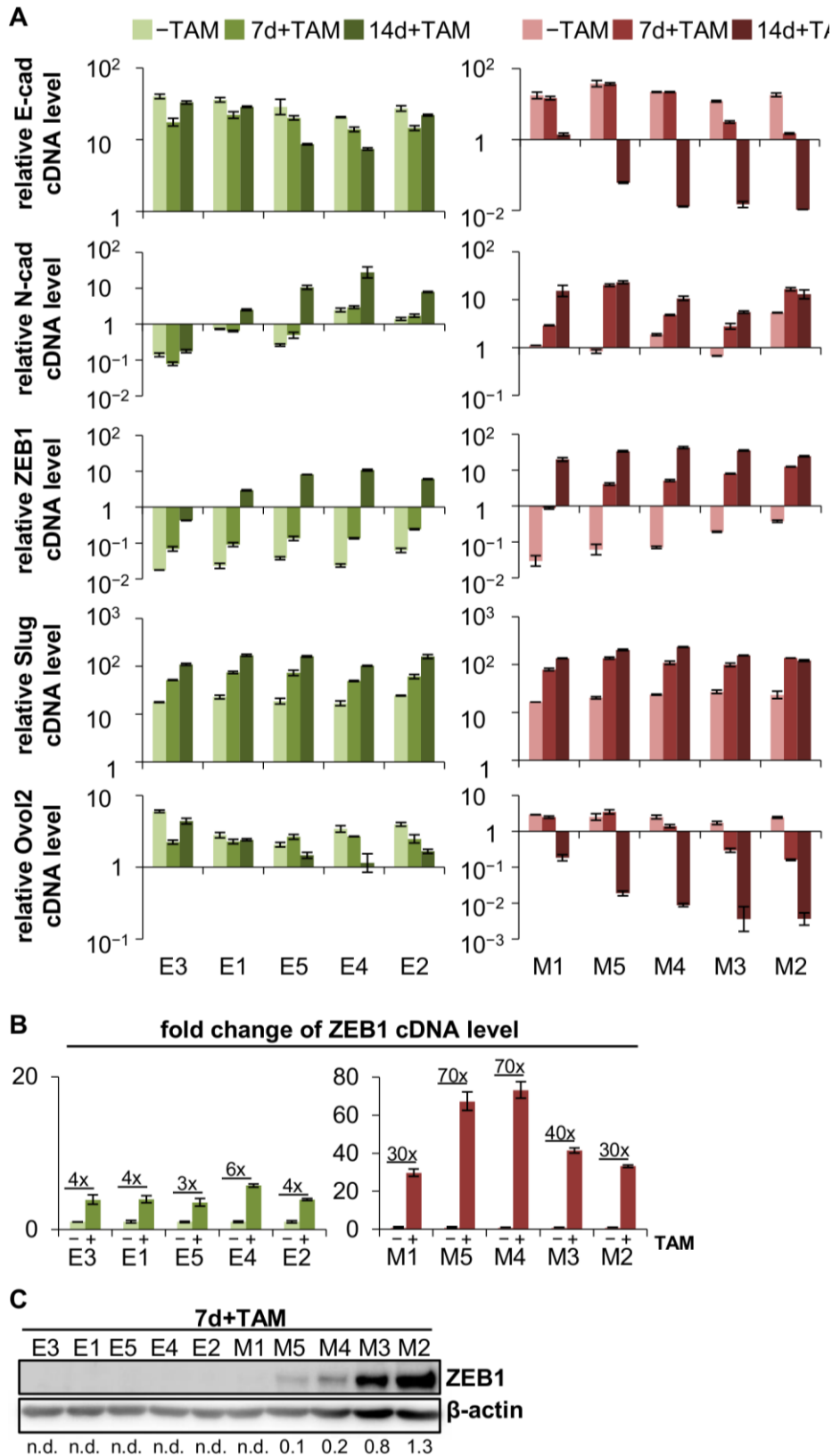


**Figure 16: Transcriptional programs in E-SCCs and M-SCCs are differentially activated upon TAM-treatment.**

(A) Relative mRNA expression of E-cadherin, N-cadherin, ZEB1, Slug and Ovol2 of E-SCCs (left panel) and M-SCCs (right panel). Cells were not treated (-TAM; light green/red) or treated with TAM for 7 days (7d+TAM; middle green/red) or 14 days (14d+TAM; dark green/red). n=3. (B)

Fold changes of the cDNA levels of ZEB1 of E-SCCs and M-SCCs not treated (-) versus treated with TAM for 7 days (+). n=3. **(C)** Western-blot analysis of ZEB1 and  $\beta$ -actin of E-SCCs and M-SCCs treated with TAM for 7 days (7d+TAM). ZEB1 protein levels were quantified relatively to  $\beta$ -actin.

Data are presented as mean  $\pm$  SEM.

### **4.16 By morphology, EMT resistant cells cannot be distinguished from EMT competent cells in co-culture**

Next, I focused on the following questions: 1) why could EMT resistant cells not be detected in the 24<sup>high</sup> HMLE bulk population cells during Twist1-activation for a period of 15 days and 2) why was MET not observed in the isolated M-SCCs after transient Twist1-activation.

Since the majority of isolated SCCs were M-SCCs (23 of 32 SCCs), I assumed that more M-SCCs than E-SCCs existed within the bulk 24<sup>high</sup> HMLE population. Based on this consideration, I developed the following hypothesis (Figure 17A): a single EMT resistant cell (\*) is surrounded by EMT competent cells. Before Twist1-activation, all HMLE cells express E-cadherin allowing the assembly of adherens junctions (I). Of note, E-cadherin protein stability is provided through heterotypic interactions with other cells expressing E-cadherin. Otherwise, adherens junctions cannot be established. I speculated that during TAM-treatment, E-cadherin expression is downregulated in EMT competent cells, which surround EMT resistant cells. Adherens junctions are dissolved and both, EMT competent and EMT resistant cells gain a single-cell state (II and III). After subsequent Twist1-deactivation, EMT resistant cells reassemble adherens junctions with their respective daughter cells and become morphologically distinguishable from surrounding mesenchymal cells (IV and V). To test this hypothesis, one representative E-SCC (E3) was transduced lentivirally with the pRRL-cPPT-CMV-GFP-W vector and mixed with one unlabeled representative M-SCC (M3) at a ratio of one E-SCC cell (GFP<sup>pos</sup>) per ten M-SCC cells (GFP<sup>neg</sup>) (Figure 17B). First, cells were analyzed by immunofluorescence before (-TAM) and after Twist1-activation (14d+TAM). Before Twist1-activation, GFP<sup>pos</sup> and GFP<sup>neg</sup> cells showed membranous E-cadherin and low vimentin protein expression. During TAM-treatment, both GFP<sup>pos</sup> and GFP<sup>neg</sup> cells acquired a

spindle-shaped morphology and high vimentin protein expression, while E-cadherin expression was lost (Figure 17C).

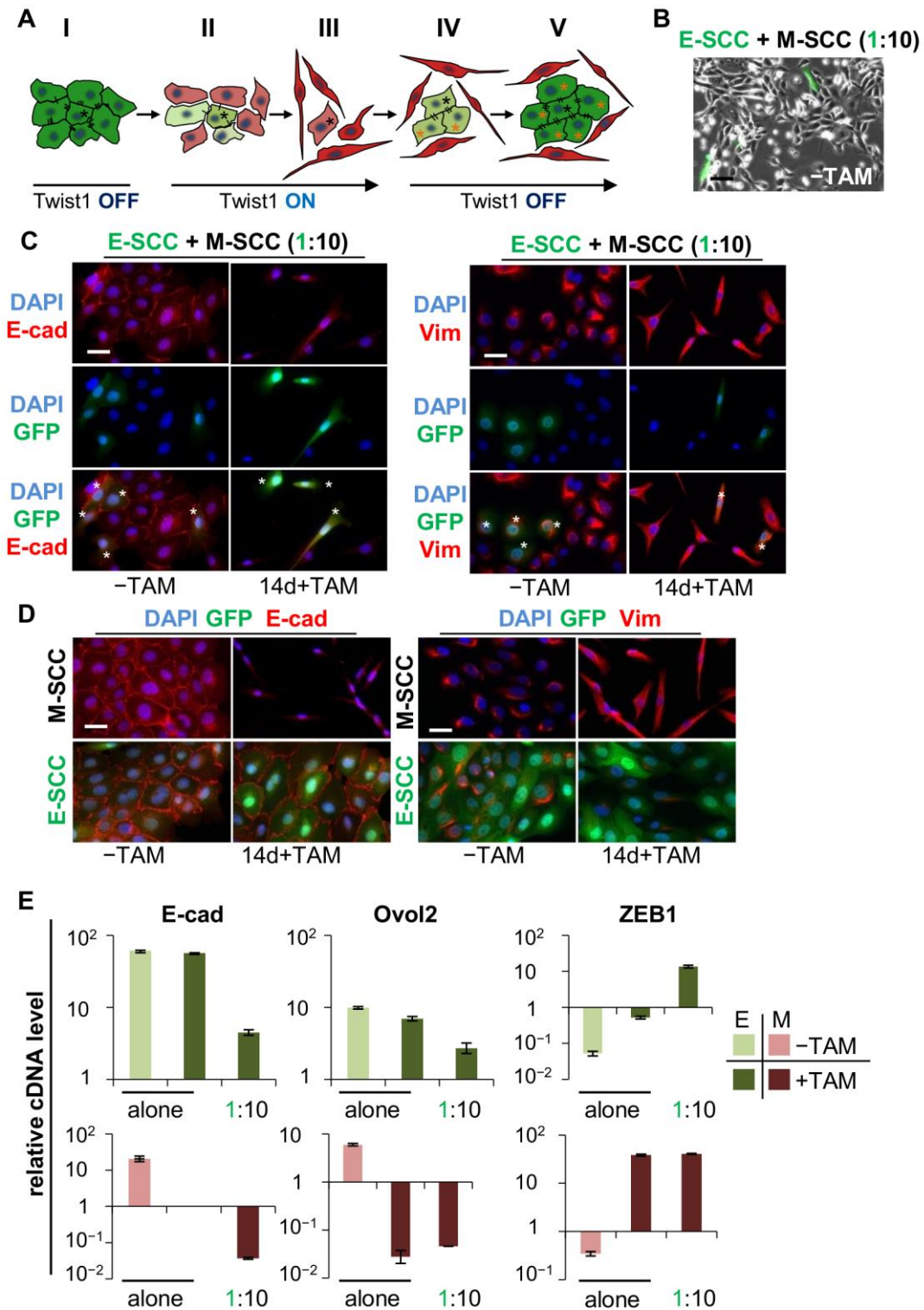


**Figure 17** By morphology, EMT resistant cells cannot be distinguished from EMT competent cells in co-culture.

(A) Schematic representation: I) Before Twist1-activation, all  $24^{\text{high}}$  HMLE cells show an epithelial phenotype (\* indicates an EMT resistant cell). II) During Twist1-activation, EMT competent cells undergo EMT and cell-cell contacts become degraded. III) After 14 days of Twist1-activation,

## Results

---

EMT resistant and EMT competent cells are morphologically indistinguishable. IV) and V) After Twist1-deactivation EMT competent cells retain a mesenchymal phenotype and EMT resistant cells become morphologically distinguishable. **(B)** Representative bright-field microscopic pictures of the co-culture of GFP-labeled EMT resistant cells (green, E-SCC) and un-labeled (GFP<sup>neg</sup>) EMT competent cells (M-SCC) not treated with TAM (-TAM). (plating ratio: one E-SCC cell per ten M-SCC cells). Scale bar: 100  $\mu$ m. **(C)** Immunofluorescence staining of E-cadherin (red; left panel) or vimentin (red; right panel) and DAPI (blue) of co-cultured E-SCC (green; indicated by \*) and M-SCC cells (plating ratio: one E-SCC cell per ten M-SCC cells). Cells were not treated (-TAM) or treated with TAM for 14 days (14d+TAM) Scale bar: 20  $\mu$ m. **(D)** Immunofluorescence staining of E-cadherin (red; upper panel) or vimentin (red; lower panel) and DAPI (blue) of one E-SCC (green; indicated by \*) and one M-SCC cultured alone. Cells were treated as described in (C). Scale bar: 20  $\mu$ m. **(E)** Relative mRNA expression of E-cadherin, *Ovol2* and *ZEB1* of SCCs treated as described in (C). Cells were either cultured alone or together (plating ratio: one E-SCC cell per ten M-SCC cells). n=3.

Data are presented as mean  $\pm$  SEM.

In addition, unlabeled GFP<sup>neg</sup> M-SSC and labeled GFP<sup>pos</sup> E-SCC cells were separately cultured as controls and monitored during Twist1-activation. During TAM-treatment, separately cultured GFP<sup>pos</sup> E-SCC cells retained high E-cadherin expression and low vimentin protein expression. In contrast, separately cultured GFP<sup>neg</sup> M-SSC cells lost E-cadherin expression and obtained high vimentin protein expression (Figure 17D). In addition, cells were analyzed for transcript levels of E-cadherin, *Ovol2* and *ZEB1* after 14 days of TAM-treatment. For this purpose, co-cultured GFP<sup>pos</sup> E-SCC and GFP<sup>neg</sup> M-SSC cells were separated by FACS prior to RNA extraction, cDNA synthesis and qRT-PCR analysis. Transcript levels of E-cadherin, *Ovol2* and *ZEB1* did not differ between co-cultured or separately cultured M-SSC cells after Twist1-activation for 14 days. Thus, M-SSC cells were not inhibited in their ability to undergo EMT by the presence of E-SCC cells. By contrast, transcript levels of E-cadherin and *Ovol2* were reduced by 50% in E-SCC cells when co-cultured with M-SSC cells during Twist1-activation. Moreover, co-cultured E-SCC cells showed 10-fold higher *ZEB1* transcript levels than separately cultured E-SCC cells after Twist1-activation for 14 days. In conclusion, expression of E-cadherin, *Ovol2* and *ZEB1* were influenced by co-culture of E-SCC with M-SSC cells. Specifically, these markers were regulated in the same direction as in M-SSC cells, but to a lesser extent. Thus, even after co-culture, *ZEB1* transcript levels merely increased to 20% of the level observed for the M-SSC (Figure 17E).

The second part of the hypothesis suggested that EMT resistant cells grow out after Twist1-deactivation and become distinguishable from surrounding mesenchymal cells. To test this part of the hypothesis, co-cultured cells were analyzed after transient Twist1-activation (14d+TAM and 9d-TAM) by immunofluorescence. After TAM-withdrawal, only GFP<sup>pos</sup> cells acquired a cobblestone-like morphology and were detected to grow in epithelial islands. Moreover, GFP<sup>pos</sup> cells re-expressed E-cadherin and showed reduced vimentin protein expression. In contrast, GFP<sup>neg</sup> M-SCC cells retained a spindle-shaped morphology, lack of E-cadherin expression and high vimentin protein expression (Figure 18).

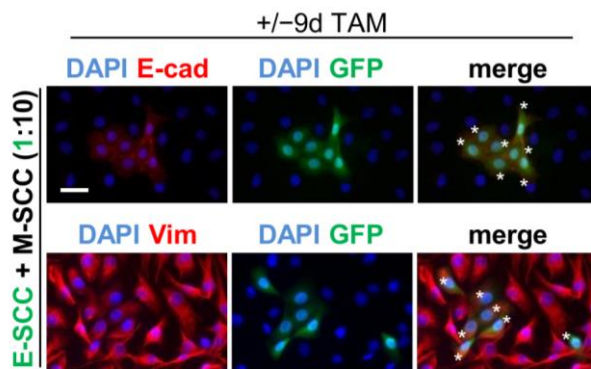


**Figure 18: EMT resistant cells reappear as epithelial islands after Twist1-deactivation.**

Immunofluorescence staining of E-cadherin (red; upper panel) or vimentin (red; lower panel) and DAPI (blue) of co-cultured E-SCC (green; indicated by \*) and M-SCC cells (plating ratio: one E-SCC cell per ten M-SCC cells). Cells were treated with TAM for 14 days followed by 9 days of TAM-withdrawal (+/-9d TAM).

Together, these data suggested that EMT resistant cells were present but not detectable within the 24<sup>high</sup> HMLE bulk population as they were morphologically indistinguishable from surrounding EMT competent cells following Twist1-activation. Moreover, these data indicated that the transcriptional EMT-program (ZEB1 up-regulation and E-cadherin as well as Ovol2 down-regulation) was not induced in E-SCCs to the same extent as in M-SCCs. Therefore, EMT resistant cells partially retained their epithelial cell state during Twist1-activation. Finally, “reappearance” of epithelial islands, consisting of E-SCC cells, suggested that MET observed for the bulk 24<sup>high</sup> cells was based on EMT resistant cells that became morphologically distinguishable once more after Twist1-deactivation.

### **4.17 ZEB1-induction is required for Twist1-mediated EMT in 24<sup>high</sup> HMLE cells**

Figure 16 showed that the EMT-TF ZEB1 was highly up-regulated at the transcriptional and protein level in M-SCCs but not in E-SCCs after TAM-treatment for 7 days. Moreover, co-culture with EMT competent cells did not increase ZEB1 transcript levels of E-SCCs to the same extent as observed for M-SCCs (Figure 17E). Therefore, I hypothesized that ZEB1-induction might be required for Twist1-mediated EMT in 24<sup>high</sup> HMLE cells. To test this hypothesis, a shRNA-mediated knockdown of ZEB1 was performed. Since M-SCC 2 showed the highest ZEB1 protein levels amongst the five M-SCCs (7 days after Twist-activation), this clone was chosen as a representative. M-SCC cells were transduced lentivirally with plasmid DNA encoding GFP and additionally either a shRNA targeting ZEB1 (sh1, sh2) or a non-targeting control shRNA (sh-nt). Of note, even in the absence of Twist1-activity, cells expressing the non-targeting shRNA showed a spindle-shaped morphology, suggesting that either the lentiviral transduction process itself or the non-targeting shRNA induced mesenchymal transdifferentiation of these cells. Importantly, M-SCC cells expressing shRNAs targeting ZEB1 retained an epithelial morphology (Figure 19A). To determine knockdown efficiency of the shRNAs targeting ZEB1, qRT-PCR and Western-blot analysis were performed. Cells expressing shRNAs targeting ZEB1 showed a greater than 90% reduction in ZEB1 transcript levels compared to cells expressing the non-targeting shRNA (Figure 19B). Accordingly, at the protein level, cells expressing sh1 or sh2 showed ZEB1 protein reduction by about 90% compared to cells expressing the non-targeting shRNA (Figure 19C). In addition, lentivirally transduced cells were analyzed for E-cadherin and vimentin protein expression by immunofluorescence. Cells expressing a shRNA targeting ZEB1 (sh1 or sh2) showed high levels of membranous E-cadherin and low vimentin protein expression. In contrast, cells expressing the non-targeting shRNA did not express E-cadherin, but displayed high vimentin protein expression (Figure 19D). During Twist1-activation for 14 days, cells expressing shRNAs targeting ZEB1 (sh1 or sh2) retained high E-cadherin and low vimentin protein expression, while cells expressing the non-targeting control shRNA retained lack of E-cadherin expression and high vimentin protein levels (Figure 19E).

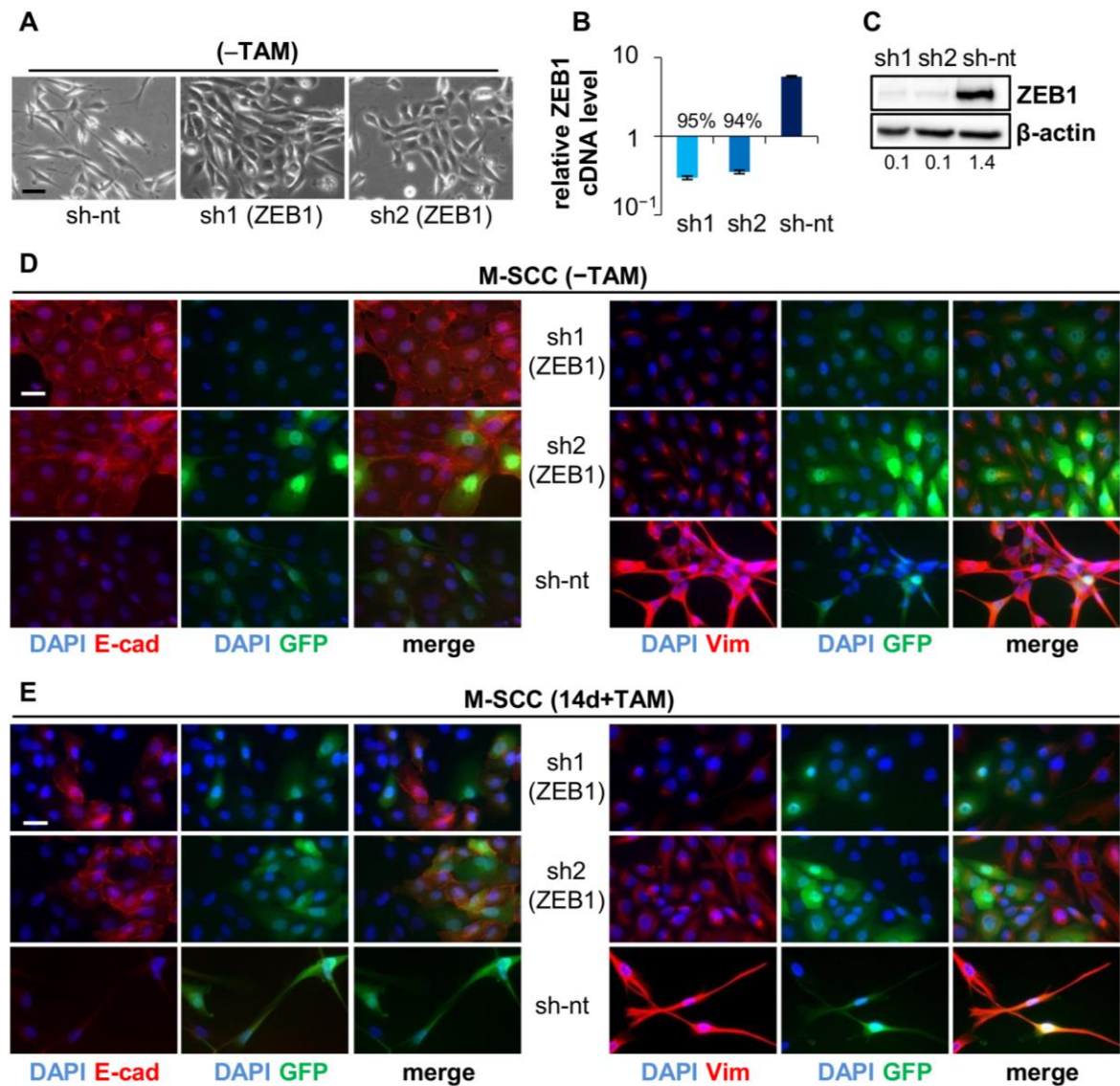


**Figure 19: ZEB1-induction is required for Twist1-mediated EMT in 24<sup>high</sup> HMLE cells.**

(A) Representative bright-field microscopic pictures of one M-SCC expressing non-targeting control shRNA (sh-nt) or shRNA targeting ZEB1 (sh1 or sh2). Cells were not treated with TAM (-TAM). Scale bar: 50  $\mu$ m. (B) Relative mRNA expression of ZEB1 of one M-SCC expressing shRNA targeting ZEB1 (sh1 or sh2) or non-targeting control shRNA (sh-nt). Cells were not treated with TAM. n=3. Percentages indicate ZEB1 knockdown compared to non-targeting control. (C) Western-blot analysis of ZEB1 and  $\beta$ -actin of one M-SCC expressing shRNA targeting ZEB1 (sh1 or sh2) or non-targeting control (sh-nt). Cells were not treated with TAM. ZEB1 protein levels were quantified relatively to  $\beta$ -actin. (D) Immunofluorescence staining of E-cadherin (red; left panel) or vimentin (red; right panel) and DAPI (blue) of one M-SCC expressing shRNA targeting ZEB1 (sh1 or sh2) or non-targeting control shRNA (sh-nt). shRNA expressing cells are labeled with GFP. Cells were not treated with TAM. Scale bar: 20  $\mu$ m. (E) Immunofluorescence staining of E-cadherin (red; left panel) or vimentin (red; right panel) and DAPI (blue) of one M-SCC expressing shRNA targeting ZEB1 (sh1 or sh2) or non-targeting control shRNA (sh-nt). shRNA expressing cells are labeled with GFP. Cells were treated with TAM for 14 days. Scale bar: 20  $\mu$ m.

Data are presented as mean  $\pm$  SEM.

In summary, these results showed that knockdown of ZEB1 was sufficient to prevent Twist1-induced EMT and demonstrated that upregulation of ZEB1 was required for Twist1-induced EMT. Consequently, these data raised the question why ZEB1 expression was differentially upregulated in M-SCCs and E-SCCs.

### **4.18 Twist1-binding to a putative enhancer region of *ZEB1* differs in M-SCCs and E-SCCs**

Using the HMLE-Twist1-ER cell line, our group recently discovered that Twist1 binds to a region 7.2 kb upstream of the transcriptional start site (TSS) of *ZEB1*, thereby inducing ZEB1 transcription and EMT (Dragoi et al., 2016). Of note, this region upstream of the TSS of *ZEB1* was identified through a recently published ChIP-sequencing data set of Twist1 (Chang et al., 2015). Based on these observations, I hypothesized that Twist1 might differentially bind to this putative enhancer region of *ZEB1* in M-SCCs and E-SCCs. To address this hypothesis, chromatin immunoprecipitation (ChIP) analysis was performed in collaboration with Dr. Vivek K. Mishra from the Department of General, Visceral and Pediatric Surgery at the University Medical Center Göttingen. ChIP analysis was performed for three E-SCCs and three M-SCCs, each before and after 7 days of Twist1-activation. To quantify Twist1-occupancy at the described region upstream of the *ZEB1* TSS, qRT-PCR analysis was performed for a DNA locus around this region (ZEB1\_+ve site). As a control, qRT-PCR analysis was performed for a DNA locus, not described to be bound by Twist1 (ZEB1\_-ve site). In untreated SCCs, ChIP did not enrich for the ZEB1\_+ve site, indicating that Twist1 was not bound to this region. In TAM-treated SCCs, ChIP enriched for the ZEB1\_+ve site (0.03% of the input for the E-SCCs and 0.12% of the input for the M-SCCs). Specifically, TAM-treatment increased Twist1-occupancy at the ZEB1\_+ve site 4-fold more in the M-SCCs than E-SCCs. At the ZEB1\_-ve site, no detectable differences between the analyzed conditions were detected (Figure 20).

In summary, these data suggested that Twist1-binding to a putative enhancer region of *ZEB1* was different for E-SCCs and M-SCCs: after TAM-treatment for 7 days, Twist1 was binding to this region more efficiently in M-SCCs compared to

E-SCCs. Based on that observation, I concluded that differential Twist1-binding to a putative enhancer region of *ZEB1* resulted in differential up-regulation of *ZEB1* and thereby either in EMT resistance or mesenchymal transdifferentiation.

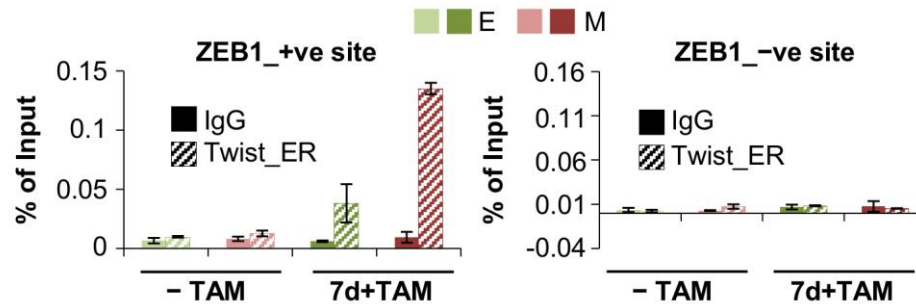


**Figure 20: Twist1-binding to a putative enhancer region of *ZEB1* differs in M-SCCs and E-SCCs.**

Chromatin Immunoprecipitation analyses of E-SCCs and M-SCCs not treated (light green/red) or treated with TAM (dark green/red) for 7 days. Data indicate percentage (%) of input. For each E-SCC and M-SCC the mean of three SCCs is shown.

Data are presented as mean  $\pm$  SD.

#### 4.19 E-SCCs and M-SCCs do not respond differentially to TGF $\beta$ 1

Figure 20 suggested Twist1 to be differentially bound to a putative enhancer region of *ZEB1* in M-SCCs and E-SCCs upon TAM-treatment. Therefore, I set out to investigate why more Twist1 was bound to this region in M-SCCs compared to E-SCCs. In addition to the discovery that Twist1 binds to this region upstream of the *ZEB1* TSS in HMLE cells, our group recently determined that Twist1-binding depends on active TGF $\beta$ -signaling and could be increased by adding additional recombinant TGF $\beta$ 1 (Dragoi, et al., 2016). Based on these data, I hypothesized that responsiveness to TGF $\beta$ -ligand might differ in M-SCCs and E-SCCs. To test this hypothesis, three E-SCCs and three M-SCCs were treated with recombinant TGF $\beta$ 1 for 30 minutes or 3 hours and phosphorylation of Smad2/3 (p-Smad2/3) was assessed by Western-blot analysis. TGF $\beta$ 1-treatment for 30 minutes strongly increased Smad2/3-phosphorylation in all representative SCCs, while p-Smad2/3 levels decreased in all SCCs 3 hours after TGF $\beta$ 1-treatment (Figure 21A). In addition, I analyzed whether expression of TGF $\beta$  target genes was equally induced in E-SCCs and M-SCCs. For this purpose, transcript levels of fibronectin and N-cadherin were determined by qRT-

PCR analysis in one representative E-SCC (E3) and one representative M-SCC (M3) treated with TGF $\beta$ 1 for 7 days. In both SCCs, TGF $\beta$ 1-treatment increased transcript levels of fibronectin and N-cadherin 10-fold compared to untreated control cells (Figure 21B).

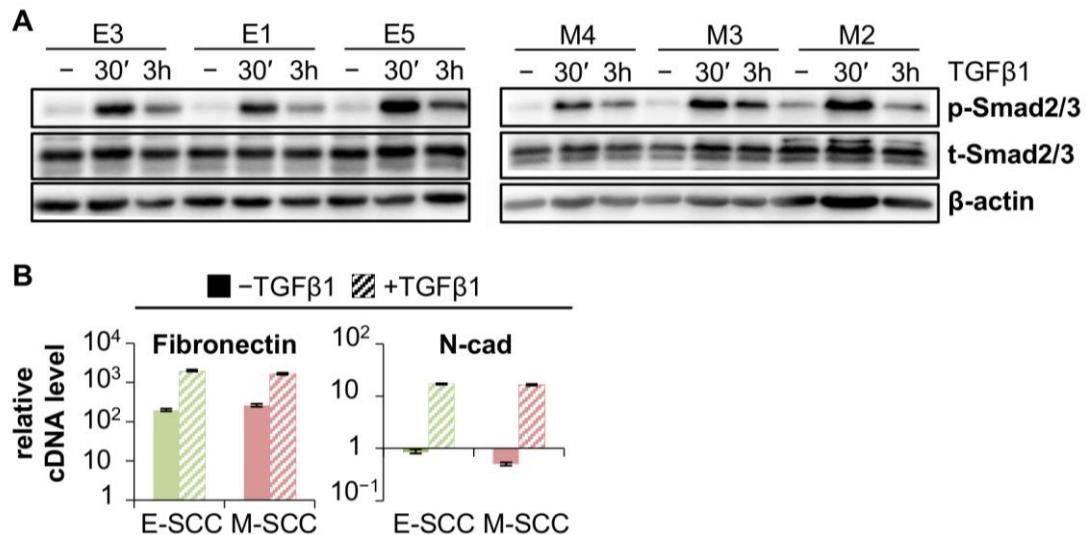


**Figure 21: E-SCCs and M-SCCs do not respond differentially to TGF $\beta$ 1.**

**(A)** Western-blot analysis of phospho-Smad2/3 (p-Smad2/3), total Smad2/3 (t-Smad2/3) and  $\beta$ -actin of E-SCCs (left panel) and M-SCCs (right panel) not treated, treated for 30 min or treated for 3 hours with TGF $\beta$ 1. **(B)** Relative mRNA expression of fibronectin and N-cadherin of one E-SCC (green) and one M-SCC (red) not treated (-TGF $\beta$ 1, filled bars) or treated with TGF $\beta$ 1 (+TGF $\beta$ 1, striped bars) for 7 days. n=3.

Data are presented as mean  $\pm$  SEM.

Together, these results suggested that E-SCCs and M-SCCs did not respond differentially to TGF $\beta$ 1-treatment. More precisely, Smad-dependent TGF $\beta$ -signaling was activated to a comparable degree in both E-SCCs and M-SCCs. Therefore, I concluded that differential Twist1-binding to the putative enhancer region of *ZEB1* was not based on different induction of the Smad-dependent TGF $\beta$ -signaling in E-SCCs and M-SCCs. Consequently, the question remained which factor(s) mediate differentially binding of Twist1 to this region in E-SCCs and M-SCCs. There are multiple scenarios that might mechanistically explain the differential Twist1-binding in E-SCCs and M-SCCs. For instance, differences in the epigenetic landscape or Smad-independent signaling could result in differential Twist1-binding. These possibilities were not addressed in this thesis, but will be examined in future studies.

### **4.20 EMT resistant and EMT competent cells show differential expression of cell surface proteins**

Upstream of epigenetic regulation and regulation by transcription factors, the transcriptional program of cells is often influenced by extracellular signaling, which might depend on ligand-receptor interactions or on interaction of cell-surface proteins present on different cells. Based on these considerations, I set out to determine whether differential extracellular signaling might provide an explanation for the differential response of E-SCCs and M-SCCs to Twist1-activation.

To examine which cell surface proteins might be differentially expressed in E-SCCs and M-SCCs, cell surface protein expression was determined for three E-SCCs and three M-SCCs, each before and after 7 days of Twist1-activation. For this purpose, glycosyl residues of cell-surface proteins were labelled and enriched with streptavidin beads. Cell surface proteomics were performed in collaboration with the laboratory of Dr. Stefanie Hauck from the Research Unit Protein Science at the Helmholtz Center Munich. In this approach, a total of 961 different cell surface proteins were identified on E-SCCs and M-SCCs. The data were filtered for those proteins that were already higher expressed on E-SCCs than M-SCCs before Twist1-activation (E/M ratio (-TAM) >1) and remained higher expressed on E-SCCs compared to M-SCCs upon TAM-treatment (E/M ratio (+TAM) >1). To identify proteins that were persistently differentially expressed on E-SCCs compared to M-SCCs, (even after Twist1-activation) proteins were sorted for E/M ratio (+TAM) (Figure 22A). Amongst the most differentially expressed proteins the epithelial cell adhesion molecules EpCAM and TACSTD2 (also named trophoblast antigen 2, Trop2) as well as desmoglein 3 (Dsg3), a glycoprotein component of desmosomes, were identified. Interestingly, for EpCAM and Dsg3 the E/M ratio increased by 55% and 67%, respectively, upon TAM-treatment. Thus, these proteins were differentially regulated in E-SCCs and M-SCCs after Twist1-activation. For validation, FACS analyses were performed for one E-SCC (E3) and one M-SCC (M3) before and after 7 days of Twist1-activation. For both EpCAM as well as TACSTD2, FACS staining confirmed higher expression on the E-SCC than M-SCC before and after

## Results

TAM-treatment (Figure 22B). FACS analysis for Dsg3 will be performed in future studies.

**A**

Gene symbol	Gene Description	ratio E/M (-TAM)	ratio E/M (+TAM)
EPCAM	epithelial cell adhesion molecule	2.50	4.63
TACSTD2	tumor-associated calcium signal transducer 2	5.08	4.45
DSG3	desmoglein 3	1.89	2.83
MST1R	macrophage stimulating 1 receptor	2.25	2.72
CA9	carbonic anhydrase IX	2.94	2.27
ADAM10	metallopeptidase domain 10	2.79	2.21
ITGB4	integrin, beta 4	2.01	2.20
TFRC	transferrin receptor	2.84	1.92
FAM49B	family with sequence similarity 49, member B	1.99	1.73
LDLR	low density lipoprotein receptor	2.44	1.71

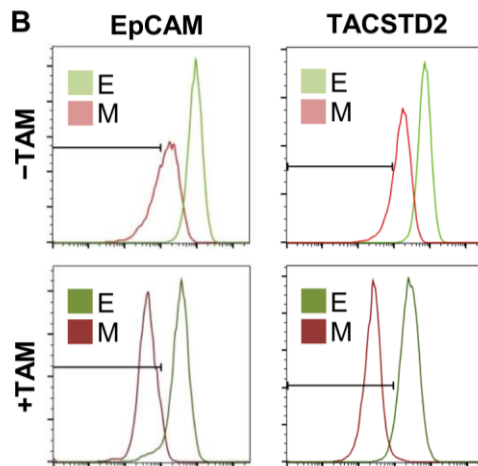


**Figure 22: EMT resistant and EMT competent cells show differential expression of cell surface proteins.**

**(A)** Top 10 upregulated cell surface proteins according to proteomics screen. Data were filtered for a peptide count of at least five, proteins with confidence score less than 100 were excluded and data were sorted for those proteins with a ratio >1 between E-SCCs versus M-SCCs before and after TAM-treatment. Values represent mean ratios for three E-SCCs or three M-SCCs, respectively. **(B)** Overlaid histogram of FACS analysis based on the surface protein EpCAM (left panel) or TACSTD2 (right panel) of one E-SCC and one M-SCC not treated with TAM (upper panel) or treated with TAM for 7 days (lower panel). Gates were set according to unstained negative control (not shown).

In summary, by cell surface proteomics I was able to identify cell surface proteins that were differentially expressed in E-SCCs and M-SCCs before and after Twist1-activation. The functional relevance of these identified cell-surface proteins will be addressed in future studies.

### **4.21 Functional relevance**

In parallel to mechanistic studies, I performed functional studies on EMT resistant and EMT competent SCCs. Based on the findings in the first part of my thesis, showing that 24<sup>high</sup> HMLE bulk cells lost colony forming ability in 3D collagen gels upon transdifferentiation to a stable mesenchymal cell state, I hypothesized that EMT resistant but not EMT competent SCCs might maintain proliferation and colony forming ability in 3D environments during Twist1-activation.

#### **4.21.1 Maintenance of an epithelial cell state is required for colony formation of 24<sup>high</sup> HMLE cells in 3D collagen gels**

To test the hypothesis that EMT resistant but not EMT competent SCCs maintain proliferation in 3D environments during Twist1-activation, five E-SCCs and five M-SCCs were analyzed for colony formation in collagen gels before and after Twist1-activation. For quantification of colony forming cells, carmine staining was performed (Figure 23A). Before Twist1-activation, both E-SCC and M-SCC cells colonized the collagen gels with similar efficiency. After Twist1-activation, E-SCC cells still formed colonies in 3D. In contrast, all M-SCCs completely lost colony forming ability (Figure 23B). In addition, I wished to analyze whether loss of colony forming ability of the M-SCCs was due to stable mesenchymal transdifferentiation during Twist1-activation. Moreover, I sought to investigate whether transient Twist1-activation induced invasive traits in SCCs as observed for the bulk 24<sup>high</sup> HMLE cells. For this purpose, colonies generated by E-SCC and M-SCC cells were assessed by immunofluorescence and subsequent confocal microscopy for expression of the mesenchymal markers vimentin and ZEB1. Before Twist1-activation, colonies formed by E-SCCs showed smooth margins and a basal layer of vimentin positive cells, suggesting a non-invasive cell state. In contrast, colonies formed by M-SCCs differed slightly: highly vimentin positive single cells were detected to detach from the margins of the colonies. Thus some M-SCC cells displayed invasive traits even before Twist1-activation (Figure 23C). Moreover, neither E-SCC nor M-SCC control cells showed ZEB1 expression (Figure 23D). Since ZEB1 is marker for mesenchymal cells, these data suggested that both, E-SCCs and M-SCCs displayed an epithelial cell state before Twist1-activation. After transient Twist1-activation,

colonies formed by E-SCCs were still characterized by a basal layer of vimentin positive cells. However, I also detected single cells, detaching from the margins of the E-SCC colonies, characterized by strong vimentin protein expression (Figure 23C). Consequently, transient Twist1 induced invasive traits in E-SCC cells. M-SCC cells were detected as dispersed, single cells displaying high vimentin protein expression. Moreover, single invading M-SCC cells showed high protein expression of ZEB1, while no ZEB1 protein expression was detectable for E-SCC cells, indicating that M-SCC cells were characterized by a mesenchymal cell state while even invasive E-SCC cells did not display a mesenchymal phenotype (Figure 23D).

Together, these data suggested that EMT resistance enabled 24<sup>high</sup> HMLE cells to retain colony forming ability and acquire invasive traits in 3D collagen gels after Twist1-activation. In contrast, EMT competence resulted in increased invasiveness but a lack of 3D colony formation. Consequently, these results confirmed the observations from the bulk 24<sup>high</sup> HMLE cells, demonstrating that stable mesenchymal transdifferentiation resulted in invasive traits and a loss of 3D colony formation, while (partial) maintenance of an epithelial cell state resulted in invasive 3D growth after Twist1-activation.

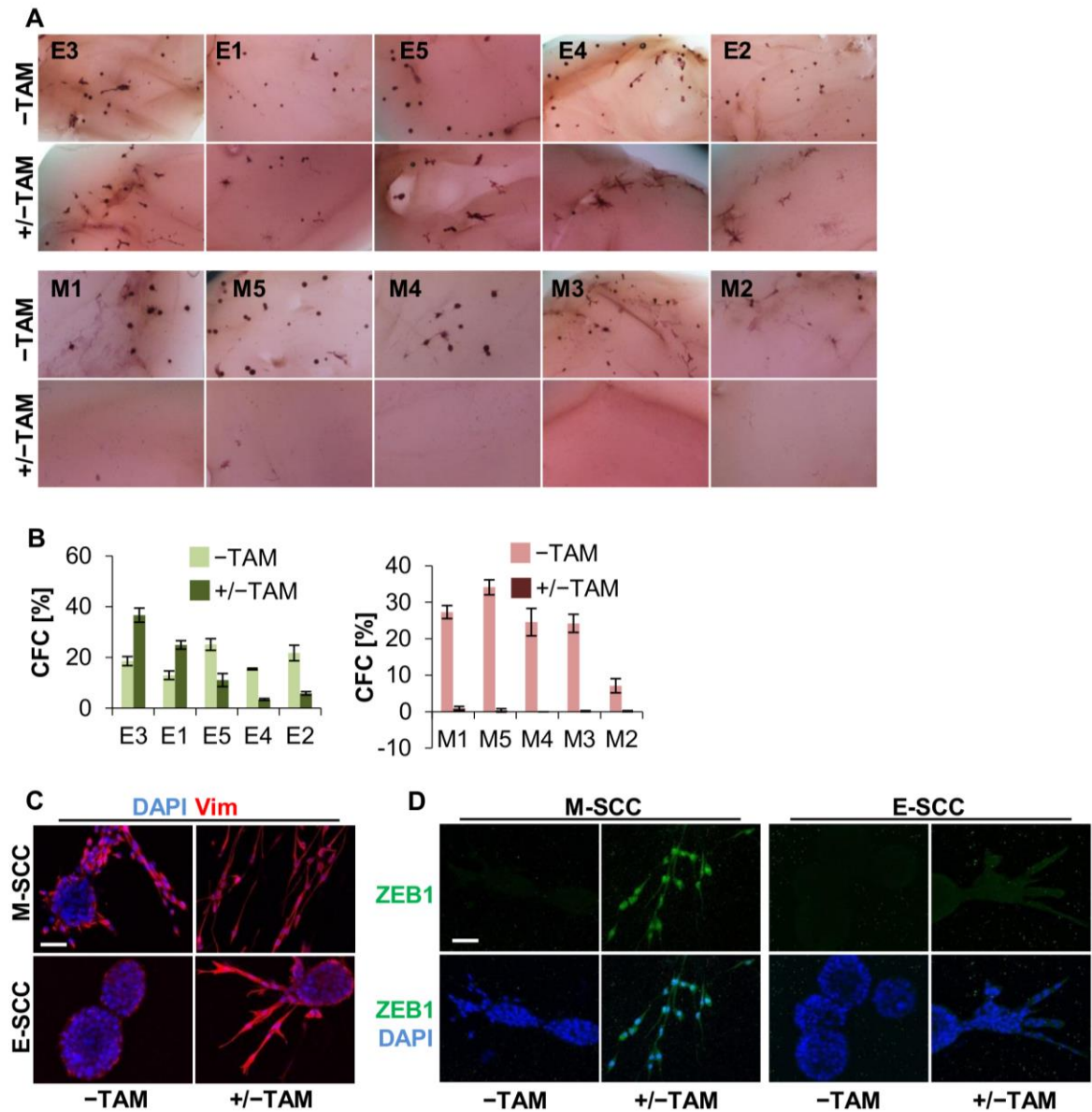


**Figure 23: Maintenance of an epithelial cell state is required for colony formation of 24<sup>high</sup> HMLE cells in 3D collagen gels.**

(A) Representative bright-field images of carmine stained colonies in 3D collagen gels formed by E-SCCs (upper panel) and M-SCCs (lower panel). Cells were not treated with TAM (-TAM) or treated with TAM for 14 days (+/-TAM) prior to plating. Cells were not further treated with TAM after plating. Plating density: 300 cells per gel. (B) Quantification of colony forming cells of E-SCCs (left panel) and M-SCCs (right panel) in 3D collagen gels. Cells were treated as described in A. n=3. CFC= colony forming cells. (C) Immunofluorescence staining of vimentin (red) and DAPI (blue) of colonies in 3D collagen gels formed by one representative M-SCC or one representative E-SCC. Cells were treated as described in A. Scale bar: 50  $\mu$ m. (D) Immunofluorescence staining of ZEB1 (green) and DAPI (blue) of colonies in 3D collagen gels formed by one representative M-SCC (left panel) or one representative E-SCC (right panel). Cells were treated as described in A. Scale bar: 50  $\mu$ m.

Data are presented as mean  $\pm$  SD.

#### **4.21.2 Maintenance of an epithelial cell state is required for colony formation of 24<sup>high</sup> HMLE cells on murine lung slices**

Since collagen is highly abundant in breast stroma, colony-formation in 3D collagen gels can be seen as a model for primary tumor formation. However, in more than 90% of breast cancer patients not the primary tumor, but distant metastases are the main cause of cancer related death (Weinberg, 2013). Since lung metastases are frequently diagnosed in breast cancer patients, I utilized murine lung slice cultures as an *in vitro* model to study metastatic outgrowth (colony formation) (Weigelt et al., 2005). Vital, 300 µm thick lung slices were obtained from the laboratory of Dr. Dr. Melanie Königshoff from the Comprehensive Pneumology Center at the Helmholtz Center Munich. To discriminate between lung and HMLE cells, one representative E-SCC (E3) was transduced lentivirally with the pRRL-cPPT-CMV-GFP-W and one representative M-SCC (M3) was transduced lentivirally with pRRL-cPPT-CMV-mCherry-W plasmid. Prior to plating, SCCs were either treated with TAM for a period of 14 days or not treated with TAM as a control. Five days after plating, colony formation was assessed by immunofluorescence and subsequent confocal microscopy. Moreover, murine lung slices were embedded in paraffin, then sectioned and stained with H&E in collaboration with Dr. Harald Bartsch from the Institute of Pathology at the Ludwig Maximilian University Munich. Whereas E-SCC control cells formed compact, round colonies, M-SCC control cells formed planar/flat colonies (Figures 24A and 24B). To quantify the cell number of the colonies, the intensity of DAPI stained nuclei was determined on confocal microscopy images. Corrected total cell fluorescence (CTCF) of DAPI was 1.5-fold higher for the untreated E-SCC compared to the untreated M-SCC (Figures 24C and 24D). After transient Twist1-activation, E-SCC cells still formed compact, round colonies, whereas M-SCC cells were detected as dispersed single cells (Figures 24A and 24B). Moreover, CTCF of DAPI increased by 30% for the E-SCCs while CTCF of DAPI decreased by 50% for the M-SCC. Thus, CTCF of DAPI was 4-fold higher for the E-SCC compared to the M-SCC after transient Twist1-activation (Figures 24C and 24D).

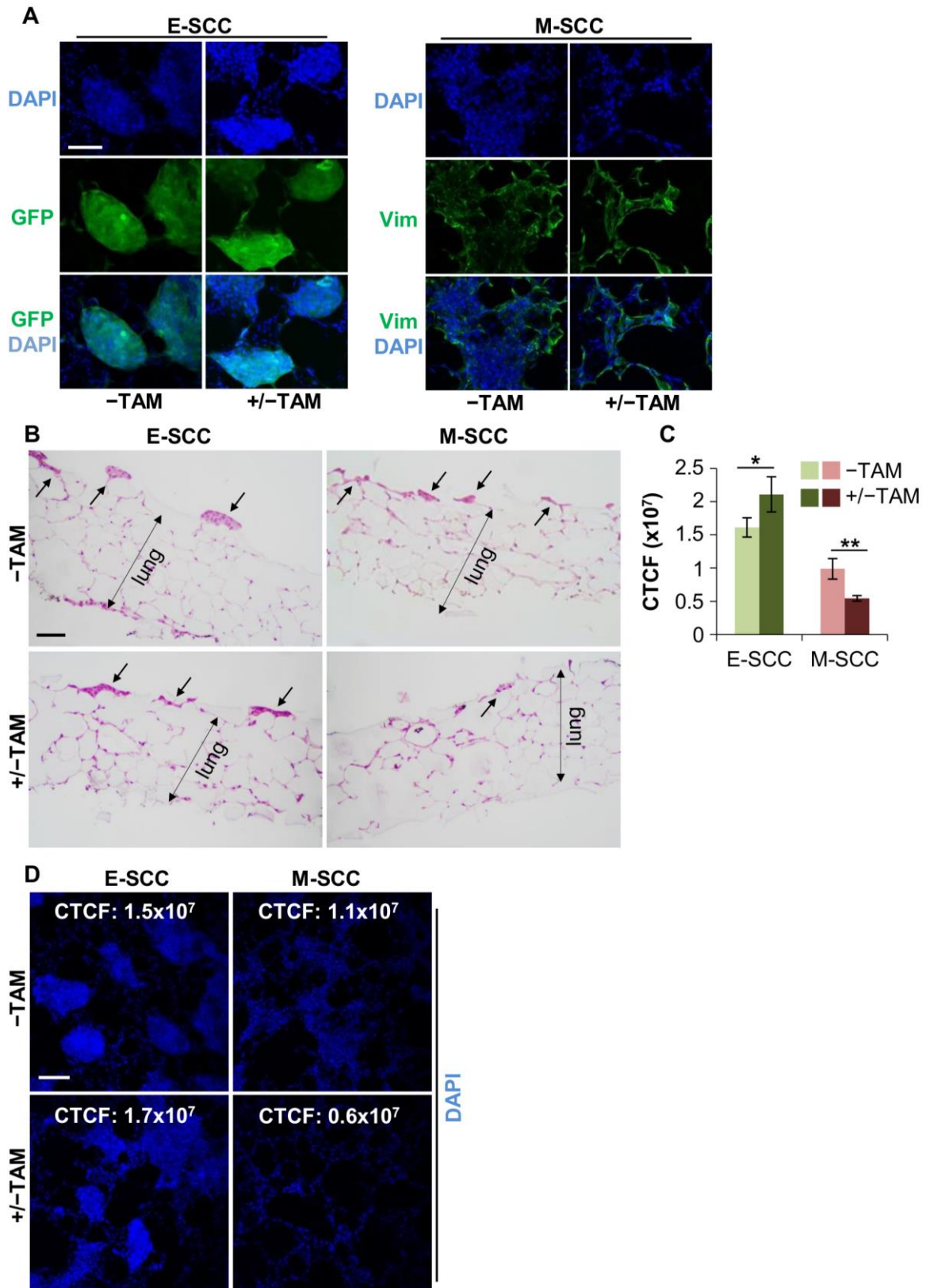


**Figure 24: Maintenance of an epithelial cell state is required for colony formation of  $24^{\text{high}}$  HMLE cells on murine lung slices.**

(A) Immunofluorescence staining of DAPI of colonies on murine lung slices formed by one representative E-SCC ( $\text{GFP}^{\text{pos}}$ ; left panel) and immunofluorescence staining of vimentin (green) and DAPI (blue) of one M-SCC (right panel). Cells were not treated with TAM (-TAM) or treated

with TAM for 14 days (+/-TAM) prior to plating. Cells were not further treated with TAM after plating. Plating density: 20.000 cells per slice. Scale bar: 50  $\mu\text{m}$ . **(B)** HE staining of cross sections of murine lung slices and colonies formed by one representative E-SCC or M-SCC. Cells were treated as described in (A). Scale bar: 50  $\mu\text{m}$ . **(C)** Quantification of DAPI intensity of representative images of colonies on murine lung slices formed by E-SCC or M-SCC cells. Cells were treated as described in A.  $n=4$ . CFCT=Corrected Total Cell Fluorescence. \* $p<0.05$ , \*\* $p<0.005$ , \*\*\* $p<0.0005$ . **(D)** Representative images of immunofluorescence staining of DAPI (blue) of murine lung slices with E-SCC or M-SCC cells used for quantification of DAPI intensity. Cells were treated as described in A. CFCT=Corrected Total Cell Fluorescence. Scale bar: 50  $\mu\text{m}$ .

Data are presented as mean  $\pm$  SD.

In summary, these results indicated that EMT resistance enabled 24<sup>high</sup> HMLE cells to retain colony forming ability on murine lung slices, while mesenchymal transdifferentiation resulted in a decrease of colony forming ability. Moreover, these data suggested that E-SCC cells already possessed a proliferative advantage before transient Twist1-activation that was even increased by transient Twist1. In contrast, M-SCCs already proliferated less before Twist1-activation and proliferative capacity was decreased by transient Twist1-activation.

### 4.22 Summary of the second part

In the second part of my thesis, I discovered that Twist1 elicited different effects in SCCs isolated from 24<sup>high</sup> HMLE cells: EMT competent M-SCCs acquired a stable mesenchymal cell state and did not undergo MET after Twist1-activation. EMT resistant E-SCCs resisted Twist1-induced EMT and retained an epithelial cell state. Although these observations initially appeared to be in conflict with those made in 24<sup>high</sup> HMLE bulk cells (no EMT resistance, but MET competence), co-culture experiments revealed that EMT resistant cells are contained within bulk cells, but become morphologically indistinguishable from EMT competent cells during Twist1-activation. Moreover, EMT resistant cells were discovered to grow as epithelial islands again, once Twist1 was deactivated, suggesting that EMT resistant and MET competent HMLE cells are the same cells within the 24<sup>high</sup> HMLE bulk cells. Mechanistic studies identified three key players (ZEB1, E-cadherin, Ovol2) that correlated with EMT competence or EMT resistance: loss of E-cadherin and Ovol2 expression and fast (7 days after Twist1-activation) ZEB1 up-regulation correlated with

mesenchymal transdifferentiation, while maintenance of E-cadherin and *Ovol2* transcript levels as well as delayed ZEB1 up-regulation correlated with EMT resistance. Moreover, sh-RNA mediated knockdown experiments revealed that ZEB1-expression was required for Twist1-induced EMT and even directly regulated by Twist1-binding to a putative enhancer region upstream of the *ZEB1* TSS. Finally, cell surface proteomics analysis identified cell surface proteins specifically higher expressed on EMT resistant cells before and after Twist1-activation. In parallel, functional studies of the SCCs suggested that maintenance of epithelial identity was required for proliferation and thus colony formation in 3D environments.

## 5 Discussion

Epithelial-Mesenchymal Transition (EMT) is a developmental program that converts epithelial cells to highly migratory mesenchymal cells. These morphological changes are accompanied by the dissolution of strong cell-cell adhesions, mainly by down-regulation of the adherens junction protein E-cadherin. Thus, observations linking the EMT program and the acquisition of aggressive traits by breast cancer cells (such as the ability to invade and intravasate) were not unexpected. However, studies connecting the EMT program to the acquisition of tumor-initiating traits (stem cell (sc)-like traits) were rather unexpected since breast cancer metastases are composed of epithelial cells with strong cell-cell adhesions (Kowalski et al., 2003). Importantly, recent studies only implicated, but did not provide evidence for a direct molecular link between EMT and acquisition of sc-like traits: only a minority of immortalized human mammary epithelial (HMLE) cells that transdifferentiated to a mesenchymal cell state additionally acquired tumor-initiating traits upon overexpression of the EMT-TF Snail or Twist1 (Mani et al., 2008; Morel et al., 2008). Thus, one could hypothesize that the EMT program might be involved but might not be sufficient for generation of sc-like traits. More precisely, acquisition of sc-like traits might be cell-specific effects of EMT inducing stimuli.

### 5.1 Twist1 induces mesenchymal transdifferentiation and mammosphere (MS)-formation independently of each other

Recent studies suggesting a link between EMT and the acquisition of sc-like traits (measured as MS-forming ability) were carried out using bulk populations of immortalized human mammary epithelial cells (HMLE) (Elenbaas et al., 2001; Mani et al., 2008). Importantly, HMLE bulk cells, additionally expressing an inducible construct of the EMT-TF Twist1 (HMLE-Twist1-ER), are heterogeneous and contain pre-existing subpopulations that are phenotypically and functionally distinct: besides epithelial cells, HMLE-Twist1-ER cells contain a small mesenchymal subpopulation enriched for sc-like traits (Mani et al., 2008; Scheel et al., 2011). Interestingly, this small CD44<sup>high</sup>/CD24<sup>neg</sup>, mesenchymal subpopulation was shown to arise spontaneously from bulk HMLE cells (Chaffer et al., 2011). Thus, one cannot distinguish whether EMT generates

mesenchymal, MS-forming cells *de novo* or whether the EMT process selects and expands pre-existing mesenchymal, MS-forming cells.

In this thesis, the heterogeneous character of the bulk HMLE cell-line was considered. By FACS sorting, phenotypically and functionally distinct subpopulations ( $24^{\text{neg}}$ ,  $24^{\text{low}}$ ,  $24^{\text{high}}$ ) within the HMLE-Twist1-ER cell-line were separated prior to Twist1-activation. I discovered that Twist1-activity induced a complete mesenchymal transdifferentiation and MS-forming ability in purified  $\text{CD24}^{\text{pos}}$  epithelial HMLE cells. Consequently, my studies provided evidence that activation of the EMT-TF Twist1 does not only select for pre-existing mesenchymal MS-forming cells, but that Twist1-activity is sufficient to induce both, conversion from epithelial to mesenchymal phenotype and conversion from non-MS-forming to MS-forming cells.

More importantly, I was able to elucidate that EMT and MS-forming ability were induced sequentially and independently of each other: 1) short-term Twist1-induction in  $24^{\text{high}}$  HMLE cells did not result in mesenchymal transdifferentiation but MS-forming capacity and 2) long-term Twist1-activation for 15 days switched all  $24^{\text{high}}$  HMLE cells to a mesenchymal phenotype, while only a small subset of them gained MS-forming ability. For the first time, I demonstrated that Twist1 conveys mesenchymal transdifferentiation and sc-like traits via distinct downstream signaling axes. Moreover, my studies provided evidence that passage through an EMT was not required for the acquisition of sc-like traits, while in turn Twist1-activity was not sufficient to induce these traits in each cell.

As mentioned in the results part of my thesis (Chapter 4), the MS-assay measures two functional parameters: 1) anoikis resistance (a form of programmed cell death/apoptosis) and 2) proliferation at clonal density (Frisch and Francis, 1994; Onder et al., 2008). One could hypothesize that MS-forming cells need to overcome apoptosis and to escape from cell cycle control. A recent review summarizes possible explanations on how Twist1 might induce these traits not necessarily linked to mesenchymal transdifferentiation (Puisieux et al., 2014). In detail, Maestro and colleagues showed that Twist is involved in inhibiting apoptosis by interfering with the p53 pathway (Maestro et al., 1999). Moreover, TWIST proteins were described to repress the transcription of  $\text{p16}^{\text{INK4A}}$ , thereby allowing escape from RB-mediated cell cycle control (Ansieau et al., 2008; Valsesia-Wittmann et al., 2004). Although these studies give an idea

on how Twist1 creates the foundation of MS-forming ability, the question remains why Twist1 was not sufficient to induce sc-like traits in each cell. One plausible explanation for the heterogeneous responses to Twist1-activation might be a cell-specific predisposition. For instance, presence or absence of specific signaling pathways, TFs or Twist1-interacting partners might determine whether Twist1-activity is sufficient to induce sc-like traits or not. In my studies, I discovered one important pre-requisite for Twist1-induced tumourigenicity: cellular plasticity (e.g. MET competence). The definition of cellular plasticity, the molecular background as well as functional consequences will be addressed in the following sections.

### **5.2 Twist1-deactivation results in a novel, hitherto unknown permanent cell state**

While monitoring the consequences of Twist1-activity in 24<sup>pos</sup> HMLE cells I observed that MS-formation only emerged after subsequent Twist1-deactivation and that pro-longed Twist1-deactivation increased MS-formation in 24<sup>high</sup> HMLE cells. Simultaneously, I detected that some 24<sup>high</sup> HMLE cells underwent MET in 2D culture after Twist1-deactivation. From these observations I initially concluded that HMLE cells needed to revert to their initial epithelial cell state in order to grow out as MS. However, when attempting to identify and enrich for MS-forming cells, I discovered that these cells were neither characterized by a fixed epithelial nor a fixed mesenchymal cell state. Instead, MS-forming cells displayed epithelial-mesenchymal plasticity, characterized by a unique gene expression profile (defined as the plasticity signature) (Schmidt et al, 2015). By identification of this unique plasticity signature I was able to provide evidence that transient EMT-TF activation primes HMLE cells for a novel permanent cell state. Even though recent *in vivo* studies suggested Twist1-deactivation and MET to be required for outgrowth at metastatic site in mouse models, these earlier studies did not focus on the precise cell state after MET (Ocana et al., 2012; Stankic et al., 2013; Tsai et al., 2012). My studies demonstrated for the first time that cells undergoing MET do not necessarily revert back to their original cell state. One possible explanation for the acquisition of a permanently altered cell state might be epigenetic modulation, which leaves a molecular footprint: epigenetic reprogramming was previously described for HMLE cells

during Twist1-induced EMT while EMT-TFs were shown to be capable of recruiting chromatin modifiers, such as Bmi1 or BRD4 (Bedi et al., 2014; Malouf et al., 2013; Shi et al., 2014; Yang et al., 2010;).

The fact that cells undergoing MET do not revert back to their original cell state might harbor dangerous consequences regarding breast cancer progression and therapy: although tumor cells that have transiently seen Twist1-activity are not detectable by morphology (or Twist1-expression), these cells might have gained tumor-initiating traits (sc-like traits) that persist after Twist1 is no longer active. The gene expression profile discovered in my thesis represents a potential tool to specifically detect these potentially metastatic cells. The identified gene expression profile could help to differ between tumors predisposed to metastasize and tumors that will not metastasize. Thus, these findings might help to improve patients' treatment by avoiding "over"- or "under-treatment". Moreover, based on the fact that the MS-assay measures anchorage independent proliferation at clonal density (traits shown by metastatic cells), I hypothesize that genes specifically expressed by MS-forming cells encode for proteins involved in molecular mechanisms required for metastatic capacity. Interfering with these mechanisms might represent a point of vantage for prevention of breast cancer progression.

### **5.3 24<sup>high</sup> HMLE cells predisposed to undergo MET retain expression of epithelial genes during Twist1-activation**

Given the fact that my results suggested MET to be required for MS-forming ability, I wished to elucidate the molecular mechanisms predisposing cells to undergo MET. Since the FACS purified 24<sup>high</sup> HMLE cells were heterogeneous with respect to Twist1-responsiveness I isolated single cell clones (SCCs) and studied the effects of Twist1 at the single cell level. Unexpectedly and contradictory to the observations from the 24<sup>high</sup> HMLE bulk cells, I identified "EMT competent" (M-SCCs) and "EMT resistant" HMLE cell clones (E-SCCs). Even more surprisingly, I did not detect any M-SCC that underwent MET after Twist1-deactivation. Studying these SCCs in more detail, I discovered that EMT resistance and EMT competence were correlated with specific changes of the transcriptional program. Specifically, I identified three key players correlated with EMT competence or EMT resistance: 1) the EMT-TF ZEB1, 2) the adherens

junction protein E-cadherin and 3) the Ovo-like zinc finger TF 2 (Ovol2). In detail, loss of E-cadherin and Ovol2 expression as well as strong and early ZEB1 up-regulation (at day 7) correlated with mesenchymal transdifferentiation, while maintenance of high E-cadherin and Ovol2 transcript levels as well as delayed ZEB1 up-regulation correlated with EMT resistance.

For reconciliation of the conflicting observations obtained from bulk 24<sup>high</sup> HMLE cells and isolated SCCs, I co-cultured E-SCC and M-SCC cells. Thereby, I discovered that E-SCCs and M-SCCs were morphologically not distinguishable (E-SCCs and M-SCCs represented as single scattered cells) as long as Twist1 was active, but became distinguishable after Twist1-deactivation (E-SCCs grew in epithelial islands while M-SCCs retained as single, scattered cells). Importantly, when SCCs from co-culture experiments were analyzed for their transcriptional program, I observed that E-SCC cells retained expression of E-cadherin and Ovol2. Based on these observations I concluded that cells predisposed for MET are characterized by the ability to maintain epithelial gene expression even in the presence of ZEB1 up-regulation.

#### **5.4 Expression of ZEB1 is directly regulated by Twist1 in 24<sup>high</sup> HMLE cells**

As described in the section above, early ZEB1 up-regulation (at day 7) correlated with mesenchymal transdifferentiation, while delayed ZEB1 up-regulation correlated with EMT-resistance. Using CD24<sup>pos</sup> HMLE-Twist1-ER cells, Diana Dragoi, a PhD student from the Scheel laboratory determined that Twist1 binds to a putative enhancer region in a TGF $\beta$ -type-I receptor (TGFBR1)-dependent manner, thereby inducing ZEB1 transcription and EMT (Chang et al., 2015; Dragoi et al., 2016). In my studies I examined whether Twist1 differentially binds to this region in M-SCCs and E-SCCs resulting in stronger and faster ZEB1-upregulation in M-SCCs compared to E-SCCs. By Immunoprecipitation (ChIP) analysis I discovered that Twist1-occupancy was higher in M-SCCs than E-SCCs at the putative enhancer region of *ZEB1* upon TAM-treatment.

Multiple scenarios might mechanistically explain the differential Twist1-binding in E-SCCs and M-SCCs. For instance, differences in Twist1-binding might be a result of epigenetic regulatory mechanisms: closed chromatin (heterochromatin) prevents access of transcriptional regulators to DNA, while open chromatin

(euchromatin) allows assembling of the transcriptional machinery and thereby gene expression (Wolffe and Matzke, 1999). Based on that, one could hypothesize that the chromatin within the putative enhancer region upstream of the *ZEB1* TSS is closed in E-SCCs, while open in M-SCCs. In future studies, it will be investigated whether E-SCCs and M-SCCs differ in chromatin marks either corresponding to active chromatin, such as H3K9 acetylation, or heterochromatin marks like H3K9 methylation.

In addition to differences in chromatin status, it is possible that E-SCCs and M-SCC might differ in their expression of (a) Twist1 interaction partner(s). Twist1 belongs to the basic Helix-loop-helix (bHLH) TFs. Activity of bHLH TFs is mainly regulated by the availability of dimerization partners and the formation of distinct homo- or heterodimers (Ellenberger et al., 1994). For example, human Twist1 was discovered to bind exclusively to E-box sequences after heterodimerization with an E-protein while Twist1 homodimers lack this ability (Chang et al., 2015). Thus, it might be conceivable that heterodimerization of Twist1 with a hitherto not identified partner, present in M-SCCs but not in E-SCCs, is prerequisite for Twist1-binding to the putative enhance region of *ZEB1*. It might also be vice versa: Twist1-binding might be negatively influenced by a dimerization partner, present in E-SCCs but not in M-SCCs. For instance, binding of Id proteins to class I or II bHLH TFs influences their function in a dominant-negative manner as Id proteins lack the DNA binding domain (Massari and Murre, 2000). Id4 was recently described to suppress invasion of glioblastoma cells by direct inhibitory interaction with Twist1 (Rahme and Israel, 2015). In addition, Id1 was found to oppose Twist1 protein activity in breast cancer cells (Stankic et al., 2013). Besides dimerization with partners belonging to the bHLH-TF family, Twist1 interacts with proteins involved in chromatin remodeling (Shi et al., 2014; Yang et al., 2010). Moreover, Twist1 contains a highly conserved domain at the carboxy-terminus (WR domain) that was found to allow interaction with proteins such as the TF RUNX2 or the NF- $\kappa$ B subunit p65 (Bialek et al., 2004; Castanon and Baylies, 2002; Li et al., 2012).

In future studies, Co-immunoprecipitation analyses will help to identify potential Twist1-binding partners that might participate in the regulation of Twist1-binding to the putative enhancer region of *ZEB1*.

### **5.5 Does *Ovol2* represent the central brake holder of *Twist1*-induced EMT?**

Although ZEB1 expression in EMT resistant cells was not up-regulated as rapid and strong as in EMT competent cells, a significant increase of ZEB1 transcript levels was detectable after long-term *Twist1*-activation. There are multiple scenarios that might explain why ZEB1 upregulation in E-SCCs was not sufficient to repress epithelial gene expression and therefore was not sufficient to mediate EMT. An explanation could be the existence of EMT-inhibiting regulatory networks, specifically present in E-SCCs. As described above, E-SCCs retained expression of the Ovo-like zinc finger TF 2 (*Ovol2*) during long-term *Twist1* activation. Interestingly, increasing evidence indicates *Ovol2* to represent a brake holder of EMT by direct inhibition of ZEB1 (Jia et al., 2015; Hong et al., 2015; Watanabe et al., 2014). Recently, Roca and colleagues identified gene expression changes induced by *Ovol2* overexpression to closely overlap with those induced by ZEB1-shRNA expression, suggesting a cross-regulation of these TFs (Roca et al., 2013). Moreover, *Ovol2* might indirectly restrict ZEB1-activity by induction of miR-200 family members (Roca et al., 2013). ZEB1 and the miR-200 family are known to repress each other in a negative feedback loop (Bracken et al., 2008; Burk et al., 2008). Furthermore, *Ovol2* might act as an EMT inhibitory factor by upregulating epithelial splicing regulatory proteins 1 and 2 (ESRP1, ESRP2). ESRP1 and ESRP2 were described to be critical for the isoform switch of the cell surface marker CD44 and thereby for EMT (Brown et al., 2004). Besides the described EMT-inhibitory networks regulated by *Ovol2*, a lack of ZEB1 interacting proteins might explain differential responses of E-SCCs and M-SCCs. For instance, the co-repressor C-terminal binding protein 1 (CTBP1) as well as the chromatin remodeling protein BRG1 were described to be required for efficient E-cadherin repression by ZEB1 (Grootclaes and Frisch, 2000; Shánchez-Tilló et al., 2010, Shi et al., 2003).

The question, to what extent *Ovol2* represents a critical gatekeeper for epithelial identity and to what extent the described EMT-inhibitory networks or the lack of ZEB1 interacting proteins are involved in EMT resistance will be addressed in future studies. In this thesis, I set out to identify regulatory mechanisms influenced by extracellular signaling, that might provide an explanation for the differential response of E-SCCs and M-SCCs to *Twist1*-activation (see 5.7).

## **5.6 EMT resistance is required for proliferation at primary tumor and metastatic site**

Since collagen is an abundant component of the extracellular matrix in human breast stroma, colony formation in 3D collagen gels can be seen as a model for primary tumor formation (Linnemann et al., 2015; Lo et al., 2012). In this study, I discovered that transient Twist1-activation induced invasive traits in 24<sup>high</sup> bulk HMLE cells while permanent Twist1-activity retained cells in a mesenchymal, non-proliferating cell state. When the isolated SCCs were grown in 3D collagen gels E-SCCs retained proliferative capacity and acquired invasiveness while M-SCCs lost proliferative capacity and represented as single cells invading the collagen gels after transient Twist1-activation. In summary, I was able to demonstrate that transient Twist1-activation elicited a proliferative and invasive cell state in EMT resistant cells, while stable mesenchymal transdifferentiation inhibited 3D growth. These data were in line with my observations from the MS-assay: as long as cells were fixed in a mesenchymal cell state (in this case by active Twist1) cells were not able to proliferate.

Based on the fact that in the majority of breast cancer patients (90%) not the primary tumor, but distant metastases are the main cause of cancer related death, I developed an *in vitro* model for metastatic outgrowth (Weinberg, 2013). In collaboration with the laboratory of Dr. Dr. Melanie Königshoff I established a method to culture HMLE cells on murine lung slices. I discovered that EMT-resistance (E-SCCs) enabled 24<sup>high</sup> HMLE cells to retain colony forming ability on murine lung slices, while mesenchymal transdifferentiation (M-SCCs) resulted in a decrease of colony forming ability. Importantly, decrease in colony formation was due to a lack of proliferation. In summary, the observations obtained from 3D-collagen gels and murine lung slice cultures imply that mesenchymal transdifferentiation decreases proliferative ability in an environment mimicking the primary tumor as well as an exemplary metastatic site.

Regarding cancer progression and metastasis many efforts have focused on targeting mesenchymal breast cancer cells in the past (Gupta et al., 2009; Pattabiraman et al., 2016; Tam et al., 2013). However, my studies and other observations caution against strategies targeting mesenchymal cancer cells (Celia-Terrassa et al., 2012; Korpál et al., 2011; Tran et al., 2014b). Whereas cells fixed in a mesenchymal cell state might remain non-proliferative and will not

grow out at metastatic site, enforced reversion to an epithelial or intermediate phenotype might harbor dangerous outcomes: 1) this approach might rather promote than prevent proliferation at primary tumor and metastatic site and 2) cells might be converted to a plastic state, enabling them to switch back and forth between different states and thereby adapt to various environments. Interestingly, recent discoveries from EMT lineage tracing strategies support the idea that EMT is not required for successful metastasis: in breast cancer mouse models, Kari and colleagues demonstrated that lung metastasis was driven by tumor cells persisting in an epithelial phenotype during the whole process (Fischer et al., 2015). In mouse models of pancreatic ductal adenocarcinoma (PDAC) loss of Twist1 or Snail1 did not influence tumor formation or metastasis to lung and liver, but suppressed EMT in the primary tumor. Moreover, EMT resulted in suppression of tumor cell proliferation (Zheng et al., 2015).

### **5.7 Does extracellular signaling explain differential response of E-SCCs and M-SCCs?**

Upstream of epigenetic regulation and regulation by transcription factors, the transcriptional program of cells is also influenced by extracellular signaling. Based on these considerations, I hypothesized that differential extracellular signaling might provide an explanation for the differential response of E-SCCs and M-SCCs to Twist1-activation. Since our group recently determined that Twist1-binding depends on active TGF $\beta$ -signaling, I investigated the influence of Smad-dependent TGF $\beta$ -signaling in a first approach (Dragoi, et al., 2016). As I did not discover significant differences in Smad-dependent TGF $\beta$ -signaling, a cell surface proteomics screen was performed. Thereby, I identified a set of 961 cell surface proteins that were differentially expressed in E-SCCs and M-SCCs before and after Twist1-activation. Amongst proteins persistently higher expressed on EMT resistant cells (before and after Twist1-activation), the tumor-associated calcium signal transducer 2 (TACSTD2), also known as trophoblast antigen 2 (Trop2), and the epithelial cell adhesion molecule (EpCAM) were found. Interestingly, both, Trop2 and EpCAM are highly expressed in variant epithelial cancers and their aberrant expression is linked to higher frequencies of metastasis (Cubas et al., 2009). Association of EpCAM and Trop2 overexpression with poor patient outcome might be explained by their ability to

stimulate tumor cell proliferation (Trzpis et al., 2007): EpCAM regulates cell cycle progression by influencing cyclin D1 expression and its overexpression was found to increase cell proliferation *in vitro* and *in vivo* (Chaves-Perez et al., 2013; Munz et al., 2004; Wenqi et al., 2009). Similarly, inhibition of Trop2 was shown to inhibit breast cancer growth *in vitro* and *in vivo* (Lin et al., 2014). Consequently, E-SCCs, expressing higher levels of EpCAM and Trop2 compared to M-SCCs, might benefit from pro-proliferative effects of these proteins. Interestingly, loss of EpCAM expression in M-SCCs during Twist1-activation might result from ZEB1 up-regulation in these cells: Vannier and colleagues discovered that ZEB1 directly represses EpCAM-expression in human pancreatic and breast cancer cell lines (Vannier et al., 2013).

Although overexpression of EpCAM and Trop2 might explain why M-SCC and E-SCC differ in their proliferation and thus colony forming capacity, the question remains why E-SCCs and M-SCCs respond differentially to Twist1-activation. Based on the discovery that Twist1 was differently bound to a region upstream of the *ZEB1* TSS in M-SCCs compared to E-SCCs 7 days after Twist1-activation, one possible scenario could be differences in the chromatin status. Interestingly, EpCAM as well as the desmosomal protein desmoglein 3 (Dsg3), also identified by the proteomics screen, were found to interact with the actin cytoskeleton: the cytoplasmic EpCAM domain contains two  $\alpha$ -actinin binding sites conferring interaction between EpCAM and actin cytoskeleton (Guillemot et al., 2001). Dsg3 was shown to interact with the actin cytoskeleton and promotes cytoskeleton organization in epithelial cells (Tsang et al., 2012). Based on that one could hypothesize that different levels of EpCAM and Dsg3 favor different cytoskeleton organizations, which might influence chromatin composition: Ramdas and Shivashankar recently discovered that the cytoskeleton modulates nuclear morphology, heterochromatin localization as well as chromatin dynamics and thereby gene expression (Ramdas and Shivashankar, 2015). Future studies investigating the importance of Trop2, EpCAM or Dsg3 on EMT resistance and metastatic competence will be performed.

### 5.8 Closing remarks

The results of my study clearly emphasize that mesenchymal transdifferentiation, tumorigenicity and metastatic capability are not necessarily linked to each other.

While transdifferentiation to a stable mesenchymal cell state might prevent metastatic outgrowth, maintenance of an epithelial or intermediate/plastic cell state might facilitate metastatic outgrowth. Moreover, the discovery that cells undergoing MET after transient Twist1-activity do not revert back to their original cell state might harbor dangerous consequences: these cells are not detectable by morphology but might have gained tumor-initiating traits (sc-like traits) that persist after Twist1 is no longer active. Consequently, this study illustrates the urgent need of considering EMT-independent molecular mechanisms, mediated by EMT-TFs, in order to develop new therapeutic strategies for breast cancer eradication. Moreover, my data clearly show the need for diagnostic tools to detect those tumor cells that have transiently seen EMT-TF activity and might thus represent potentially metastatic cells. My study provides two promising datasets for the development of new diagnostic criteria: a unique gene expression profile specifically expressed in MS-forming cells and a set of 961 cell surface proteins differentially expressed in “metastatic” and “non-metastatic” HMLE clones.

## 6 References

Al-Hajj, M., Wicha, M.S., Benito-Hernandez, A., Morrison, S.J., and Clarke, M.F. (2003). Prospective identification of tumorigenic breast cancer cells. *Proceedings of the National Academy of Sciences of the United States of America* 100, 3983-3988.

Ansieau S, Bastid J, Doreau A, Morel AP, Bouchet BP, Thomas C, Fauvet F, Puisieux I, Doglioni C, Piccinin S, Maestro R, Voeltzel T, Selmi A, Valsesia-Wittmann S, Caron de Fromental C, Puisieux A. (2008). Induction of EMT by twist proteins as a collateral effect of tumor-promoting inactivation of premature senescence. *Cancer Cell* 14: 79-89.

Ansieau, S., Morel, A.P., Hinkal, G., Bastid, J., and Puisieux, A. (2010). TWISTing an embryonic transcription factor into an oncoprotein. *Oncogene* 29, 3173-3184.

Ansieau S. (2013). EMT in breast cancer stem cell generation. *Cancer Lett*; 338: 63-8.

Arnoux, V., Nassour, M., L'Helgoualc'h, A., Hipskind, R.A., and Savagner, P. (2008). Erk5 controls Slug expression and keratinocyte activation during wound healing. *Molecular biology of the cell* 19, 4738-4749.

Barrallo-Gimeno, A., and Nieto, M.A. (2005). The Snail genes as inducers of cell movement and survival: implications in development and cancer. *Development* 132, 3151-3161.

Bedi, U., Mishra, V.K., Wasilewski, D., Scheel, C., and Johnsen, S.A. (2014). Epigenetic plasticity: A central regulator of epithelial-to-mesenchymal transition in cancer. *Oncotarget* 5, 2016–2029.

Bialek P., Kern B., Schrock M., Hong N., Wu H.,Ornitz D.M., Justice M.J., Yang X., Sobic D., Yu K., Olson E.N., Karsenty G. (2004). A Twist Code Determines the Onset of Osteoblast Differentiation. *Developmental Cell*, Vol. 6, 423–435.

Bonnet, D., and Dick, J. (1997). Human acute myeloid leukemia is organized as a hierarchy that originates from a primitive hematopoietic cell. *Nat. Med.* 3, 730–737.

Boyer B., Thiery J.P. (1993). Epithelium-mesenchyme interconversion as example of epithelial plasticity. *APMIS*. 1993 Apr;101(4):257-68.

Bracken, C.P., Gregory, P.A., Kolesnikoff, N., Bert, A.G., Wang, J., Shannon, M.F., and Goodall, G.J. (2008). A double-negative feedback loop between ZEB1-SIP1 and the microRNA-200 family regulates epithelial-mesenchymal transition. *Cancer research* 68, 7846-7854.

Brown, K.A., Aakre, M.E., Gorska, A.E., Price, J.O., Eltom, S.E., Pietenpol, J.A., and Moses, H.L. (2004). Induction by transforming growth factor-beta1 of

epithelial to mesenchymal transition is a rare event in vitro. Breast cancer research : BCR 6, R215-231.

Burk, U., Schubert, J., Wellner, U., Schmalhofer, O., Vincan, E., Spaderna, S., and Brabletz, T. (2008). A reciprocal repression between ZEB1 and members of the miR-200 family promotes EMT and invasion in cancer cells. EMBO reports 9, 582-589.

Campbell, K., Whissell, G., Franch-Marro, X., Batlle, E., and Casanova, J. (2011). Specific GATA factors act as conserved inducers of an endodermal-EMT. Developmental cell 21, 1051-1061.

Cano A<sup>1</sup>, Pérez-Moreno MA, Rodrigo I, Locascio A, Blanco MJ, del Barrio MG, Portillo F, Nieto MA. (2000). The transcription factor snail controls epithelial-mesenchymal transitions by repressing *E-cadherin* expression. Nature Cell Biol. 2, 76-83 (2000).

Casas, E., Kim, J., Bendesky, A., Ohno-Machado, L., Wolfe, C.J., and Yang, J. (2011). Snail2 is an essential mediator of Twist1-induced epithelial mesenchymal transition and metastasis. Cancer research 71, 245-254.

Castanon I., Baylies M.K. (2002). A Twist in fate: evolutionary comparison of Twist structure and function. Gene 287 (2002) 11-22.

Celia-Terrassa, T., Meca-Cortes, O., Mateo, F., de Paz, A.M., Rubio, N., Arnal-Estape, A., Ell, B.J., Bermudo, R., Diaz, A., Guerra-Rebollo, M., et al. (2012). Epithelial-mesenchymal transition can suppress major attributes of human epithelial tumor-initiating cells. The Journal of clinical investigation 122, 1849-1868.

Chaffer C.L, Brueckmann I., Scheel C., Kaestli A.J., Wiggins P.A., Rodrigues L.O., Brooks M., Reinhardt F., Su Y., Polyak K., Arendt L.M., Kuperwasser C., Bieri B., Weinberg R.A. (2011). Normal and neoplastic nonstem cells can spontaneously convert to a stem-like state. Proc Natl Acad Sci U S A. 2011 May 10;108(19):7950-5.

Chang, A.T., Liu, Y., Ayyanathan, K., Benner, C., Jiang, Y., Prokop, J.W., Paz, H., Wang, D., Li, H.R., Fu, X.D., et al. (2015). An evolutionarily conserved DNA architecture determines target specificity of the TWIST family bHLH transcription factors. Genes & development 29, 603-616.

Chapman, H.A. (2011). Epithelial-mesenchymal interactions in pulmonary fibrosis. Annual review of physiology 73, 413-435.

Chaves-Perez, A., Mack, B., Maetzel, D., Kremling, H., Eggert, C., Harreus, U., and Gires, O. (2013). EpCAM regulates cell cycle progression via control of cyclin D1 expression. Oncogene 32, 641-650.

Chen Z.F., Behringer R.R. (1995). twist is required in head mesenchyme for cranial neural tube morphogenesis. Genes Dev. 1995 Mar 15;9(6):686-99.

## References

---

- Comijn J, Berx G, Vermassen P, Verschueren K, van Grunsven L, Bruyneel E, Mareel M, Huylebroeck D, van Roy F. (2001). The two-handed E box binding zinc finger protein SIP1 downregulates E-cadherin and induces invasion. *Mol Cell* 2001; 7: 1267-78.
- Cubas, R., Li, M., Chen, C., and Yao, Q. (2009). Trop2: a possible therapeutic target for late stage epithelial carcinomas. *Biochimica et biophysica acta* 1796, 309-314.
- Dave, N., Guaita-Esteruelas, S., Gutarra, S., Frias, A., Beltran, M., Peiro, S., and de Herreros, A.G. (2011). Functional cooperation between Snail1 and twist in the regulation of ZEB1 expression during epithelial to mesenchymal transition. *The Journal of biological chemistry* 286, 12024-12032.
- Davies J.A. (1996). Mesenchyme to epithelium transition during development of the mammalian kidney tubule. *Acta Anat (Basel)*. 1996;156(3):187-201.
- De Craene, B., and Berx, G. (2013). Regulatory networks defining EMT during cancer initiation and progression. *Nature reviews Cancer* 13, 97-110.
- Dontu, G., Abdallah, W.M., Foley, J.M., Jackson, K.W., Clarke, M.F., Kawamura, M.J., and Wicha, M.S. (2003). In vitro propagation and transcriptional profiling of human mammary stem/progenitor cells. *Genes & development* 17, 1253-1270.
- Dragoi D., Krattenmacher A., Mishra V.K., Schmidt J.M., Kloos U.J., Meixner L.K., Hauck S.M., Buggenthin F., Schwartz D., Marr C., Johnsen S.A., Scheel C.H. (2016). Twist1 induces distinct cell states depending on TGFBR1-activation. *Oncotarget*, Vol. 7, No. 21, 30396-30407.
- DuBridge R.B., Tang P., Hsia H.C., Leong P.M., Miller J.H., Calos M.P. (1987). Analysis of mutation in human cells by using an Epstein-Barr virus shuttle system. *Mol Cell Biol*. 1987 Jan;7(1):379-87.
- Eger, A., Aigner, K., Sonderegger, S., Dampier, B., Oehler, S., Schreiber, M., Berx, G., Cano, A., Beug, H., and Foisner, R. (2005). DeltaEF1 is a transcriptional repressor of E-cadherin and regulates epithelial plasticity in breast cancer cells. *Oncogene* 24, 2375-2385.
- Eijkelenboom, A., and Burgering, B.M. (2013). FOXOs: signalling integrators for homeostasis maintenance. *Nature reviews Molecular cell biology* 14, 83-97.
- Ell, B., and Kang, Y. (2013). Transcriptional control of cancer metastasis. *Trends in cell biology* 23, 603-611.
- Elenbaas B., Spirio L., Koerner F., Fleming M.D., Zimonjic D.B., Donaher J.L., Popescu N.C., Hahn W.C., Weinberg R.A. (2001). Human breast cancer cells generated by oncogenic transformation of primary mammary epithelial cells. *Genes Dev*. 2001 Jan 1;15(1):50-65.

- Ellenberger T., Fass D., Arnaud M., Harrison S.C. (1994). Crystal structure of transcription factor E47: E-box recognition by a basic region helix-loop-helix dimer. *Genes Dev.* 1994 Apr 15;8(8):970-80.
- Elloul, S., Elstrand, M.B., Nesland, J.M., Trope, C.G., Kvalheim, G., Goldberg, I., Reich, R., and Davidson, B. (2005). Snail, Slug, and Smad-interacting protein 1 as novel parameters of disease aggressiveness in metastatic ovarian and breast carcinoma. *Cancer* 103, 1631-1643.
- Fillmore, C.M., and Kuperwasser, C. (2008). Human breast cancer cell lines contain stem-like cells that self-renew, give rise to phenotypically diverse progeny and survive chemotherapy. *Breast cancer research : BCR* 10, R25.
- Fischer, K.R., Durrans, A., Lee, S., Sheng, J., Li, F., Wong, S.T., Choi, H., El Rayes, T., Ryu, S., Troeger, J., et al. (2015). Epithelial-to-mesenchymal transition is not required for lung metastasis but contributes to chemoresistance. *Nature*.
- Franco D.L, Mainez J., Vega S., Sancho P., Murillo M.M., de Frutos C.A., Del Castillo G., López-Blau C., Fabregat I., Nieto M.A. (2010). Snail1 suppresses TGF-beta-induced apoptosis and is sufficient to trigger EMT in hepatocytes. *J Cell Sci.* 2010 Oct 15;123(Pt 20):3467-77.
- Frisch, S.M., and Francis, H. (1994). Disruption of epithelial cell-matrix interactions induces apoptosis. *J. Cell Biol.* 124, 619–626.
- Geradts, J., de Herreros, A.G., Su, Z., Burchette, J., Broadwater, G., and Bachelder, R.E. (2011). Nuclear Snail1 and nuclear ZEB1 protein expression in invasive and intraductal human breast carcinomas. *Human pathology* 42, 1125-1131.
- Graessel A., Hauck S.M., von Toerne C., Kloppmann E., Goldberg T., Koppensteiner H., Schindler M., Knapp B., Krause L., Dietz K., Schmidt-Weber C.B., Suttner K. A. (2015). A combined Omics Approach to Generate the Surface Atlas of Human Naïve CD4+ T Cells during Early T-Cell Receptor Activation. *Mol. Cell Proteomics* 14, 2085-2102.
- Grooteclaes, M. L., & Frisch, S. M. (2000). Evidence for a function of CtBP in epithelial gene regulation and anoikis. *Oncogene*, 19(33), 3823–3828.
- Grosche A., Hauser A., Lepper M.F., Mayo R., von Toerne C., Merl-Pham J., Hauck S.M. (2015). The proteome of native adult Muller glial cells from murine retina. *Mol. Cell Proteomics* [Epub ahead of print].
- Guaita, S., Puig, I., Franci, C., Garrido, M., Dominguez, D., Batlle, E., Sancho, E., Dedhar, S., De Herreros, A.G., and Baulida, J. (2002). Snail induction of epithelial to mesenchymal transition in tumor cells is accompanied by MUC1 repression and ZEB1 expression. *The Journal of biological chemistry* 277, 39209-39216.

## References

---

- Guillemot J.C., Naspetti M., Malergue F., Montcourrier P., Galland F., Naquet P. (2001). Ep-CAM transfection in thymic epithelial cell lines triggers the formation of dynamic actin-rich protrusions involved in the organization of epithelial cell layers. *Histochem Cell Biol.* 2001 Oct;116(4):371-8.
- Gupta, P.B., Onder, T.T., Jiang, G., Tao, K., Kuperwasser, C., Weinberg, R.A., and Lander, E.S. (2009). Identification of selective inhibitors of cancer stem cells by high-throughput screening. *Cell* 138, 645-659.
- Hauck S.M., Dietter J., Kramer R.L., Hofmaier F., Zipplies J.K., Amann B., Feuchtinger A., Deeg C.A., Ueffing M. (2010). Deciphering membrane-associated molecular processes in target tissue of autoimmune uveitis by label-free quantitative mass spectrometry. *Mol.Cell Proteomics* 9, 2292-305.
- Hajra K.M., Chen D.Y., Fearon E.R. (2002). The SLUG zinc-finger protein represses E-cadherin in breast cancer. *Cancer Res.* 2002 Mar 15;62(6):1613-8.
- Hay E.D.. (1968). Organization and fine structure of epithelium and mesenchyme in the developing chick embryos. In *Epithelial-Mesenchymal Interactions: 18th Hahnemann Symposium*, ed. R. Fleischmajer, R.E. Billingham, pp. 31–35. Baltimore: Williams & Wilkins.
- Hay, E.D. (1995). An overview of epithelial-mesenchymal transformation. *Acta Anat. (Basel).* 154, 8–20.
- Hong, J., Zhou, J., Fu, J., He, T., Qin, J., Wang, L., Liao, L., and Xu, J. (2011). Phosphorylation of serine 68 of Twist1 by MAPKs stabilizes Twist1 protein and promotes breast cancer cell invasiveness. *Cancer research* 71, 3980-3990.
- Hong, T., Watanabe, K., Ta, C.H., Villarreal-Ponce, A., Nie, Q., and Dai, X. (2015). An Ovol2-Zeb1 Mutual Inhibitory Circuit Governs Bidirectional and Multi-step Transition between Epithelial and Mesenchymal States. *PLoS computational biology* 11, e1004569.
- Howe LR, Watanabe O, Leonard J, Brown AM. (2003). Twist is up-regulated in response to Wnt1 and inhibits mouse mammary cell differentiation. *Cancer Res* 63: 1906-13.
- Ince, T.A., Richardson, A.L., Bell, G.W., Saitoh, M., Godar, S., Karnoub, A.E., Iglehart, J.D., and Weinberg, R. a (2007). Transformation of different human breast epithelial cell types leads to distinct tumor phenotypes. *Cancer Cell* 12, 160–170.
- Jia D., Jolly M.K., Boareto M., Parsana P., Mooney S.M., Pienta K.J., Levine H., Ben-Jacob E. (2015). OVOL guides the epithelial-hybrid-mesenchymal transition. *Oncotarget*, Vol. 6, No. 17.
- Kalluri, R., and Weinberg, R.A. (2009). The basics of epithelial-mesenchymal transition. *The Journal of clinical investigation* 119, 1420-1428.

## References

---

- Knight RD, Shimeld SM. (2001). Identification of conserved C2H2 zinc-finger gene families in the Bilateria. *Genome Biol.* 2001;2(5):RESEARCH0016. Epub 2001 Apr 24.
- Korpai, M., Ell, B.J., Buffa, F.M., Ibrahim, T., Blanco, M.A., Celia-Terrassa, T., Mercatali, L., Khan, Z., Goodarzi, H., Hua, Y., et al. (2011). Direct targeting of Sec23a by miR-200s influences cancer cell secretome and promotes metastatic colonization. *Nature medicine* 17, 1101-1108.
- Kowalski, P.J., Rubin, M.A., and Kleer, C.G. (2003). E-cadherin expression in primary carcinomas of the breast and its distant metastases. *Breast cancer research : BCR* 5, R217-222.
- Kwok W.K., Ling M.T., Lee T.W., Lau T.C., Zhou C., Zhang X., Chua C.W., Chan K.W., Chan F.L., Glackin C., Wong Y.C., Wang X. (2005). Up-regulation of TWIST in prostate cancer and its implication as a therapeutic target. *Cancer Res.* 2005 Jun 15;65(12):5153-62.
- Lai Z.C., Fortini M.E., Rubin G.M. (1991). The embryonic expression patterns of zfh-1 and zfh-2, two Drosophila genes encoding novel zinc-finger homeodomain proteins. *Mech Dev.* 1991 Jun;34 (2-3):123-34.
- Lamouille, S., Xu, J., and Derynck, R. (2014). Molecular mechanisms of epithelial-mesenchymal transition. *Nature reviews Molecular cell biology* 15, 178-196.
- Le T.L., Yap A.S., Stow J.L. (1999). Recycling of E-Cadherin: A Potential Mechanism for Regulating Cadherin Dynamics. *The Journal of Cell Biology*, Volume 146, Number 1, July 12, 1999 219–232.
- Lee S., Lee S., Jung Y.S., Xu Y., Ho Sung Kang H.S., Ha N., Park B. (2009). Blocking of p53-Snail Binding, Promoted by Oncogenic K-Ras, Recovers p53 Expression and Function<sup>1,2</sup>. *Neoplasia* (2009) 11, 22–31.
- Lee, T.K., Poon, R.T., Yuen, A.P., Ling, M.T., Kwok, W.K., Wang, X.H., Wong, Y.C., Guan, X.Y., Man, K., Chau, K.L., et al. (2006). Twist overexpression correlates with hepatocellular carcinoma metastasis through induction of epithelial-mesenchymal transition. *Clinical cancer research : an official journal of the American Association for Cancer Research* 12, 5369-5376.
- Leptin M. (1991). twist and snail as positive and negative regulators during Drosophila mesoderm development. *Genes Dev.* 1991 Sep;5(9):1568-76.
- Lester, R.D., Jo, M., Montel, V., Takimoto, S., and Gonias, S.L. (2007). uPAR induces epithelial-mesenchymal transition in hypoxic breast cancer cells. *The Journal of cell biology* 178, 425-436.
- Li S., Kendall S.E., Raices R., Finlay J., Covarrubias M., Liu Z., Lowe G., Lin Y., The Y. H., Leigh V., Dhillon S., Flanagan S., Aboody K.S., Glackin C.A. (2012).

## References

---

TWIST1 associates with NF- $\kappa$ B subunit RELA via carboxyl-terminal WR domain to promote cell autonomous invasion through IL8 production. *BMC Biology* 2012, 10:73.

Lin, H., Zhang, H., Wang, J., Lu, M., Zheng, F., Wang, C., Tang, X., Xu, N., Chen, R., Zhang, D., et al. (2014). A novel human Fab antibody for Trop2 inhibits breast cancer growth in vitro and in vivo. *International journal of cancer Journal international du cancer* 134, 1239-1249.

Lin, T., Ponn, A., Hu, X., Law, B.K., and Lu, J. (2010). Requirement of the histone demethylase LSD1 in Snai1-mediated transcriptional repression during epithelial-mesenchymal transition. *Oncogene* 29, 4896-4904.

Linnemann, J.R., Miura, H., Meixner, L.K., Irmeler, M., Kloos, U.J., Hirschi, B., Bartsch, H.S., Sass, S., Beckers, J., Theis, F.J., et al. (2015). Quantification of regenerative potential in primary human mammary epithelial cells. *Development* 142, 3239-3251.

Lo, A.T., Mori, H., Mott, J., and Bissell, M.J. (2012). Constructing three-dimensional models to study mammary gland branching morphogenesis and functional differentiation. *Journal of mammary gland biology and neoplasia* 17, 103-110.

Long, J., Zuo, D., and Park, M. (2005). Pc2-mediated sumoylation of Smad-interacting protein 1 attenuates transcriptional repression of E-cadherin. *The Journal of biological chemistry* 280, 35477-35489.

Maestro, R. *et al.* Twist is a potential oncogene that inhibits apoptosis. *Genes Dev.* 13, 2207–2217 (1999).

Malouf, G.G., Taube, J.H., Lu, Y., Roysarkar, T., Panjarian, S., Estecio, M.R., Jelinek, J., Yamazaki, J., Raynal, N.J., Long, H., et al. (2013). Architecture of epigenetic reprogramming following Twist1-mediated epithelial-mesenchymal transition. *Genome biology* 14, R144.

Mani, S.A., Guo, W., Liao, M.J., Eaton, E.N., Ayyanan, A., Zhou, A.Y., Brooks, M., Reinhard, F., Zhang, C.C., Shipitsin, M., et al. (2008). The epithelial-mesenchymal transition generates cells with properties of stem cells. *Cell* 133, 704-715.

Massague, J. (2008). TGFbeta in Cancer. *Cell* 134, 215-230.

Massari M.E., Murre C. (2000). Helix-loop-helix proteins: regulators of transcription in eucaryotic organisms. *Mol Cell Biol.* 2000 Jan;20(2):429-40.

Mironchik, Y., Winnard, P.T., Jr., Vesuna, F., Kato, Y., Wildes, F., Pathak, A.P., Kominsky, S., Artemov, D., Bhujwalla, Z., Van Diest, P., et al. (2005). Twist overexpression induces in vivo angiogenesis and correlates with chromosomal instability in breast cancer. *Cancer research* 65, 10801-10809.

## References

---

- Moody, S.E., Perez, D., Pan, T.C., Sarkisian, C.J., Portocarrero, C.P., Sterner, C.J., Notorfrancesco, K.L., Cardiff, R.D., and Chodosh, L.A. (2005). The transcriptional repressor Snail promotes mammary tumor recurrence. *Cancer cell* 8, 197-209.
- Morel A.P., Lièvre M., Thomas C., Hinkal G., Ansieau S., Puisieux A. (2008). Generation of Breast Cancer Stem Cells through Epithelial-Mesenchymal Transition. *PLoS One*. 2008 Aug 6;3(8):e2888. doi: 10.1371/journal.pone.0002888.
- Munz, M., Kieu, C., Mack, B., Schmitt, B., Zeidler, R., and Gires, O. (2004). The carcinoma-associated antigen EpCAM upregulates c-myc and induces cell proliferation. *Oncogene* 23, 5748-5758.
- Nagarajan, S., Hossan, T., Alawi, M., Najafova, Z., Indenbirken, D., Bedi, U., Taipaleenmaki, H., Ben-Batalla, I., Scheller, M., Loges, S., et al. (2014). Bromodomain protein BRD4 is required for estrogen receptor-dependent enhancer activation and gene transcription. *Cell reports* 8, 460-469.
- Nieto, M.A. (2002). The snail superfamily of zinc-finger transcription factors. *Nature reviews Molecular cell biology* 3, 155-166.
- Nieto, M.A. (2011). The ins and outs of the epithelial to mesenchymal transition in health and disease. *Annual review of cell and developmental biology* 27, 347-376.
- Ocana, O.H., Corcoles, R., Fabra, A., Moreno-Bueno, G., Acloque, H., Vega, S., Barrallo-Gimeno, A., Cano, A., and Nieto, M.A. (2012). Metastatic colonization requires the repression of the epithelial-mesenchymal transition inducer Prrx1. *Cancer cell* 22, 709-724.
- Ohashi, S., Natsuizaka, M., Wong, G.S., Michaylira, C.Z., Grugan, K.D., Stairs, D.B., Kalabis, J., Vega, M.E., Kalman, R.A., Nakagawa, M., et al. (2010). Epidermal growth factor receptor and mutant p53 expand an esophageal cellular subpopulation capable of epithelial-to-mesenchymal transition through ZEB transcription factors. *Cancer research* 70, 4174-4184.
- Onder, T.T., Gupta, P.B., Mani, S.A., Yang, J., Lander, E.S., and Weinberg, R.A. (2008). Loss of E-cadherin promotes metastasis via multiple downstream transcriptional pathways. *Cancer research* 68, 3645-3654.
- Panzilius E. (2014). Molecular links between epithelial-mesenchymal transition and tumorigenicity in breast cancer. (Master Thesis).
- Parvani, J.G., Taylor, M.A., and Schiemann, W.P. (2011). Noncanonical TGF-beta signaling during mammary tumorigenesis. *Journal of mammary gland biology and neoplasia* 16, 127-146.
- Pattabiraman, D.R., Bierie, B., Kober, K.I., Thiru, P., Krall, J.A., Zill, C., Reinhardt, F., Tam, W.L., and Weinberg, R.A. (2016). Activation of PKA leads to

## References

---

mesenchymal-to-epithelial transition and loss of tumor-initiating ability. *Science* 351, aad3680.

Peinado H., Del Carmen Iglesias-de la Cruz M., Olmeda D., Csiszar K., Fong K.S., Vega S., Nieto M.A., Cano A., Portillo F. (2005). A molecular role for lysyl oxidase-like 2 enzyme in snail regulation and tumor progression. *EMBO J.* 2005 Oct 5;24(19):3446-58. Epub 2005 Aug 18.

Peinado, H., Olmeda, D., and Cano, A. (2007). Snail, Zeb and bHLH factors in tumour progression: an alliance against the epithelial phenotype? *Nature reviews Cancer* 7, 415-428.

Peto, R., Boreham, J., Clarke, M., Davies, C., and Beral, V. (2000). UK and USA breast cancer deaths down 25% in year 2000 at ages 20–69 years. *The Lancet* 355, 1822.

Podo, F., Buydens, L.M., Degani, H., Hilhorst, R., Klipp, E., Gribbestad, I.S., Van Huffel, S., van Laarhoven, H.W., Luts, J., Monleon, D., et al. (2010). Triple-negative breast cancer: present challenges and new perspectives. *Molecular oncology* 4, 209-229.

Postigo A.A., Dean D.C. (2000). Differential expression and function of members of the zfh-1 family of zinc finger/homeodomain repressors. *Proc Natl Acad Sci U S A.* 2000 Jun 6;97(12):6391-6.

Postigo A.A., Depp J.L., Taylor J.J., Kroll K.L.(2003). Regulation of Smad signaling through a differential recruitment of coactivators and corepressors by ZEB proteins. *EMBO J.* 2003 May 15;22(10):2453-62.

Prat, A., and Perou, C.M. (2011). Deconstructing the molecular portraits of breast cancer. *Molecular oncology* 5, 5-23.

Puisieux, A., Brabletz, T., and Caramel, J. (2014). Oncogenic roles of EMT-inducing transcription factors. *Nature cell biology* 16, 488-494.

R Development Core Team (2008). R: A language and environment for statistical computing (Vienna, Austria: R Foundation for Statistical Computing).

Rahme, G.J., and Israel, M.A. (2015). Id4 suppresses MMP2-mediated invasion of glioblastoma-derived cells by direct inactivation of Twist1 function. *Oncogene* 34, 53-62.

Rainer, J., Sanchez-Cabo, F., Stocker, G., Sturn, A., and Trajanoski, Z. (2006). CARMAweb: comprehensive R- and bioconductor-based web service for microarray data analysis. *Nucleic acids research* 34, W498-503.

Ramdas, N.M., and Shivashankar, G.V. (2015). Cytoskeletal control of nuclear morphology and chromatin organization. *Journal of molecular biology* 427, 695-706.

Ramón y Cajal S. (1890). *Manual de Anatomía Patológica General*. Barcelona: Casa Provincial Caridad.

Remacle J.E., Kraft H., Walter Lerchner W., Wuytens G., Collart C., Kristin Verschueren K., Smith J.C., Huylebroeck D. (1999). New mode of DNA binding of multi-zinc finger transcription factors:  $\delta$ EF1 family members bind with two hands to two target sites. *The EMBO Journal* Vol.18 No.18 pp.5073–5084, 1999.

Reya, T., Morrison, S.J., Clarke, M.F., and Weissman, I.L. (2001). Stem cells, cancer, and cancer stem cells. *Nature* 414, 105–111.

Reynolds, B.A., and Weiss, S. (1992). Generation of neurons and astrocytes from isolated cells of the adult mammalian central nervous system. *Science* 255, 1707–1710.

Reynolds, B.A., and Weiss, S. (1996). Clonal and population analyses demonstrate that an EGF-responsive mammalian embryonic CNS precursor is a stem cell. *Dev. Biol.* 175, 1–13.

RKI (2010). Robert Koch Institut und die Gesellschaft der epidemiologischen Krebsregister in Deutschland e.V. *Krebs in Deutschland 2005/2006. Häufigkeiten und Trends*. 7. Ausgabe. Berlin 2010.

Roca, H., Hernandez, J., Weidner, S., McEachin, R.C., Fuller, D., Sud, S., Schumann, T., Wilkinson, J.E., Zaslavsky, A., Li, H., et al. (2013). Transcription factors OVOL1 and OVOL2 induce the mesenchymal to epithelial transition in human cancer. *PloS one* 8, e76773.

Rota L.M., Lazzarino D.A., Ziegler A.N., LeRoith D. and Wood T.L. (2012). Determining mammosphere-forming potential: application of the limiting dilution analysis. *Journal of mammary gland biology and neoplasia* 17, 119-123.

Roy, H.K., Smyrk, T.C., Koetsier, J., Victor, T.A., and Wali, R.K. (2005). The Transcriptional Repressor SNAIL Is Overexpressed in Human Colon Cancer. *Digestive Diseases and Sciences* 50, 42-46.

Sánchez-Tilló, E., Lázaro, A., Torrent, R., Cuatrecasas, M., Vaquero, E. C.,..., Castells, A., Postigo, A. (2010). ZEB1 represses E-cadherin and induces an EMT by recruiting the SWI/SNF chromatin-remodeling protein BRG1. *Oncogene*, 29(24), 3490–3500.

Scheel C, Eaton EN, Li SH, Chaffer CL, Reinhardt F, Kah KJ, Bell G, Guo W, Rubin J, Richardson AL, Weinberg RA. (2011). Paracrine and autocrine signals induce and maintain mesenchymal and stem cell states in the breast. *Cell* 145(6):926-40.

Scheel, C., and Weinberg, R.A. (2012). Cancer stem cells and epithelial-mesenchymal transition: concepts and molecular links. *Seminars in cancer biology* 22, 396-403.

## References

---

Schmidt, J.M., Panzilius, E., Bartsch, H.S., Irmeler, M., Beckers, J., Kari, V., Linnemann, J.R., Dragoi, D., Hirschi, B., Kloos, U.J., et al. (2015). Stem-cell-like properties and epithelial plasticity arise as stable traits after transient Twist1 activation. *Cell reports* 10, 131-139.

Shi J., Wang Y., Zeng L., Wu Y., Deng J., Zhang Q., Lin Y., Li J., Kang T., Tao M., et al. (2014). Disrupting the interaction of BRD4 with diacetylated Twist suppresses tumorigenesis in basal-like breast cancer. *Cancer Cell* 25, 210–225.

Shi, Y., Sawada, J., Sui, G., Affar, E. B., Whetstone, J. R., Lan, F., Shi, Y. (2003). Coordinated histone modifications mediated by a CtBP co-repressor complex. *Nature*, 422(6933), 735–738.

Shioiri, M., Shida, T., Koda, K., Oda, K., Seike, K., Nishimura, M., Takano, S., and Miyazaki, M. (2006). Slug expression is an independent prognostic parameter for poor survival in colorectal carcinoma patients. *British journal of cancer* 94, 1816-1822.

Shirakihara, T., Saitoh, M., and Miyazono, K. (2007). Differential regulation of epithelial and mesenchymal markers by deltaEF1 proteins in epithelial mesenchymal transition induced by TGF-beta. *Molecular biology of the cell* 18, 3533-3544.

Simpson P. (1983). Maternal-Zygotic Gene Interactions during Formation of the Dorsal-Ventral Pattern in *Drosophila* Embryos. *Genetics* 1983 ; 105: 615-32.

Stankic, M., Pavlovic, S., Chin, Y., Brogi, E., Padua, D., Norton, L., Massague, J., and Benezra, R. (2013). TGF-beta-Id1 signaling opposes Twist1 and promotes metastatic colonization via a mesenchymal-to-epithelial transition. *Cell reports* 5, 1228-1242.

Tam, W.L., Lu, H., Buikhuisen, J., Soh, B.S., Lim, E., Reinhardt, F., Wu, Z.J., Krall, J.A., Bieri, B., Guo, W., et al. (2013). Protein kinase C alpha is a central signaling node and therapeutic target for breast cancer stem cells. *Cancer cell* 24, 347-364.

Thiery, J.P., Acloque, H., Huang, R.Y., and Nieto, M.A. (2009). Epithelial-mesenchymal transitions in development and disease. *Cell* 139, 871-890.

Thomson, C.S., Brewster, D.H., Dewar, J.A., Twelves, C.J., and Scottish Cancer Therapy, N. (2004). Improvements in survival for women with breast cancer in Scotland between 1987 and 1993: impact of earlier diagnosis and changes in treatment. *European journal of cancer* 40, 743-753.

Thuault, S., Valcourt, U., Petersen, M., Manfioletti, G., Heldin, C.H., and Moustakas, A. (2006). Transforming growth factor-beta employs HMGA2 to elicit epithelial-mesenchymal transition. *The Journal of cell biology* 174, 175-183.

Thuault, S., Tan, E.J., Peinado, H., Cano, A., Heldin, C.H., and Moustakas, A. (2008). HMGA2 and Smads co-regulate SNAIL1 expression during induction of

epithelial-to-mesenchymal transition. *The Journal of biological chemistry* 283, 33437-33446.

Timmerman, L.A., Grego-Bessa, J., Raya, A., Bertran, E., Perez-Pomares, J.M., Diez, J., Aranda, S., Palomo, S., McCormick, F., Izpisua-Belmonte, J.C., et al. (2004). Notch promotes epithelial-mesenchymal transition during cardiac development and oncogenic transformation. *Genes & development* 18, 99-115.

Tong, Z.T., Cai, M.Y., Wang, X.G., Kong, L.L., Mai, S.J., Liu, Y.H., Zhang, H.B., Liao, Y.J., Zheng, F., Zhu, W., et al. (2012). EZH2 supports nasopharyngeal carcinoma cell aggressiveness by forming a co-repressor complex with HDAC1/HDAC2 and Snail to inhibit E-cadherin. *Oncogene* 31, 583-594.

Tran, D.D., Corsa, C.A., Biswas, H., Aft, R.L., and Longmore, G.D. (2011). Temporal and spatial cooperation of Snail1 and Twist1 during epithelial-mesenchymal transition predicts for human breast cancer recurrence. *Molecular cancer research : MCR* 9, 1644-1657.

Tran, H.D., Luitel, K., Kim, M., Zhang, K., Longmore, G.D., and Tran, D.D. (2014). Transient SNAIL1 Expression is Necessary for Metastatic Competence in Breast Cancer. *Cancer research*.

Trzpis, M., McLaughlin, P.M., de Leij, L.M., and Harmsen, M.C. (2007). Epithelial cell adhesion molecule: more than a carcinoma marker and adhesion molecule. *The American journal of pathology* 171, 386-395.

Tsai, J.H., Donaher, J.L., Murphy, D.A., Chau, S., and Yang, J. (2012). Spatiotemporal regulation of epithelial-mesenchymal transition is essential for squamous cell carcinoma metastasis. *Cancer cell* 22, 725-736.

Tsai, J.H., and Yang, J. (2013). Epithelial-mesenchymal plasticity in carcinoma metastasis. *Genes & development* 27, 2192-2206.

Tsang, S.M., Brown, L., Gadmor, H., Gammon, L., Fortune, F., Wheeler, A., and Wan, H. (2012). Desmoglein 3 acting as an upstream regulator of Rho GTPases, Rac-1/Cdc42 in the regulation of actin organisation and dynamics. *Experimental cell research* 318, 2269-2283.

Uhl, F.E., Vierkotten, S., Wagner, D.E., Burgstaller, G., Costa, R., Koch, I., Lindner, M., Meiners, S., Eickelberg, O., and Konigshoff, M. (2015). Preclinical validation and imaging of Wnt-induced repair in human 3D lung tissue cultures. *The European respiratory journal* 46, 1150-1166.

Valentin, M.D., da Silva, S.D., Privat, M., Alaoui-Jamali, M., and Bignon, Y.J. (2012). Molecular insights on basal-like breast cancer. *Breast cancer research and treatment* 134, 21-30.

Vallin J, Thuret R, Giacomello E, Faraldo MM, Thiery JP, Broders F. (2001). Cloning and characterization of three *Xenopus* slug promoters reveal direct regulation by Lef/beta-catenin signaling. *J Biol Chem* 276: 30350-8.

## References

---

- Valsesia-Wittmann, S., Magdeleine, M., Dupasquier, S., Garin, E., Jallas, A.C., Combaret, V., Krause, A., Leissner, P., and Puisieux, A. (2004). Oncogenic cooperation between H-Twist and N-Myc overrides failsafe programs in cancer cells. *Cancer cell* 6, 625-630.
- Vannier, C., Mock, K., Brabletz, T., and Driever, W. (2013). Zeb1 regulates E-cadherin and Epcam (epithelial cell adhesion molecule) expression to control cell behavior in early zebrafish development. *The Journal of biological chemistry* 288, 18643-18659.
- Viebahn C. (1995). Epithelial-mesenchymal transformation during formation of the mesoderm in the mammalian embryo. *Acta Anat (Basel)*. 1995;154(1):79-97.
- Watanabe, K., Villarreal-Ponce, A., Sun, P., Salmans, M.L., Fallahi, M., Andersen, B., and Dai, X. (2014). Mammary morphogenesis and regeneration require the inhibition of EMT at terminal end buds by *Ovol2* transcriptional repressor. *Developmental cell* 29, 59-74.
- Watanabe O., Imamura H., Shimizu T., Kinoshita J., Okabe T., Hirano A., Yoshimatsu K., Konno S., Aiba M., Ogawa K. (2004). Expression of Twist and Wnt in Human Breast Cancer. *Anticancer Res*. 2004 Nov-Dec;24(6):3851-6.
- Wei, S.C., Fattet, L., Tsai, J.H., Guo, Y., Pai, V.H., Majeski, H.E., Chen, A.C., Sah, R.L., Taylor, S.S., Engler, A.J., et al. (2015). Matrix stiffness drives epithelial-mesenchymal transition and tumour metastasis through a TWIST1-G3BP2 mechanotransduction pathway. *Nature cell biology*.
- Weigelt, B., Peterse, J.L., and van 't Veer, L.J. (2005). Breast cancer metastasis: markers and models. *Nature reviews Cancer* 5, 591-602.
- Weinberg, R.A. (2013). Moving Out: Invasion and Metastasis. In *The Biology of Cancer*, 2nd Edition, (New York, London: Garland Science), p. 642.
- Wenqi, D., Li, W., Shanshan, C., Bei, C., Yafei, Z., Feihu, B., Jie, L., and Daiming, F. (2009). EpCAM is overexpressed in gastric cancer and its downregulation suppresses proliferation of gastric cancer. *Journal of cancer research and clinical oncology* 135, 1277-1285.
- Wolffe A.P., Marjori A. Matzke M.A. (1999). Epigenetics: Regulation Through Repression. *Science* 15 Oct 1999. Vol. 286, Issue 5439, pp. 481-486.
- Wu, W.S., Heinrichs, S., Xu, D., Garrison, S.P., Zambetti, G.P., Adams, J.M., and Look, A.T. (2005). Slug antagonizes p53-mediated apoptosis of hematopoietic progenitors by repressing puma. *Cell* 123, 641-653.
- Xu, J., Lamouille, S., and Derynck, R. (2009). TGF-beta-induced epithelial to mesenchymal transition. *Cell research* 19, 156-172.
- Yang, J., Mani, S.A., Donaher, J.L., Ramaswamy, S., Itzykson, R.A., Come, C., Savagner, P., Gitelman, I., Richardson, A., and Weinberg, R.A. (2004). Twist, a

## References

---

master regulator of morphogenesis, plays an essential role in tumor metastasis. *Cell* 117, 927-939.

Yang, J., and Weinberg, R.A. (2008). Epithelial-mesenchymal transition: at the crossroads of development and tumor metastasis. *Developmental cell* 14, 818-829.

Yang, M.H., Hsu, D.S., Wang, H.W., Wang, H.J., Lan, H.Y., Yang, W.H., Huang, C.H., Kao, S.Y., Tzeng, C.H., Tai, S.K., et al. (2010). Bmi1 is essential in Twist1-induced epithelial-mesenchymal transition. *Nature cell biology* 12, 982-992.

Yang Z., Rayala S., Nguyen D., Vadlamudi R.K., Chen S., Kumar R. (2005). Pak1 phosphorylation of snail, a master regulator of epithelial-to-mesenchyme transition, modulates snail's subcellular localization and functions. *Cancer Res.* 2005 Apr 5;65(8):3179-84.

Yuen, H.F., Chan, Y.P., Wong, M.L., Kwok, W.K., Chan, K.K., Lee, P.Y., Srivastava, G., Law, S.Y., Wong, Y.C., Wang, X., et al. (2007). Upregulation of Twist in oesophageal squamous cell carcinoma is associated with neoplastic transformation and distant metastasis. *Journal of clinical pathology* 60, 510-514.

Zheng, X., Carstens, J.L., Kim, J., Scheible, M., Kaye, J., Sugimoto, H., Wu, C.C., LeBleu, V.S., and Kalluri, R. (2015). Epithelial-to-mesenchymal transition is dispensable for metastasis but induces chemoresistance in pancreatic cancer. *Nature*.

Zhou, B.P., Deng, J., Xia, W., Xu, J., Li, Y.M., Gunduz, M., and Hung, M.C. (2004). Dual regulation of Snail by GSK-3beta-mediated phosphorylation in control of epithelial-mesenchymal transition. *Nature cell biology* 6, 931-940.

## **Eidesstattliche Versicherung**

Schmidt, Johanna Maria

Ich erkläre hiermit an Eides statt,

dass die vorliegende Dissertation mit dem Thema

### **Temporal and cell-specific effects of the basic Helix-Loop-Helix Transcription factor Twist1 during breast cancer progression**

selbständig verfasst, mich außer der angegebenen keiner weiteren Hilfsmittel bedient und alle Erkenntnisse, die aus dem Schrifttum ganz oder annähernd übernommen sind, als solche kenntlich gemacht und nach ihrer Herkunft unter Bezeichnung der Fundstelle einzeln nachgewiesen habe.

Ich erkläre des Weiteren, dass die hier vorgelegte Dissertation nicht in gleicher oder in ähnlicher Form bei einer anderen Stelle zur Erlangung eines akademischen Grades eingereicht wurde.

Grassau Mietenkam, 30.05.2017

---

Unterschrift Doktorandin

### **Acknowledgments**

I have never been afraid of facing the unknown and in Doctor Christina Scheel I found both, a great advisor and a good friend facing the challenge of science. I am very thankful that she always had motivating and positive words for me and a sympathetic ear to my needs.

My special thanks go to Professor Magdalena Götz for giving me the opportunity to perform my doctoral thesis at her Institute of Stem Cell research. Thank you for all the great discussions, your guidance and listening to my problems.

Next I would like to thank all the members of the Scheel group. Thanks to Diana Dragoi, Jelena Linnemann, Elena Panzilius, Benjamin Hirschi, Lisa Meixner, Anja Krattenmacher and Laura Eichelberger for being reliable colleagues and friends. Uwe Kloos provided excellent technical support. Much progress was made in collaboration with Elena Panzilius, who became one of my best friends.

During my whole project I received precious input and great support from the members of my thesis committee: Professor Magdalena Götz, Professor Andreas Jung and Doctor Christina Scheel. Thank you for productive meetings and great back up.

All this work could not have been established if I had not had the opportunity to collaborate with excellent scientists from most different departments. Thanks to Doctor Martin Irmeler and Doctor Steffen Sass for expression profiling and statistical transcriptome analysis, Doctor Stefanie Hauck for proteomics analysis of cell surface proteins, Professor Steven Johnson and Doctor Vivek Mishra for ChIP analysis, Professor Karl Sotlar and Doctor Harald Bartsch for histological sections and clinical data and Doctor Doctor Melanie Königshoff and Doctor Mareike Lehmann for providing murine lung slices. Thank you for productive meetings and excellent cooperation on interesting scientific questions.

Furthermore, I want to acknowledge all the members of the Institute of Stem Cell Research for your advices, help and suggestions.

I also want to thank Elsa Melo, Nina Fuchs and Karen Biniossek for administrative and organizational support.

Last but not least, I want to extend my gratitude to my family and my friends. I want to thank all of you for your support, your constant motivation and for always being there for me.